The Role of MeCP2 in the Regulation of Alternative Splicing

By

Ronghui Li

A dissertation submitted in partial fulfillment of

the requirements of the degree of

Doctor of Philosophy

(Cellular and Molecular Biology)

at the

UNIVERSITY OF WISCONSIN-MADISON

2016

Date of final oral examination: 05/02/2016

The dissertation is approved by the following members of the Final Oral Committee:

Qiang Chang, Associate professor, Genetics
Timothy J. Kamp, Professor, Medicine
Su-Chun Zhang, Professor, Neuroscience and Neurology
Xin Sun, Professor, Genetics
John Svaren, Professor, Comparative Biosciences

Abstract

Mutations in the human *MECP2* gene cause Rett syndrome (RTT), a severe neurodevelopmental disorder that predominantly affects girls. Despite decades of work, the molecular function of MeCP2 is not fully understood. Here we report a systematic identification of MeCP2-interacting proteins in the mouse brain. In addition to transcription regulators, we found that MeCP2 physically interacts with several modulators of RNA splicing, including LEDGF and DHX9. These interactions are disrupted by RTT causing mutations, suggesting that they may play a role in RTT pathogenesis. Consistent with the idea, deep RNA sequencing revealed misregulation of hundreds of splicing events in the cortex of *Mecp2* knockout mice. To reveal the functional consequence of altered RNA splicing due to the loss of MeCP2, we focused on the regulation of the splicing of the flip/flop exon of *Gria2* and other AMPAR genes. We found a significant splicing shift in the flip/flop exon toward the flop inclusion, leading to a faster decay in the AMPAR gated current and altered synaptic transmission. In summary, our study identified direct physical interaction between MeCP2 and splicing factors, a novel MeCP2 target gene, and established functional connection between a specific RNA splicing change and synaptic phenotypes in RTT mice. These results not only help our understanding of the molecular function of MeCP2 but also reveal potential drug targets for future therapies.

Acknowledgments

First, I would like to thank my thesis advisor, Dr. Qiang Chang, for his strong support and tremendous guidance throughout the Ph.D. training. He not only offered me great opportunity to work on interesting and challenging projects, but also trained me how to think critically and act responsibly. I appreciate a lot all the time he spent talking to me, and all the advices he shared with me on how to become a scientist. I would also like to thank all of my thesis committee members, Dr. Timothy Kamp, Dr. Su-Chun Zhang, Dr. Xin Sun, Dr. Emery Bresnick, and Dr. John Svaren, for giving great guidance and advices on my research projects and career planning.

Second, I am very grateful for all the current and former Chang lab members. Hongda Li and Xiaofen Zhong not only helped me in my projects but also became great friends to me. Qiping Dong is a wonderful labmate and contributed a lot to the project. Qian Bu and Anxin Wang shared a lot of thoughts with me. Shruti Marwaha, Fei Yu and Xiaoji Zhang helped me a lot with mouse work. In addition, I want to acknowledge the help from our collaborators, Dr. Zefeng Wang, Dr. Xinyu Zhao, and Dr. Sunduz Keles. I would never be able to accomplish anything without their contribution.

Third, I want to thank Dr. Barry Ganetzky for playing table tennis with me. We have a lot of fun together. I owe a lot to all of my friends, Yu Gao, Anqi Wang, Zhangli Su, Xinmin Zhang and Hao Zeng. They have made my life much more interesting.

Last but not least, I would like to give special thanks to my wife, Jiewen Huang, and all of my family members. They have always understood me and supported me unconditionally.

Table of Contents

Abstract ..... **i**

Acknowledgments ..... **ii**

Table of Contents ..... **iii**

Chapter 1: Introduction **1**

1.1 Rett syndrome **1**

1.1.1 Clinical features 1

1.1.2 Pathophysiology 2

1.2 RTT genetics **3**

1.2.1 The *MECP2* gene: structure and transcription 3

1.2.2 The MeCP2 protein 4

1.2.3 Causative mutations 5

1.2.4 *MECP2* duplication syndrome 7

1.3 RTT model systems **8**

1.3.1 Mouse models 8

1.3.2 Patient-specific induced pluripotent stem cells (iPSCs) 11

1.3.3 Genetically engineered human stem cell model 12

1.4 RTT disease mechanism **13**

1.4.1 MeCP2 target genes 13

1.4.2 Molecular function of MeCP2 14

1.5 MeCP2 posttranscriptional modification **18**

1.5.1 Phosphorylation 18

1.5.2 Other posttranslational modifications 19

1.6 Alternative splicing and neurological disorders 20

1.6.1 Alternative splicing 20

1.6.2 Splicing regulation 21

1.6.3 Epigenetic regulation of alternative splicing 22

1.6.4 Splicing regulation and neurological disorder 23

Chapter 2: Systematic identification of MeCP2-interacting proteins in the mouse brain ... 25

2.1 Introduction 25

2.2 Results 27

2.2.1 Co-immunoprecipitation optimization 27

2.2.2 Co-immunoprecipitation and mass spectrometry 30

2.2.3 Validation of MeCP2-interacting proteins 33

2.2.4 Interaction between MeCP2 and splicing factors in human neural progenitor cells 35

2.2.5 Essential domain in MeCP2 for interaction with splicing factors 37

2.2.6 MeCP2 phosphorylation does not influence interaction with splicing factors 41

2.3 Discussion 45

2.4 Materials and Methods 46

2.4.1 Animals 46

2.4.2 Plasmids 47

2.4.3 Co-immunoprecipitation and Mass spectrometry 47

2.4.4 Co-immunoprecipitation and Western blot 48

2.4.5 Transfection and Co-immunoprecipitation 48

Chapter 3: Loss of MeCP2 affects alternative splicing 50

3.1 Introduction 50

3.2 Results 51

3.2.1 RNA-Seq reveals alteration of alternative splicing upon loss of MeCP2 51

3.2.2 Altered splicing of the AMPAR genes in the cortex of *Mecp2* KO mice 60

3.2.3 AMPA receptor flip/flop splicing is not regulated by activity dependent MeCP2 phosphorylation 65

3.2.4 LEDGF is involved in the regulation of *Gria2* flip/flop splicing 68

3.2.5 Functional link between altered flip/flop splicing and synaptic phenotypes in the *Mecp2* KO mice 72

3.2.6 Pharmaceutical correction of AMPA receptor desensitization defect might delay disease progression in *Mecp2* KO mouse 79

3.3 Discussion 81

3.4 Methods and Materials 84

3.4.1 RNA-Seq Analysis 84

3.4.2 Gene Ontology Analysis 85

3.4.3 RNA extraction and qRT-PCR 85

3.4.4 Chromatin Immunoprecipitation 85

3.4.5 ChIP-seq data analysis 86

3.4.6 Gria2 minigene splicing assay 87

3.4.7 Electrophysiology 87

3.4.8 Lentivirus preparation and stereotaxic injection. 89

3.4.9 AAV infection. 89

3.4.10 Statistics. 89

Chapter 4: Conclusions and future directions 90

4.1 MeCP2-interacting proteins 90

4.1.1 Cell-type specific protein-protein interaction 90

4.1.2 Functional importance of MeCP2-interacting proteins 91

4.2 MeCP2 and alternative splicing 94

4.2.1 Brain region specific splicing changes 94

4.2.2 Profiling splicing changes in specific cell types 95

4.2.3 Dynamics of flip/flop splicing changes 95

4.2.4 Contribution of splicing changes to RTT phenotypes 96

4.2.5 Mechanism underlying MeCP2-mediated splicing regulation on *Gria2* flip/flop exons 97

4.2.6 Correction of aberrant flip/flop splicing in *Mecp2* KO mice 98

References 100

Chapter 1: Introduction

1.1 Rett syndrome

Rett syndrome (RTT [MIM #312750]) is a progressive neurodevelopmental disorder that predominantly affects females. RTT occurs in 1:10,000 to 1: 15,000 female live birth(Hagberg, 1985) and is the second most frequent cause for intellectual instability in females. RTT was firstly described by a Viennese pediatrician, Dr. Andreas Rett, in 1966(Rett, 1966) and was later brought to international recognition by Hagberg in 1983(Hagberg et al., 1983).

1.1.1 Clinical features

Typical RTT patients are born healthy and do not manifest any developmental abnormalities in the first 6-18 months. Affected girls can learn to walk and even speak a few words. After this period, patients cease to achieve developmental milestone and experience a developmental stagnation. The disease progression follows a distinct developmental course that can be roughly divided into four stages(Chahrour and Zoghbi, 2007; Hagberg, 2002). In stage I (6-18 months), their head growth decelerates, which results in microcephaly by the second year of age. Affected girls also display general body growth arrest and have a weak posture due to muscle hypotonia. In stage II (age 1-4 years), patients exhibit a rapid deterioration of higher brain functions, including loss of purposeful hand movement, speech, and social interaction deficit. The onset of rapid neurological regression is accompanied by development of stereotypic hand wringing, ataxia, and seizures. Breathing is normal during sleep but appears irregular during active wakefulness, with hyperventilation followed by periods of apnea(Cirignotta et al., 1986; Lugaresi et al., 1985). Syndromes seem to stabilize after this rapid regression stage. This marks the beginning of a stationary stage (stage III, age 3-10 years). Patients suffer from autonomic

dysfunction at this stage, and a proportion of sudden death of girls with RTT has been attributed to improper autonomic function(Kerr et al., 1997). Additional syndrome includes development of scoliosis and anxiety. Although seizure is less frequent after patients turn teenage (Stage IV, 10 year and older), loss of mobility worsens and render patients wheelchair-bound. Some patients can survive up to decades of life.

Besides typical RTT cases, several atypical RTT variants has been proposed based on clinical severity(Hagberg and Skjeldal, 1994). Milder variants are the forme fruste ("worn-down form"), the late regression and the preserve speech variant(Hagberg, 2002). In contrast, severe variants include congenital variant and the early seizure-onset form(Hagberg and Skjeldal, 1994; Rajaei et al., 2011).

1.1.2 Pathophysiology

Consistent with the observation of microcephaly, RTT girls have reduced brain weight and volume compared with age- and gender-matched control subjects(Jellinger et al., 1988; Jellinger and Seitelberger, 1986; Reiss et al., 1993). Anatomical studies did not reveal gross cell loss and neuronal atrophy(Jellinger et al., 1988; Reiss et al., 1993), arguing against the early assumption that RTT has a neurodegeneration root. Instead, neurons in RTT patients are smaller in size and more densely packed in cortical and subcortical region(Bauman et al., 1995), suggestive of delayed neuronal development. Morphological examination of pyramidal neurons showed decrease in dendritic length and complexity in the frontal, motor, and limbic cortex(Armstrong et al., 1995; Armstrong et al., 1998), further supporting RTT is a neurodevelopmental disorder. Reduction of dendritic complexity is also accompanied by dendritic spine dysgenesis, with reduction in spine density and lower proportion of mushroom type spine(Belichenko et al., 1994;

Phillips and Pozzo-Miller, 2015). Interestingly, dendritic spine dysgenesis has been observed in a number of autism-related disorders, such as Fragile X syndrome, Down syndrome, and Angelman syndrome, indicating spine dysgenesis could be a convergent mechanism for intellectual disability(Phillips and Pozzo-Miller, 2015).

1.2 RTT genetics

Dominant occurrence of RTT in females strongly indicates that RTT results from mutations in X-linked genes, and hemizygous male cannot survive(Hagberg et al., 1983; Zoghbi, 1988). Traditional linkage analysis, however, is challenging because more than 99% of RTT cases are sporadic. Nevertheless, exclusion mapping was performed on rare familial cases and successfully identified Xq28 as the candidate region. Subsequent systematic gene screening approach identified *MECP2* gene as the causative locus(Amir et al., 1999). More than 95% RTT cases have mutation in the *MECP2* gene, and most of the mutations are de novo mutations of paternal origin(Trappe et al., 2001).

1.2.1 The *MECP2* gene: structure and transcription

The *MECP2* locus spans 76kb in the human Xq28 region(Quaderi et al., 1994). It has four exons and has an exceptionally 8.5kb long 3' untranslated region (UTR)(Reichwald et al., 2000). Depending on the alternative usage of the polyadenylation signal in the 3'UTR, the *MECP2* gene can generate three transcripts with differential length (1.8, ~7.5kb and ~10kb)(Balmer et al., 2003; Coy et al., 1999). The longest isoform (~10kb) is predominantly expressed in the fetal brain and is subjected to miR-483-5p-mediated repression(Han et al., 2013). Consequently, MeCP2 has a low expression level during embryonic development.

1.2.2 The MeCP2 protein

1.2.2.1 Isoforms and expression

Tow MeCP2 protein isoforms have been reported, MeCP2e1 and MeCP2e2. The MeCP2e1 isoform is translated from an mRNA containing all four exons; the MeCP2e2 is a product of *Mecp2* mRNA containing exon 1, 3 and 4 (Mnatzakanian et al., 2004). Although *Mecp2e1* mRNA is longer, translation starts at exon2 instead of exon1, and therefore MeCP2e1 has a slightly shorter N-terminal than MeCP2e2(Kriaucionis and Bird, 2004). The two MeCP2 isoforms display distinct tissue-specific expression pattern. MeCP2e2 is abundantly expressed in the brain; MeCP2e1 is more prevalent in in placenta, liver, and skeletal muscle(Itoh et al., 2012; Kriaucionis and Bird, 2004). Consistently, specific loss of MeCP2e1 does not cause RTT syndrome but results in defects in the development of extraembryonic tissue (Itoh et al., 2012).

The MeCP2 protein is expressed at a low level during embryonic development and increases during early postnatal brain development (Kishi and Macklis, 2004). In the central nervous system (CNS), MeCP2 is most abundantly expressed in postmitotic neurons. Low level of MeCP2 is present in glial cells, including astrocytes, microglia, and oligodendrocytes (Ballas et al., 2009; Maezawa and Jin, 2010; Maezawa et al., 2009).

1.2.2.2 MeCP2 functional domains

Several functional domains in MeCP2 protein have been characterized, including methyl-DNA-binding domain (MBD, amino acid 78-163) (Nan et al., 1993), transcriptional repression domain (TRD, amino acid 205-310) (Nan et al., 1997), the nuclear localization signal (NLS, amino acid 173-193 and 255-271) (Nan et al., 1996), and the carboxyl terminal domain (CTD, amino acid

380-492) (Chandler et al., 1999). MeCP2 binding to methylated DNA is dependent on MBD. The discovery of MBD established MeCP2 as the founding member of the MBD protein family. Recently, MeCP2 was shown to be able to bind 5-hydroxymethylcytosine (5hmC) through the MBD domain(Mellen et al., 2012). Interestingly, $MeCP2^{R133C}$ specifically abolishes the capability of binding to 5hmC but not 5mC(Mellen et al., 2012), suggesting the residues on MBD for binding to 5hmC might differ from those required for binding to 5mC. TRD is able to induce transcriptional repression in a reporter assay(Nan et al., 1997). TRD does not process enzymatic activity but instead assemble a repressor complex by binding to transcriptional co-repressors, mSin3a and histone deacetylases (HDACs). This repressor complex induces chromatin compaction by modifying the histone tail and leads to a repressive chromatin environment(Jones et al., 1998; Nan et al., 1997). The NLS is responsible for importing MeCP2 into the nucleus, where most of its functions are executed. The CTD in MeCP2 is thought to be important in mediates oligomerization of nucleosome arrays and chromatin compaction(Nikitina et al., 2007). Recently, three AT-hook domains (amino acids 185–194; 265–272; 31-364) were found in MeCP2 that align well with protein in the high-mobility group AT-hook (HMGA) family. AT-hook is responsible for binding to AT-rich DNA. Disruption of one of the AT-hook domain, amino acids 265-272, abolishes the ability to facilitate nucleosome oligomerization *in vitro*(Baker et al., 2013).

1.2.3 Causative mutations

1.2.3.1 Mode of causative mutations

MeCP2 mutations are primarily originated from paternal *de novo* mutations in the germline, leading to high percentage of RTT cases being sporadic and high female/male ratio in RTT

patients(Trappe et al., 2001). The predominance of paternal *de novo* mutations has been attributed to the hypermutability of some CpG sites in the male germ cells, but the underlying mechanism is still not clear. Rare familial cases have been reported and are usually due to inheritance from a carrier mother. Although most RTT patients are heterozygous females, some hemizygous male patients have been described. Hemizygous RTT males tend to have more severe syndromes and die quickly after birth.

1.2.3.2 Effect of XCI in disease presentation

Mecp2 is a X-linked gene; the allelic expression of *Mecp2* is subjected to X chromosome inactivation (XCI). Because most RTT female patients are heterozygous, X chromosome random inactivation results in somatic mosaicism throughout the body. Depending on the pattern of the X inactivation, the severity of syndromes varies from patient to patient. In some extreme cases, a carrier female with skewed X inactivation will not be diagnosed as a RTT patient because of favored inactivation of the mutant X chromosome(Amir and Zoghbi, 2000). Such RTT females can only be inferred from their children with RTT phenotypes.

1.2.3.3 Type and severity of mutations

Over 800 different types of mutations have been observed, including missense mutation, nonsense mutation, deletion, insertion, and large chromosomal rearrangement (RettBASE: RettSyndrome.org). Although RTT mutations span the whole gene, several types of mutation seem to be over-represented in RTT patients. Eight frequent mutations, including four missense mutations (R106W, R133C, T158M, and R306C) and four nonsense mutations (R168X, R255X, R270X, and R294X), account for over 65% of all classic RTT cases(Calfa et al., 2011). Deletion

is another over-represented type of mutation in RTT patients, causing over 15% of all cases(Calfa et al., 2011).

Efforts to establish relationship between genotype and phenotype in RTT female patients have generated conflicting results. But some patterns can be seen when comparing specific mutations. Mutations that result in early truncation of the proteins tend to have more severe phenotypes than those localized toward the C-terminal domain(Calfa et al., 2011). For example, patients with R168X mutations usually have more severe syndrome than those carrying R294X and small deletions in the C-terminal domain(Neul et al., 2008). Missense mutations also exhibit positional preference. A large proportion of missense mutations clusters on two region of the MeCP2 protein, one in MBD and the other in TRD, emphasizing the importance of these two functional domains(Lyst et al., 2013). The severity of missense mutations was probably determined by the functions disrupted. Individual with R133C is usually mild in phenotype probably because R133C mutation does not affect the binding of MeCP2 to 5mC but instead abolish its capability to bind a much less frequently modified cytosine, 5hmC(Mellen et al., 2012).

1.2.4 *MECP2* duplication syndrome

Boys with duplicated genomic region spanning *MECP2* are usually autistic and display progressive neurodevelopmental syndrome(Ramocki et al., 2009). Rare triplicated *MECP2* patients have also been reported and showed more severe syndrome than *MECP2* duplication patients(del Gaudio et al., 2006).

1.3 RTT model systems

1.3.1 Mouse models

To confirm the causal relationship between loss of function of MeCP2 and RTT, and to investigate the molecular mechanism underlying RTT, two separate groups generated *Mecp2* knockout (KO) mouse. Targeted deletion of exon3 or exon3 plus part of exon4 results in null allele and recapitulates phenotypes present in RTT patients(Chen et al., 2001; Guy et al., 2001). Hemizygous male mice usually develop normally until 3-5 weeks, and then start to show typical RTT syndrome such as stereotypic hindlimb clasping, tremor, irregular breathing, and usually die prematurely at between 6-12 weeks. Anatomical dissection of brain from these mice showed substantially smaller brain size as well as reduction in neuronal cell size. Heterozygous female mice also develop symptoms, although at a late onset(Guy et al., 2001).

Besides *Mecp2* null mice, mouse lines carrying various RTT mutations have been generated. Mouse with truncation after amino acid 308 ($Mecp2^{308}$), mimicking deletions in the C-terminal domain, showed normal motor activity until 6 weeks and then undergo progressive deterioration of neurological syndromes(Shahbazian et al., 2002). $Mecp2^{308}$ mice usually survive over a year, supporting the notion that C-terminal deletion of *Mecp2* gene is a less several allele in the RTT mutation spectrum. In contrast, mouse with R168X mutations reproduces many aspects of Rett syndrome and experience early death(Lawson-Yuen et al., 2007), confirming observation in human patient that R168X is associated with severe phenotypic consequences. T158M (in some cases T158A also occurs) is a frequent RTT mutation localized in the MBD domain. $Mecp2^{T158A}$ knockin mice develop progressive neurological syndromes resembling those present in the null mice(Goffin et al., 2012). Consistent with *in vitro* observations, $MeCP2^{T158A}$ protein showed reduced binding to methylated DNA and decreased protein stability. To model a missense

mutation in the TRD, *Mecp2*^{R306C} mice were created. These mice display a number of RTT-like phenotypes probably due to disruption of interaction between MeCP2 and NcoR/SMRT co-repressor complexes(Lyst et al., 2013). To understand the phenotypic difference between R270fs and R273fs in male patients, mouse lines expressing MeCP2^{R270X} and MeCP2^{R273X}, respectively, have been generated(Baker et al., 2013). R270fs in male results in neonatal encephalopathy and death, whereas patient with similar mutation at a few amino acids away, R273fs, survived with defects. Interestingly, although both *Mecp2*^{R270X} and *Mecp2*^{G273X} mice develop RTT-like phenotypes, the onset of syndrome is strikingly different: *Mecp2*^{G273X} showing later onset and slower progression of disease syndrome. ATRX localization is disrupted in *Mecp2*^{R270X} neurons but is less significantly changed in *Mecp2*^{G273X} neurons. Mechanistically, a AT hook domain at around 270 (amino acids 257–272) is disrupted in *Mecp2*^{R270X}, but is still preserved in *Mecp2*^{G273X}, suggestive of important function of the AT hook domain.

MECP2 duplication syndrome has also been modeled in mouse by overexpressing a human MeCP2 protein in wild type mice. These mice express MeCP2 at about two fold of the wild type level and show enhanced motor and contextual learning at 10 weeks of age but start to develop RTT-like phenotypes at about 20 weeks, including seizures and hypoactivity(Collins et al., 2004). About 30% of these mice die within one year. These results confirm clinical observations that boys with duplicated genomic region spanning MECP2 show progressive neurodevelopment syndromes.

To examine the spatial and temporal requirement of MeCP2 in the brain, researchers have used Cre-loxP recombination system to generate conditional *Mecp2* KO mouse. Using a Nestin-Cre that expresses in neuronal progenitors at embryonic day 12 enables generation of mice with specific deletion of *Mecp2* in the whole brain. These mice showed a phenotype similar to that of

germline null mice, suggesting loss of MeCP2 in the brain is sufficient for the manifestation of Rett syndrome(Chen et al., 2001; Guy et al., 2001). Ca^{2+}-calmodulin-dependent protein kinase (CamK)-cre93-mediated deletion of MeCP2 specifically in postnatal forebrain neurons results in delayed onset of RTT-like phenotypes, including ataxia gait and hypoactivity(Chen et al., 2001; Gemelli et al., 2006), indicating an essential role of MeCP2 in maintaining the proper function of postmitotic neurons. Selective deletion of *Mecp2* in Single-minded homolog 1 (*Sim1)* expressing neurons in the hypothalamus mimics the abnormal stress response and aggressive social behavior observed in *Mecp2* null mice(Fyffe et al., 2008). In addition, mice with deletion of MeCP2 in Tyrosine hydroxylase (TH)-expressing dopaminergic and noradrenergic neurons are hypoactive and have reduced dopamine and norepinephrine concentration(Samaco et al., 2009). Loss of MeCP2 in PC12 ets factor 1 (PET1)-positive serotonergic neurons reduces secretion of serotonin (5-HT) and results in increased aggression and hyperactivity in mice(Samaco et al., 2009). Surprisingly, conditional knockout of *Mecp2* in *Viaat* expressing GABAergic neurons in mice displays phenotypes in resemblance with the null mutation, including repetitive behavior (overgrooming)(Chao et al., 2010). *Dlx5/6*-mediated deletion of *Mecp2* only in forebrain GABAergic neurons also reproduces many RTT-like features, such as hypoactivity(Chao et al., 2010). In summary, these results suggest an essential role of MeCP2 in maintaining the proper function of various kinds of neurons.

The Cre-loxP technology also enables examination of temporal requirement of MeCP2 in the brain. Tamoxifen-induced deletion of *Mecp2* in adult mice (more than 8-weeks old) results in development of phenotypes comparable to null mice, including abnormal gait, hindlimb clasping, impaired motor activity, and premature death(McGraw et al., 2011). Another study compared inactivation of MeCP2 in three different time points, 3, 11, and 20 weeks of age and showed that

these treatments all led to RTT-like phenotypes and premature death regardless of age of onset(Cheval et al., 2012). In the other hand, re-expression of *Mecp2* in syndromatic mice mitigates the syndromes and prevents premature death in male as well as female mice, which are more relevant to human RTT patients(Guy et al., 2007). Reactivation of *Mecp2* expression only in neurons of postnatal mice also significantly extends the lifespan of the mutant mice and delays onset of RTT phenotypes(Giacometti et al., 2007; Luikenhuis et al., 2004). Taken together, these experiments support an essential role of MeCP2 in maintaining the normal function of the brain throughout life.

The non-cell autonomous effect of astrocytes on Rett syndrome was investigated using RTT mouse model. Although astrocytes only express MeCP2 at the level of about one third of that in neurons, MeCP2 deficient astrocytes negatively influence dendritic morphology of wild type neurons, suggesting a non-cell autonomous effect of astrocyte on RTT pathology(Ballas et al., 2009). Importantly, specific reactivation of *Mecp2* in astrocytes significantly rescues many RTT phenotypes and prolongs lifespan of germline null mice(Lioy et al., 2011). In the cellular level, re-expression of *Mecp2* in mutant astrocytes rescues defects of dendritic morphology of the neurons *in vivo*.

1.3.2 Patient-specific induced pluripotent stem cells (iPSCs)

Although mouse model of Rett syndrome is useful in modeling the disease, distinct structure and cell composition in mouse brain prevents it from faithfully reproducing all aspects of Rett syndrome. Studies using human postmortem brain tissues have generated some insights for the disease pathogenesis, but tissue source is limited. Induced pluripotent stem cells (iPSCs) allow generation of human cells identical to those from Rett syndrome patients by first converting

human somatic cells into pluripotent stem cells and then differentiating these cells into disease-related cell types. The first report of modeling RTT using iPSCs came from a group at the Salk Institute in 2008. Neurons differentiated from RTT iPSCs recapitulate many aspects of cellular changes previously described in human patients and mouse models, including decreased dendritic complexity, fewer synapse, smaller soma, abnormal calcium transient, and alteration of electrophysiological properties(Marchetto et al., 2010). In addition, RTT iPSCs-derived neurons also enable evaluation of the efficacy of potential drugs(Marchetto et al., 2010), representing a valuable platform for screening drugs specifically targeting a certain cellular phenotype. Despite the promising results, the control in this study is an unaffected non-relevant subject that has a different genetic background from the patients, and usage of this control would confound the subsequent characterization of phenotypes in RTT iPSCs-derived cells. To overcome this drawback, researchers took advantage of non-random X chromosome inactivation during the reprogramming process and derived iPSCs that only differ in the status of X-inactivation being either paternal or maternal chromosome(Ananiev et al., 2011; Cheung et al., 2011). Such congenic iPSCs pairs allow more objective characterization of phenotypic changes due to mutations in the *MECP2* allele.

1.3.3 Genetically engineered human stem cell model

Recent advance in genetic engineering tools holds great promise in treating as well as modeling genetic disorders. Targeted disruption of *MECP2* locus in human embryonic stem cells has been achieved,z and neurons differentiated from these cells showed abnormalities in all aspects of cellular functions previously found in patients and primary culture cells(Li et al., 2013). The faithful recapitulation of RTT-related defects in cells with specific loss of MeCP2 function

further supports the causative relationship between loss of MeCP2 and Rett syndrome. Engineered human stem cell model represents a valuable tool to dissect molecular mechanism underlying Rett syndrome.

1.4 RTT disease mechanism

1.4.1 MeCP2 target genes

Tremendous effort has been put into identifying MeCP2 target genes because it is not only important for understanding the RTT pathology but also critical for the development of therapeutic treatments. A number of MeCP2 target genes have been studied in detail over the last two decades. Brain Derived Neurotropic Factor (BDNF) plays important roles in brain development and neuronal plasticity. Although the mRNA level of *Bdnf* is only modestly changed in MeCP2 deficient brain, the protein level is decreased to about 70% of that in wild type mice(Chang et al., 2006). Importantly, deletion of *Bdnf* in forebrain neurons of *Mecp2* null mice accelerates the disease progression, and overexpression of *Bdnf* delays the onset of RTT phenotypes, suggesting the level of BDNF modulates the RTT disease progression(Chang et al., 2006). Consistently, administration of BDNF agonist in *Mecp2* null mice prolongs lifespan and recues many aspects of RTT phenotypes, including breathing irregularity(Johnson et al., 2012; Schmid et al., 2012).

Increased anxiety response and abnormal social behaviors has been observed in the $MECP2^{Tg}$ mice. Mechanistically, doubling the MeCP2 level significantly increases the expression of neuropeptide corticotropin-releasing hormone (Crh) and G protein–coupled μ-opioid receptor MOR (Oprm1). Interestingly, genetic reduction or pharmaceutical inactivation of Crh receptor attenuates the heightened anxiety response in $MECP2^{Tg}$ mice. Similarly, genetic reduction of

Oprm1 rescues the social behavior defects in the MECP2 duplication mice. These observations suggest treatments targeting Crh and Oprm1 can be potential therapies for *MECP2* duplication syndrome(Samaco et al., 2012).

1.4.2 Molecular function of MeCP2

1.4.2.1 MeCP2 localization and function

MeCP2 was initially isolated through an affinity pull-down assay for methylated-DNA binding protein(Lewis et al., 1992; Meehan et al., 1992). The discovery of MeCP2 founded the methyl-DNA binding protein family. At the microscopic level, MeCP2 is localized in centromeric heterochromatin region where methylated CpGs are clustered(Nan et al., 1996). The binding of MeCP2 to heterochromatin is dependent on methylation and the methyl-CpG binding domain(Nan et al., 1996). In agreement with *in vitro* data, high-throughput sequencing of MeCP2 bound DNA showed that MeCP2 selectively binds to methylated CpG *in vivo* and tracks the density of methylated CpG site globally(Chen et al., 2015; Skene et al., 2010). The genome wide binding of MeCP2 is associated with repression of dispersed repetitive elements, and in MeCP2 deficient cells, expression of Line-1 retrotransposon is significantly upregulated (Muotri et al., 2010; Skene et al., 2010).

Despite the high affinity of MeCP2 binding to methylated DNA, it does not preclude its binding to unmethylated DNA. *In vitro* chromatin assembly assay showed that MeCP2 can bind to unmethylated nucleosome and mediate assembly of secondary structure chromatin independent of DNA methylation(Georgel et al., 2003; Nikitina et al., 2007). The nonspecific binding to unmethylated DNA might be mediated by the intrinsic disordered domain(Adams et al., 2007) or the A/T hook domain(Baker et al., 2013).

Cytosine methylation is traditionally thought to be restricted to CpG dinucleotide. Non-CpG (CpH, where H is A, T or C) methylation, however, was also observed in pluripotent stem cells and in the brain. Interestingly, MeCP2 can recognize and bind to both CpG and CpH methylation *in vitro* as well as in neurons(Guo et al., 2014). High-throughput sequencing also revealed that MeCP2 binding positively correlates with CpH methylation(Chen et al., 2015). In addition, CpH methylation is established during postnatal neuronal maturation, coincident with the rise of MeCP2 expression, suggesting binding of MeCP2 to CpH methylation might play an important role in postnatal brain development(Guo et al., 2014). Moreover, enriched occupancy of MeCP2 and CpH methylation was observed on genes affected by MeCP2 deficiency or overexpression, suggesting MeCP2 binds to CpH methylation to regulate gene expression(Chen et al., 2015). Lastly, a meta-analysis of transcriptional profiling across multiple brain regions in the brain revealed that MeCP2 might preferentially repressed expression of long genes(Gabel et al., 2015). Interestingly, long genes are enriched with mCA and MeCP2 binding to mCA is essential for repressing expression of long genes.

MeCP2 was also reported to bind to another type of modified cytosine, 5hmC, in the mouse brain(Mellen et al., 2012). *In vitro* assay showed that MeCP2 binds to 5hmC and 5mC at similar affinity mediated by the MBD domain. But the biochemical motif for binding to 5hmC is different from that for 5mC because a RTT mutation, R133C, affects binding to 5hmC without altering affinity to 5mC, and RTT mutations that disrupt binding to 5mC do not influence binding to 5hmC. Genome wide study showed that 5hmC is enriched in the gene body of highly expressed genes(Mellen et al., 2012; Song et al., 2011). Consistent with this observation, the binding of MeCP2 to 5hmC enhances chromatin accessibility and facilitates gene expression.

1.4.2.2 MeCP2-interacting proteins

MeCP2 recognizes and binds to methylated cytosine across the genome, and therefore MeCP2 is thought to be the interpreter of information encoded by DNA methylation. Because DNA methylation is associated with transcriptional repression, early studies focused on deciphering how MeCP2 mediates transcriptional regulation. Pull-down assay showed that MeCP2 could form a complex with transcriptional co-repressors, mSin3a and histone deacetylases (HDACs), and repress transcription by modifying chromatin structure(Jones et al., 1998; Nan et al., 1998). Besides mSin3a and HDACs, MeCP2 can physically interact with a number of co-repressors, including HP1, co-REST, Suv39h1, c-Ski, and NcoR(Agarwal et al., 2007; Kokura et al., 2001; Lunyak et al., 2002). Moreover, MeCP2 represses expression of a few imprinted genes by associating with ATRX and Cohesin(Kernohan et al., 2010).

Despite the extensive association of MeCP2 and transcriptional repressors, gene expression profiling in brain tissues failed to reveal widespread gene activation(Nuber et al., 2005; Tudor et al., 2002). MeCP2 deficiency might affect gene transcription differently in different brain regions, and analyzing gene expression changes in whole brain tissue homogenate might dilute the effect(Sugino et al., 2014). To overcome this problem, transcriptional profiling was performed in a small region of the brain, hypothalamus, of *Mecp2* null and overexpression ($MECP2^{Tg}$) mice(Chahrour et al., 2008). MeCP2 dysfunction results in misregulation of thousands of genes. Interestingly, a large number of genes altered in *Mecp2* null show opposite changes to $MECP2^{Tg}$ mice. Unexpectedly, most of the affected genes were MeCP2-activated genes, indicating that MeCP2 can function as both transcriptional repressor and activator. In support with this idea, MeCP2 interacts with a transcriptional activator, CREB1, and the MeCP2-

CREB1 complex occupies on the promoter of a MeCP2-activated target but not a repressed target(Chahrour et al., 2008).

In addition to the regulation of gene expression, MeCP2 has also implicated in the regulation of alternative splicing. The first evidence came from the discovery of interaction between MeCP2 and a RNA-binding protein, Y box-binding protein 1 (YB-1), and the MeCP2-YB-1 complex regulates alternative splicing of reporter minigenes(Young et al., 2005). In addition, alteration of alternative splicing in dozens of genes was found in the brain of a RTT mouse. Another evidence came from an integrated analysis of genome binding of MeCP2, splicing data, and patterns of methylation in a cancer cell line(Maunakea et al., 2013). DNA methylation and MeCP2 binding are significantly enriched on alternative spliced exons, and MeCP2 promotes inclusion of alternative exon by recruiting HDACs and modulating the kinetics of DNA polymerase complex II (PolII).

Recently, the finding that MeCP2 physically interacts with DiGeorge syndrome critical region 8 (DGCR8) adds regulation of microRNA biogenesis to the ever-growing list of functions of MeCP2. The association between MeCP2 and DGCR8 prevents the assembly of Drosha and DGCR8 complex and leads to suppression of nuclear microRNA biogenesis(Cheng et al., 2014b). Loss of MeCP2 in the hippocampus of mice leads to misregulation of a number of microRNAs(Cheng et al., 2014b; Urdinguio et al., 2010). miR-134, one of MeCP2 targets, regulates the protein levels of CREB, LIMK1, and Pumilio2, which are critical for dendritic growth in neurons, and the misregulation of miR-134 might mediate dendritic defects in MeCP2 deficient neurons.

1.5 MeCP2 posttranscriptional modification

1.5.1 Phosphorylation

Multiple serine and threonine residues of the MeCP2 protein can be phosphorylated in response to external stimulus such as neuronal activity or neurotrophic factors. In silent neurons, MeCP2 binds to the promoter III of BDNF gene and represses gene expression. Upon neuronal activation, MeCP2 is released from the BDNF promoter III(Martinowich et al., 2003). This process is dependent on an event of calcium influx-induced phosphorylation(Chen et al., 2003). Serine 421 is later identified as the residue required for membrane depolarization-induced phosphorylation of MeCP2(Zhou et al., 2006). The phosphor dead mutant S421A abolishes the activity-dependent induction of *Bdnf* expression, and affects dendritic growth and spine maturation in neurons. Loss of S421 phosphorylation *in vivo* results in subtle defects in synapse formation and loss of response to novel experience(Cohen et al., 2011). Interestingly, another study disrupted the activity-dependent phosphorylation of both S421 and the adjacent S424 residues, and mice with S421A;S424A mutation have enhanced synaptogenesis, LTP, and spatial memory(Li et al., 2011).

Phosphorylation at S421 on MeCP2 is also regulated by extracellular stimulus other than neuronal activity. In neural progenitor cells isolated from adult mouse hippocampus, cell cycle triggers MeCP2 S421 phosphorylation through aurora kinase B(Li et al., 2014). MeCP2 S421 phosphorylation modulates the balance of proliferation and differentiation of aNPCs through regulation of Notch signaling pathway, suggesting the stimulus-induced MeCP2 phosphorylation acts as an additional epigenetic regulatory module.

A number of other phosphorylation site for MeCP2 have also been reported(Tao et al., 2009). Interestingly, serine 80 (S80) displays an opposite phosphorylation pattern as S421(Tao et al.,

2009). S80 is phosphorylated in resting neurons and loses phosphorylation in stimulated neurons, whereas S421 is phosphorylated when neurons are activated and undergoes dephosphorylation when neurons are silent. Substitution of serine to alanine at S80 results in mice with motor defects. S80A also affects binding of MeCP2 to gene promoters and leads to misregulation of a small number of genes.

Recently, T308 site has been identified as a novel activity-dependent MeCP2 phosphorylation site(Ebert et al., 2013). Phosphorylation of T308 disrupts the interaction of MeCP2 and the nuclear receptor co-repressor (NcoR) complex and renders MeCP2 unable to repress transcription. T308A mutation in mice fails to induce the expression of a subset of activity-regulated genes and triggers the appearance of RTT-like phenotype. Taken together, phosphorylation status modulates the function of MeCP2.

1.5.2 Other posttranslational modifications

MeCP2 is also subjected to other posttranslational modification, including acetylation, Poly(ADP-ribosyl)ation and ubiquitination. Poly(ADP-ribosyl)ation of MeCP2 modulates the heterochromatin clustering ability(Becker et al., 2016). The small ubiquitin-like modifier (SUMO) can be attached to multiple lysine residues of the MeCP2 protein. SUMOylation of MeCP2 at lysine 223 is critical for association with HDAC complex and repression of gene expression(Cheng et al., 2014a). Mutation of lysine 223 affects the formation of synapse in rat hippocampus. Another study showed that lysine 412 SUMOylation is mediated by an E3 ligase PIAS1 and modulated by activity-dependent MeCP2 phosphorylation at S421 or R308(Tai et al., 2016). MeCP2 SUMOylation can be induced by NMDA, IGF-1, and CRF, suggesting the dynamic SUMOylation might mediate the integration of external stimuli and transcriptional

regulation. In support of this idea, MeCP2 SUMOylation increases *Bdnf* expression by releasing CREB from the repressor complex. Importantly, over-expression of MeCP2-SUMO fusion protein, which mimics the constitutively SUMOylated MeCP2, in the null mice rescues multiple aspects of RTT phenotypes, including abnormal social behavior, fear memory, and LTP(Tai et al., 2016).

1.6 Alternative splicing and neurological disorders

1.6.1 Alternative splicing

Pre-mRNA undergoes multiple posttranscriptional processing steps before exporting to the cytoplasm for translation. Spliceosome, which is assembled by five small nuclear ribonucleoprotein particles (snRNP) and a large number of auxiliary protein factors, recognizes the splice signals and carries out the splicing reaction to remove intron sequence between protein-coding exons(Chen and Manley, 2009). Depending on the differential combination of splice sites being recognized, certain exons can be included within or excluded from the final mature mRNA transcripts, resulting in generation of different mRNA isoforms from one single pre-mRNA. This process is termed alternative splicing or differential splicing. The different mRNA isoforms encode proteins with different amino acid sequence and often, different biological functions. In this way, alternative splicing greatly expand the proteome diversity of the cells in spite of the seemingly limited number of protein-coding genes in the human genome. Recent high-throughput sequencing data estimated that over 90% of human multi-exon genes undergo alternative splicing(Pan et al., 2008; Wang et al., 2008). More than 22,000 alternative splicing events were defined as tissue-specific, suggesting alternative splicing might play important roles in differentiation and development and might be a determinant of cell fate and

identity(Luco et al., 2011; Wang et al., 2008). Multiple modes of alternative splicing have been observed, including skipped exon (SE), mutually exclusive exon (MXE), retained introns (RI), alternative 5' splice site (A5SS), and alternative 3' splice site (A3SS). SE is the most common type and the best annotated type in the genome, in which a certain exon is included in a fraction of mature transcripts of the gene and excluded in other transcripts.

1.6.2 Splicing regulation

Alternative splicing is regulated collectively by a group of trans-acting proteins and functional cis-acting sequence resided in the transcript. Cis-acting splicing motif is usually about 10nt long and is critical for assistance of accurate recognition of true splice sites. Empirical experiments coupled with computational predictions have generated a long list of cis-acting splicing enhancers or silencers(Chasin, 2007; Goren et al., 2006; Wang et al., 2012; Wang et al., 2004). Depending on the localization, these elements can be further divided into exonic splicing enhancers (ESEs), exonic splicing silencers (ESSs), intronic splicing enhancers (ISEs), and intronic splicing silencers (ISSs). These cis-acting elements function by recruiting tran-acting protein factors that positively or negatively interact with core spliceosome components, such as U1 or U2 snRNP. For example, ESE can recruit serine-arginine-rich (SR) proteins that interact favorably with snRNPs, and ESS recruits members of the heterogeneous nuclear ribo-nucleoprotein (hnRNP) family to inhibit the recognition of adjacent splice site(Han et al., 2010; Long and Caceres, 2009).

1.6.3 Epigenetic regulation of alternative splicing

Traditionally RNA posttranscriptional processing is thought to occur after the transcript is finished and released from the DNA template. Mounting evidence, however, suggests that splicing occurs cotranscriptionally; splicing machinery starts assembling even before the transcript is release from RNA polymerase II complex(Beyer and Osheim, 1988; Tennyson et al., 1995). It has been proposed that PolII C-terminal domain (CTD) can recruit splicing factors. The coupling of transcription and splicing suggests epigenetic mechanisms might be involved in the regulation of alternative splicing. Several models have been proposed. One model involves the regulation of elongation rate of the PolII complex. Fast PolII elongation exposes a strong splice site to compete for splicing factors with a weak splice site and leads to skipped usage of the weak splice site, whereas slow PolII elongation allows the splicing factor to assemble on the weak splice site before exposing the strong splice site and hence results in inclusion of the alternative exon(Luco et al., 2011). Examination of the inclusion of cassette exon 33 of the human *FN* gene revealed that inhibition of elongation rate or a slow mutant of PolII leads to increased E33 inclusion, supporting that PolII kinetics directly modulate alternative splicing(de la Mata et al., 2003; de la Mata et al., 2010; Kadener et al., 2001).

Chromatin structure is also implicated in the regulation of alternative splicing. Several *in vitro* studies on splicing of minigene reporter revealed the involvement of histone modification enzymes in the regulation of exon splicing(Auboeuf et al., 2002; Kadener et al., 2001). A chromatin-adaptor model has been proposed for the regulation of alternative splicing by histone modification marks. In polypyrimidine tract-binding protein (PTB)-dependent splicing events, H3K36me3 recruits chromatin-binding factor MRG15 that acts as an adaptor to recruit PTB to the weak splice site and promote exon skipping.

Interestingly, DNA methylation has also been reported to modulate alternative splicing. CCCTC-binding factor (CTCF) favors the inclusion of alternative exon in CD45 exon 5 by pausing the PolII(Shukla et al., 2011). Methylation on exon 5 of the CD45 gene precludes binding of CTCF and induces exon skipping. Integrated analysis of methylation and splicing data revealed enriched methylation in included exons(Chodavarapu et al., 2010) and enriched occupancy of MeCP2 in included alternative exons (Maunakea et al., 2013).

1.6.4 Splicing regulation and neurological disorder

Aberrant alternative splicing has been implicated in a number of diseases, including neurological diseases. Mutations in either cis-acting elements or trans-acting proteins could lead to splicing defects that underlie the neurological diseases. A single nucleotide substitution in the exon 7 of survival of motor neuron 2 (*SMN2*) gene results in preferential exclusion of exon7 and production of a truncated SMN2 protein that is usually inactive and unstable(Lorson et al., 1999). This substitution converts the original ESE, which facilitates the inclusion of exon7, to an ESS, which favors the exclusion of exon7 (Cartegni and Krainer, 2002; Kashima et al., 2007). Deficiency of functional SMN protein caused by loss of function of SMN2 and deletions in the SMN1 gene triggers the appearance of spinal muscular atrophy (SMA), a fatal motor neuron degenerative disorder. A large number of synonymous mutations have been identified in patients with genetic disorders. For a long time, the functional implications of these silent mutations are unknown. Using the cystic fibrosis transmembrane conductance regulator (CFTR) exon 12 as a model, it was estimated at lease one quarter of synonymous mutations disrupt splicing and cause frequent skipping of the exon(Pagani et al., 2005).

The expression level and localization of trans-acting splicing factors are critical for regulation of alternative splicing. Cytoplasmic aggregates of TDP-43 are found in the brain of affected individuals with fronto-temporal dementia (FTD), Alzheimer's disease, and amyotrophic lateral sclerosis (ALS)(Ule, 2008). TDP-43 is an hnRNP A-like splicing regulator, and mutations in the *TARDBP* gene that encodes TDP-43 have been causally linked with sporadic and familial cases of ALS and in rare cases of FTD(Daoud et al., 2009; Kabashi et al., 2008). Consistently, Deletion of *Tardbp* in the mouse brain causes aberrant splicing in hundreds of RNA transcripts(Polymenidou et al., 2011). But it still remained elusive whether loss of TDP-43 in the nucleus or the gain-of-function of TDP-43 aggregates or both mediates the pathological effects in related diseases.

Chapter 2: Systematic identification of MeCP2-interacting proteins in the mouse brain

2.1 Introduction

It has been estimated that over 80% of proteins do not act alone but form protein complexes to perform biological functions(Phizicky and Fields, 1995). Proteins participated in the same biological processes are often interacting with each other(von Mering et al., 2002). Therefore, one can infer the potential functions of a protein from its interaction with other proteins, whose functions are known. Many proteins have been identified to physically interact with MeCP2. Based on the known functions of identified MeCP2-interacting proteins, previous studies have suggested a role for MeCP2 in maintaining DNA methylation(Kimura and Shiota, 2003), regulating transcription(Chahrour et al., 2008; Forlani et al., 2010; Kokura et al., 2001; Lunyak et al., 2002; Lyst et al., 2013), chromatin structure(Agarwal et al., 2007; Fuks et al., 2003; Jones et al., 1998; Kernohan et al., 2010; Nan et al., 2007; von Mering et al., 2002), and RNA processing(Cheng et al., 2014b; Long et al., 2011; Young et al., 2005). These results greatly advance our understanding of the molecular functions of MeCP2, but it is unlikely that all the MeCP2-involved biological functions are revealed.

To identify novel functions of MeCP2, researchers have used several systematic approaches to screen for MeCP2-interacting proteins. Yeast two-hybrid (Y2H) screening is an *in vivo* method to detect protein-protein interaction: two candidate proteins are fused to a DNA-binding domain (DBD) and an activation domain (AD), respectively, and if they interact with each other, DBD and AD join together and activate the expression of a reporter gene. So far two studies had performed Y2H screening to systematically identify MeCP2-interacting proteins. One study used the N-terminal half of the e2 isoform of rat MeCP2 (amino acids 1–206) as bait to screen a human fetal brain library and successfully identified ATRX as a novel MeCP2-interacting

protein(Nan et al., 2007). In another study, researchers used transcriptional repression domain (TRD) and the upstream linker region of MeCP2 fused to the GAL4 DNA-binding domain (DBD-linkTRD) as bait and discovered homeodomain-interacting protein kinase 2 (HIPK2) as a novel MeCP2-interacting kinase, which phosphorylates MeCP2 at Serine 80(Bracaglia et al., 2009). Despite these successes, neither of these studies disclosed the validation rate of the screen, thus it is impossible to estimate the effectiveness of using Y2H, a method notoriously known for high false positive and negative discovery rate, to identify MeCP2-interacting proteins.

Co-expression analysis has also been used to screen for MeCP2-interacting proteins on the basis that proteins highly correlated in expression levels are components in the same complex. By performing co-expression analysis in two datasets, Forlani et al found that Ying Yang 1 (YY1) is the only common candidate protein that co-expresses with MeCP2. Further biochemical experiments confirmed the physical interaction between MeCP2 and YY1, and the regulation of ANT1 expression by MeCP2/YY1 complex(Forlani et al., 2010).

Co-immunoprecipitation is a gold standard assay for detecting protein-protein interaction. Coupled with mass spectrometry, co-immunoprecipitation allows systematic identification of protein-protein interaction in physiological conditions. Previously our lab had created a mouse line that expresses an endogenous MeCP2-flag fusion protein by inserting a Flag sequence into the C-termal of the *Mecp2* gene (*Mecp2*-Flag). This unique tool gives us two main advantages. First, it ensures that the MeCP2-Flag protein is expressed at the physiological level, so that non-specific protein-protein interactions caused by the overexpression of MeCP2-Flag is minimized. Second, it allows us to use a highly efficient anti-Flag antibody in the co-immunoprecipitation. The choice of antibody is not a trivial issue, because in the past, different anti-MeCP2 antibodies

in co-immunoprecipitation experiments have generated conflicting results in the identification of MeCP2-interacting proteins(Harikrishnan et al., 2005; Hu et al., 2006).

Here we report a systematic identification of MeCP2-interacting protein using co-immunoprecipitation and mass spectrometry. In addition to proteins previously known for interacting with MeCP2, we identified a number of novel candidates that are enriched with proteins involved in the regulation of alternative splicing. Although the screening was performed in mouse brain, we found that MeCP2 also interact with splicing regulators in human neural progenitor cells differentiated from embryonic stem cells. Moreover, the interaction between MeCP2 and two of these splicing regulators, LEDGF and DHX9, relies on the existence of the transcriptional repression domain; Rett syndrome mutations within TRD disrupt interaction with LEDGF or DHX9. Lastly, phosphorylation status at MeCP2 S421 does not affect the interaction with splicing factors.

2.2 Results

2.2.1 Co-immunoprecipitation optimization

MeCP2 is highly abundant in the brain and can be easily detected in brain lysate using an ionic detergent-containing buffer such as RIPA buffer. But SDS in RIPA buffer disrupts antigen-antibody interaction and is not compatible with co-immunoprecipitation. Generally, non-ionic detergent such as NP-40 is used to replace SDS for co-immunoprecipitation, but the amount of MeCP2 isolated under this condition was beyond the detection limit of Western blot (**Fig 1a, left panel**). To enhance the MeCP2 signal, we tested the effect of extracting nuclear fraction because MeCP2 is a nuclear protein. Nuclei were purified from whole mouse brain and lysed by sonication. We observed that nuclear extract did show stronger MeCP2 signal than whole cell

lysate (**Fig 1a**). To further optimize the procedure of nuclei extraction from mouse brain, we tested the effect of supplementing different concentration of NP-40 in the lysis buffer in the yield of nuclei number. We found that 0.2% and 0.5% NP-40 yielded similar nuclei number (**Fig 1b**); therefore, we stick to 0.2% NP-40 in all subsequent experiments.

One reason that direct lysis of brain tissue cannot produce high MeCP2-containing lysate is that mild non-ionic detergent fail to release MeCP2 from methylated DNA because of the high binding affinity. To further increase MeCP2 yield in the lysate, we supplemented Benzonase, which can digest both DNA and RNA efficiently, during lysis of nuclei and found that MeCP2 was significantly increased (**Fig 1c**).

In order to identify specific MeCP2-interacting protein, it is critical to optimize the wash conditions for the co-immunoprecipitation procedure. To that end, third wash and sixth wash was collected, resolved into a SDS-PAGE gel, and stained with silver. Although detectable amount of protein was observed in the third wash, almost nothing was retained in the sixth wash (**Fig 1d**).

Although traditional SDS-containing loading buffer can efficiently elute protein from beads, it is not compatible with downstream mass spectrometry analysis because IgG would be eluted and interfere with mass spectrometry analysis. Therefore, we tested using free Flag peptide to elute proteins from beads by saturating the binding capability of the antibody. We found that most of proteins can be released from beads by incubating with 100ug/ml of Flag peptide and only trace amount of protein was remained, which was subsequently eluted by adding LDS loading buffer (**Fig 1e**). Importantly, IgG heavy chain is not detected in flag eluate.

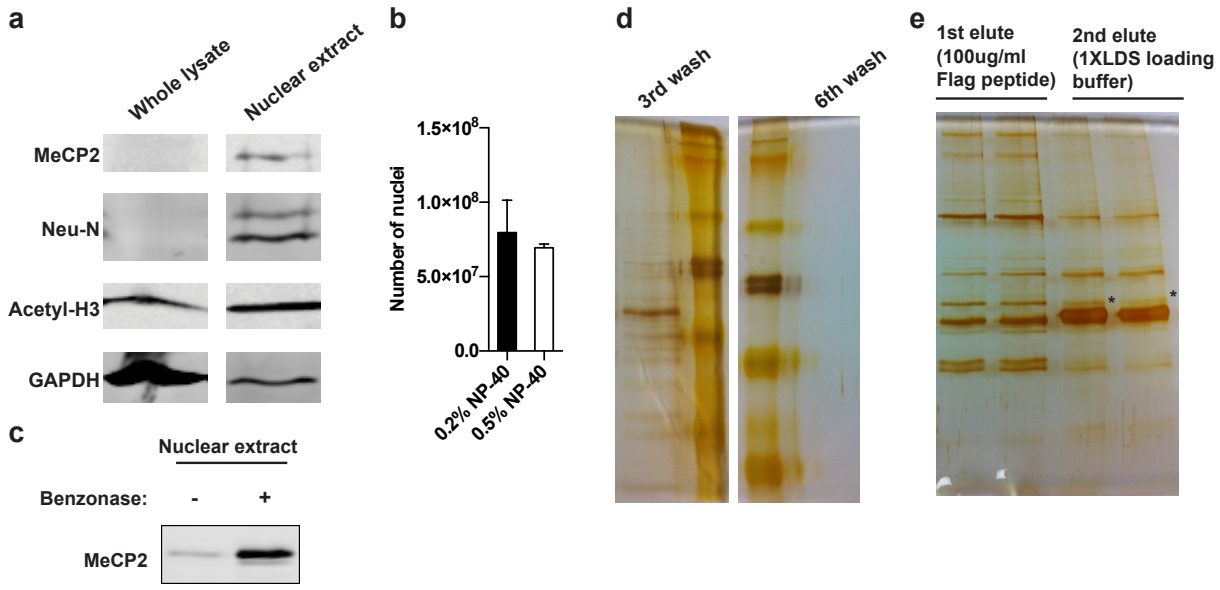

Fig 1. Optimization of co-immunoprecipitation conditions.

(a) Western blot analysis of MeCP2, Neu-N, Acetyle-H3 and GAPDH in whole brain lysate (left lane) and nuclear extract from brain (right lane). Neu-N and Acetyl-H3 is nuclear marker; GAPDH is a cytoplasmic marker.

(b) Average number of nuclei from one mouse brain using lysis buffer containing indicated percentage of NP-40. n=3 for 0.2% NP-40 group, n=2 for 0.5% NP-40 group.

(c) Western blot analysis of MeCP2 in nuclear extract pre-treated with or without Benzonase.

(d) Silver staining of xth wash resolved in SDS-PAGE.

(e) Silver staining of eluted proteins using different methods. * indicates IgG heavy chain.

2.2.2 Co-immunoprecipitation and mass spectrometry

To facilitate identification of MeCP2 interacting proteins in the mouse brain, we generated the *Mecp2-Flag* knockin mouse line that expresses Flag-tagged wild-type MeCP2 from the endogenous locus. We purified nuclei from the brains of male *Mecp2-Flag* mice, prepared nuclear extract, and performed co-immunoprecipitation (co-IP) using the anti-Flag antibody. Eluted protein sample was then subjected to protein identification by mass spectrometry. Fourty-eight proteins were identified using highly stringent statistical filters (**Table 1**). Identified proteins included previously known MeCP2-interacting transcriptional regulators and chromatin remodeling proteins, such as HDAC1 and components of the SWI/SNF complex(Harikrishnan et al., 2005; Jones et al., 1998; Nan et al., 1998). Consistently, gene ontology analysis showed that proteins identified by co-IP/MS were enriched with GO terms of chromatin organization, chromatin modification and regulation of transcription. Interestingly, these proteins were also enriched for RNA splicing (**Fig 2a**).

Table 1. MeCP2-interacting proteins identified by co-immunoprecipitation and mass spectrometry

Protein	Spectral count	No. of unique peptides	Protein	Spectral count	No. of unique peptides
53BP1	3	3	LAP2B	1	1
CA077	1	1	LEDGF	6	5
CaMK2A	3	3	MATR3	3	2
CaMK2B	1	1	MBD2	1	1
CaMK2D	1	1	MBD3	1	1
CAMK2G	1	1	NEUA	1	1
CDK7	1	1	NPM1	3	2
CSK2B	1	1	p66B	1	1
DDX5	1	1	PRPF19	1	1
DHX9	1	1	PURA	1	1
eIF5b	1	1	RbAp48	1	1
FUS	1	1	SAFB2	1	1
HDAC1	1	1	SAP18	1	1
HDGR3	5	3	SMARCA2	1	1
hnRNPC	2	1	SMARCA4	2	2
hnRNPF	2	2	SMARCC2	1	1
hnRNPH1	3	3	SMARCD1	1	1
hnRNPH2	3	3	SMARCD2	1	1
hnRNPM	2	1	SMARCD3	1	1
hnRNPUL2	7	6	SMC1A	2	2
HP1α	2	2	SMC3	1	1
HP1β	1	1	SmD3	1	1
HP1γ	3	3	TDP-43	2	1
LAP2A	1	1	TMOD3	2	2

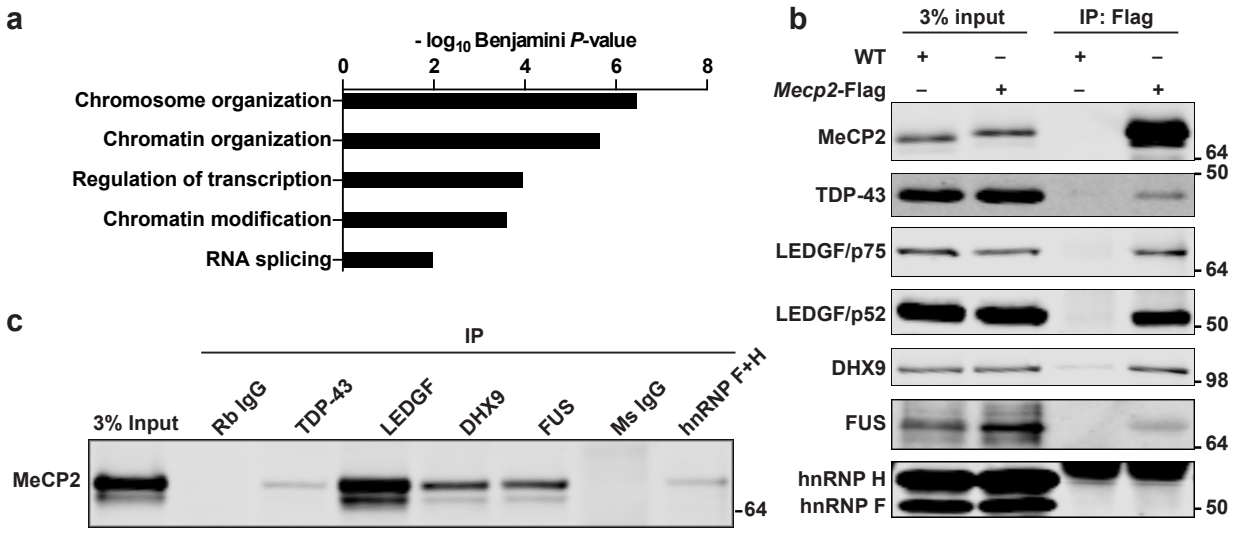

Fig 2. MeCP2 interacts with multiple splicing regulators.

(a) Gene ontology (GO) analysis of proteins identified from anti-Flag co-immunoprecipitation and mass spectrometry (Co-IP/MS) analysis in *Mecp2-Flag* knockin mouse brain. Top five GOTERM_BP_FAT terms were shown and $-\log_{10}$ Benjamini *P*-value is plotted.

(b) Western blot validation of interactions between MeCP2 and splicing regulators identified in Co-IP/MS. Anti-Flag immunoprecipitate in nuclear extract from WT and *Mecp2-Flag* knockin mouse brain is resolved in SDS-PAGE and probed with antibodies against indicated proteins.

(c) Western blot analysis of MeCP2 in anti-TDP-43, anti-LEDGF, anti-DHX9, anti-FUS and anti-hnRNP F+H immunoprecipitate. Rabbit (Rg) IgG is negative control for rabbit antibody (anti-TDP-43, LEDGF, DHX9 and FUS) and mouse (Ms) IgG is negative control for mouse antibody (anti-hnRNP F+H).

2.2.3 Validation of MeCP2-interacting proteins

To validate the physical interaction between MeCP2 and splicing factors, we performed anti-Flag co-IP in nuclear extract from the *Mecp2*-Flag knockin mouse brain and probed it with antibodies against TDP-43, LEDGF, DHX9, FUS, hnRNP H, and hnRNP F, respectively. Western blot results showed that TDP-43, LEDGF, DHX9, and FUS were co-immunoprecipitated with MeCP2, whereas hnRNP H and hnRNP F were not (**Fig 2b**). Next, we performed reverse co-IP and detected MeCP2 in immunoprecipitate of anti-TDP-43, anti-LEDGF, anti-DHX9, anti-FUS, and anti-hnRNPH+F (**Fig 2c**), further confirming that MeCP2 physically interacts with these proteins in the mouse brain. In addition, the interaction between MeCP2 and splicing factors were not sensitive to Benzonase treatment, which digest and remove all nucleic acids, suggesting that these interactions were most likely direct interactions independent of either DNA or RNA (**Fig 3**).

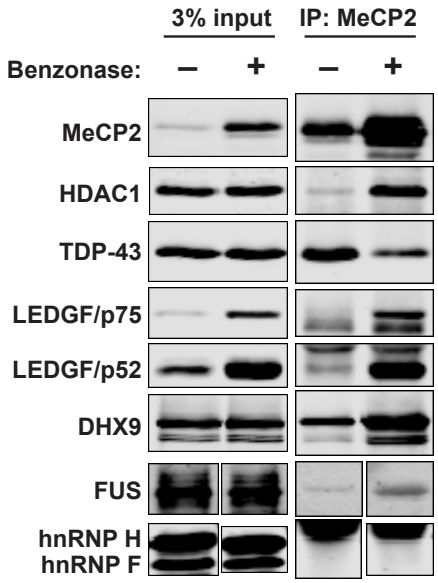

Fig 3. Interaction between MeCP2 and splicing factors is not dependent on DNA or RNA. Co-immunoprecipitation was performed in nuclear extract pretreated with or without Benzonase, which degrades nucleic acids in the lysate. Proteins were resolved in SDS-PAGE and probed with indicated antibodies. A previously known MeCP2-interacting protein, HDAC1, is shown as a control.

2.2.4 Interaction between MeCP2 and splicing factors in human neural progenitor cells

To test whether MeCP2 interacts with these novel splicing related proteins in human cells, we performed a co-immunoprecipitation in nuclear extract prepared from human neural progenitor cells derived from embryonic stem cells. Although MeCP2 is expressed at a low level in these cells, which is consistent with previous observation(Li et al., 2013), upon enrichment by co-immunoprecipitation, MeCP2 becomes detectable (**Fig 4**). Western blot analysis of immunoprecipitate showed that DHX9, TDP-43 and LEDGF can be co-purified using an anti-MeCP2 antibody but not an anti-IgG, supporting that DHX9, TDP-43 and LEDGF physically interact with MeCP2 in human neural progenitor cells.

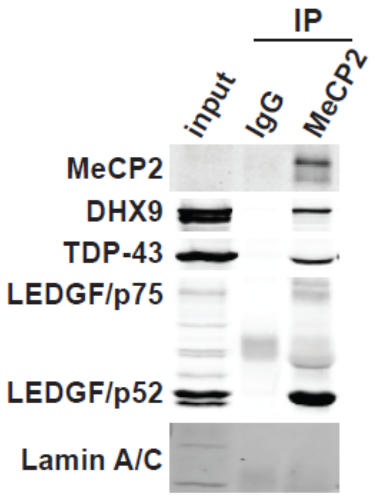

Fig 4. MeCP2 interacts with splicing regulators in human neural progenitors.

MeCP2 immunoprecipitate in neural progenitors derived from human embryonic stem cells was resolved in SDS-PAGE and probed with indicated antibody. Lamin A/C is used as a negative control.

2.2.5 Essential domain in MeCP2 for interaction with splicing factors

2.2.5.1 TRD domain is required for interaction of MeCP2 and splicing factors

The interaction between MeCP2 and LEDGF has been previously reported in cancer cells(Leoh et al., 2012), but not in the brain. MeCP2 interacts with the N-terminal PWWP-CR1 domain of LEDGF, but which domain of MeCP2 that LEDGF binds to is not defined. DHX9 has recently been revealed as an interacting partner of MeCP2(Maxwell et al., 2013), but the interaction domain is not known either. To examine which domain of MeCP2 is required for interaction with LEDGF and DHX9, we expressed HA-tagged MeCP2 with different deletions (**Fig 5a**) and Myc-tagged full-length LEDGF/p52, LEDGF/p75 and DHX9, respectively, in HEK293 cells. Co-IP with anti-HA antibody followed by Western blot with anti-Myc antibody showed that deletion of amino acids 163-380 of the MeCP2 protein completely abolished the interaction between MeCP2 and LEDGF/p52, LEDGF/p75, or DHX9 (**Fig 5b-c; Fig 6a**). Reverse co-IP with anti-Myc antibody followed by Western blot with anti-HA antibody also demonstrated that amino acids 163-380 of the MeCP2 protein was required for interaction between MeCP2 and LEDGF/p52 (**Fig 6b**). Collectively, these results strongly suggested that the transcription repression domain (TRD) of MeCP2 is essential for the interaction of MeCP2 with RNA binding proteins.

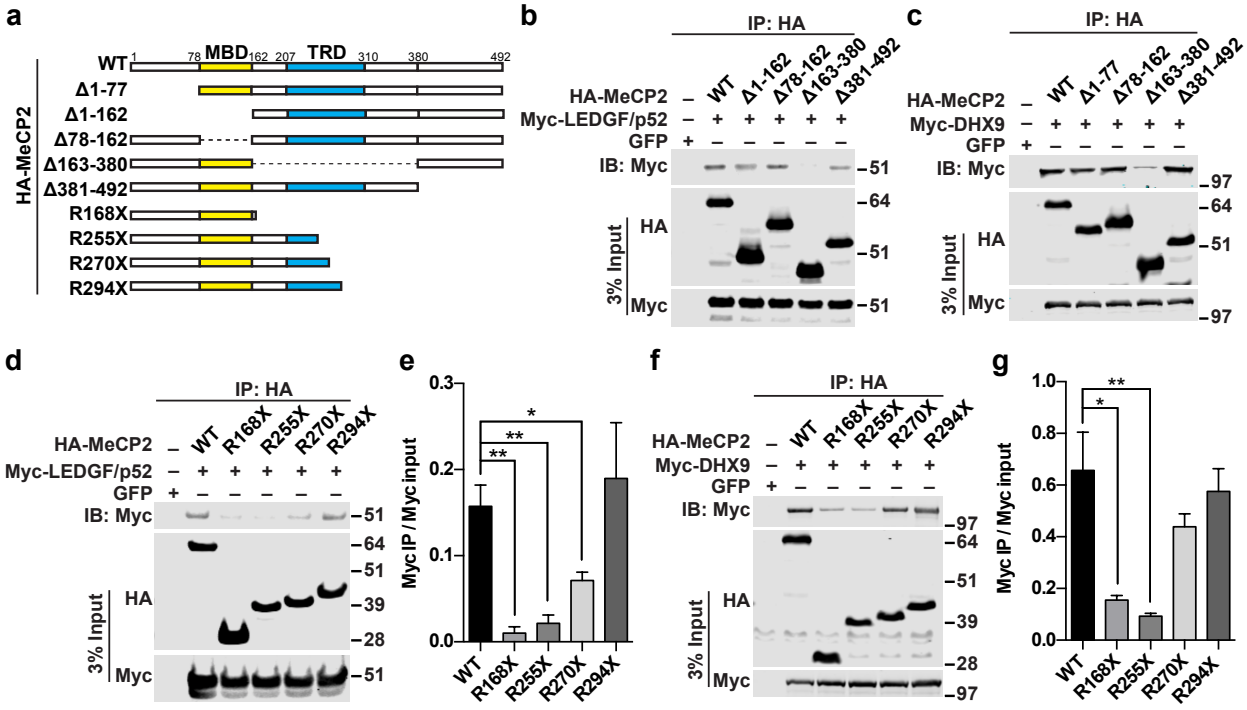

Fig 5. RTT mutations disrupt MeCP2 interaction with LEDGF and DHX9.

(a) Schematic diagram of HA-MeCP2 constructs used in this study. The methyl-CpG-binding domain (MBD) domain is shown in yellow and the transcription repression domain (TRD) in blue.

(b) Western blot analysis of Myc-LEDGF/p52 in anti-HA immunoprecipitate (top panel) from cells transfected with different combinations of plasmids as labeled on top. HA-MeCP2 (middle panel) and Myc-LEDGF/p52 (bottom panel) in input were also analyzed by Western blot.

(c) Western blot analysis of Myc-DHX9 in anti-HA immunoprecipitate (top panel) from cells transfected with different combinations of plasmids as labeled on top. HA-MeCP2 (middle panel) and Myc-DHX9 (bottom panel) in input were also analyzed by Western blot.

(d) Representative Western blot analysis of Myc-LEDGF/p52 in HA immunoprecipitate (top panel) from cells transfected with different combinations of plasmids as labeled on top. HA-

MeCP2 (middle panel) and Myc-LEDGF/p52 (bottom panel) in input were also analyzed by Western blot.

(e) Quantification of Myc-LEDGF/p52 IP over input signal intensity of three independent experiments. Error bar represents S.E.M; $**P < 0.01$, $*P < 0.05$; two-tailed *t*-test.

(f) Representative Western blot analysis of Myc-DHX9 in HA immunoprecipitate (top panel) from cells transfected with different combinations of plasmids as labeled on top. HA-MeCP2 (middle panel) and Myc-DHX9 (bottom panel) in input were also analyzed by Western blot.

(g) Quantification of Myc-DHX9 IP over input signal intensity of four independent experiments. Error bar represents S.E.M; $**P < 0.01$, $*P < 0.05$; two-tailed *t*-test.

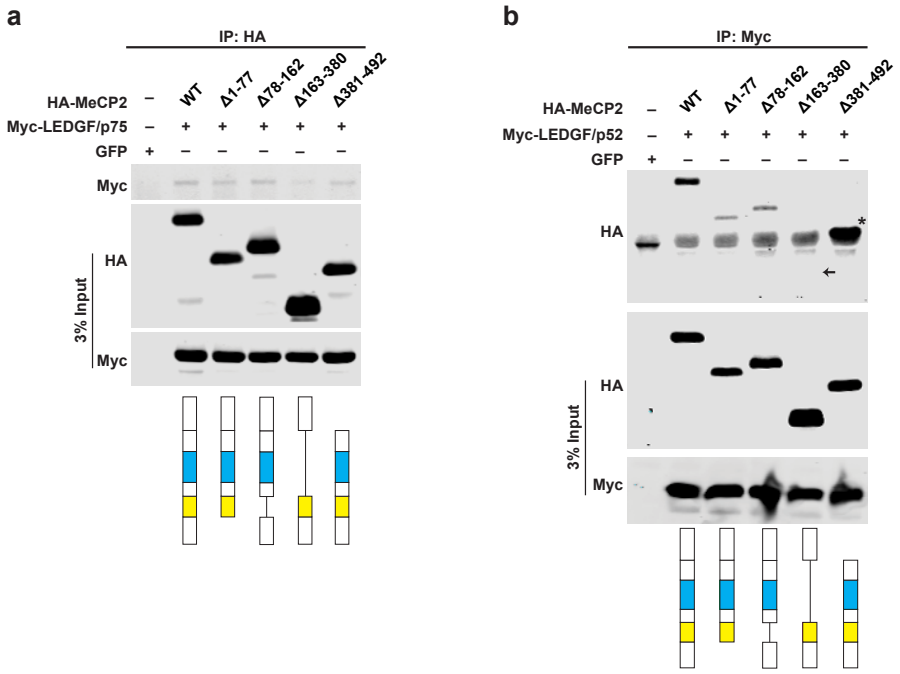

Fig 6. Deletion of amino acids 163-380 in MeCP2 disrupted interaction with LEDGF.

(a) Western blot analysis of Myc-LEDGF/p75 in anti-HA Immunoprecipitate. HA-MeCP2 and Myc-LEDGF/p75 were co-transfected into HEK293 cells. Anti-HA immunoprecipitate was resolved in SDS-PAGE and probed with anti-Myc antibody (Top panel). HA-MeCP2 (middle panel) and Myc-LEDGF/p52 (bottom panel) in input were also analyzed by Western blot. Schematics below blots show the configuration of each MeCP2 deletion construct.

(b) Western blot analysis of HA-MeCP2 in anti-Myc immunoprecipitate. HA-MeCP2 and Myc-LEDGF/p52 were co-transfected into HEK293 cells. Anti-Myc immunoprecipitate was resolved in SDS-PAGE and probed with anti-HA antibody (Top panel). HA-MeCP2 (middle panel) and Myc-LEDGF/p52 (bottom panel) in input were also analyzed by Western blot. Arrow indicates where MeCP2$^{\Delta 163\text{-}380}$ band would be if there is one. Star indicates the MeCP2$^{\Delta 381\text{-}492}$ band overlapping with IgG. Schematics below blots show the configuration of each MeCP2 deletion construct.

2.2.5.2 RTT mutations disrupt interactions between MeCP2 and LEDGF or DHX9

Several RTT disease causing mutations in the region of amino acids 163-380 (R168X, R255X, R270X and R294X) may disrupt the TRD domain; we asked whether these mutations affect the interaction between MeCP2 and LEDGF or DHX9. To test this, we co-transfected MeCP2 construct encoding MeCP2 WT, MeCP2^{R168X}, MeCP2^{R255X}, MeCP2^{R270X}, and MeCP2^{R294X}, respectively, with LEDGF/p52 or DHX9 in HEK293 cells. Co-IP assay showed that interaction between LEDGF/p52 and MeCP2^{R168X}, MeCP2^{R255X}, and MeCP2^{R270X} was significantly impaired (**Fig 5d-e**). Interestingly, the interaction between MeCP2^{R294X} (retaining a large fraction of TRD) and LEDGF/p52 was not significantly different from that between wild type MeCP2 and LEDGF/p52, suggesting that amino acids 270-294 of MeCP2 are required for its binding to LEDGF/p52 (**Fig 5d-e**). Similarly, we found that MeCP2^{R168X} and MeCP2^{R255X} interacted poorly with DHX9, but MeCP2^{R270X} and MeCP2^{R294X} had intact binding capability, indicating that amino acids 255-270 of MeCP2 are required for its binding to DHX9 (**Fig 5f-g**).

2.2.6 MeCP2 phosphorylation does not influence interaction with splicing factors

Previous studies showed that MeCP2 phosphorylation modulates protein-protein interaction with chromatin factors HP1, SMC3, the cofactors Sin3A, RNA-binding factor YB-1 and microRNA processor DGCR8(Cheng et al., 2014b; Gonzales et al., 2012). To test whether neuronal activity-induced phosphorylation modulates interaction between MeCP2 and splicing factors, we injected mice with kainic acid (KA) to induce seizure and performed co-immunoprecipitation with an anti-MeCP2 antibody. Western blot analysis showed that although KA treatment drastically increases MeCP2 S421 phosphorylation in wild type animal, it does not alter the protein level of

MeCP2, DHX9, TDP-43 and LEDGF in the input, nor does it change the amount of DHX9, TDP-43 and LEDGF co-immunoprecipitated with MeCP2 (**Fig 7a-b**).

Kainic acid might induce phosphorylation changes in multiple residues of MeCP2 and the combinatorial phosphorylation changes might confound the effect of some phosphorylation events modulating protein-protein interaction. To that end, we tested the interaction between a phosphor dead mutant at S421 and S424 residues ($MeCP2^{S421A;S424A}$) or a phosphor mimic mutant at S421 ($MeCP2^{S421E}$) and splicing factors. Co-immunoprecipitation followed by Western blot analysis showed that $MeCP2^{S421A;S424A}$ or $MeCP2^{S421E}$ interacts with DHX9, TDP-43 and LEDGF similarly to wild type MeCP2, suggesting S421 phosphorylation status does not modulates interaction with splicing factors.

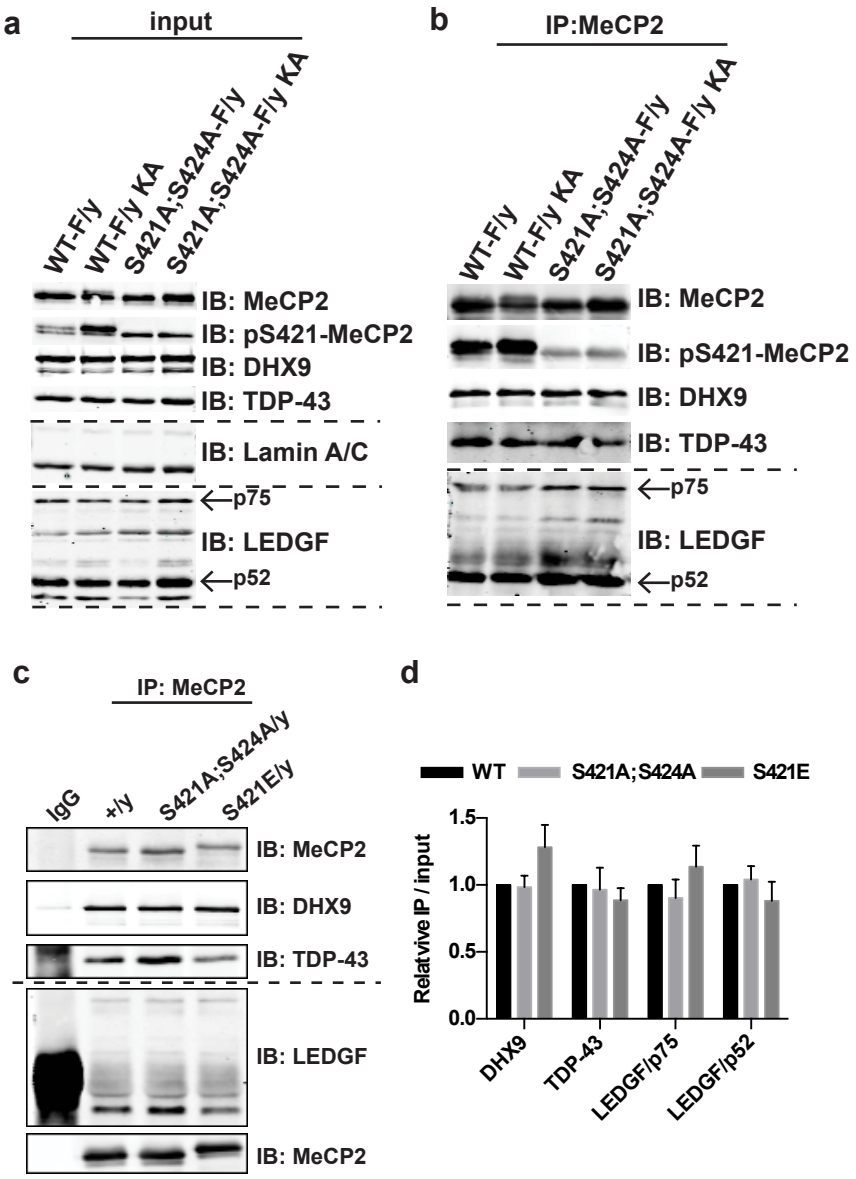

Fig 7. MeCP2 phosphorylation at S421 does not affect its interaction with splicing factors.

(a) Protein level of DHX9, TDP-43 and LEDGF is not altered upon kainate acid (KA)-induced MeCP2 S421 phosphorylation. S421A;S424A/y mice is used as negative control for KA-induced phosphorylation.

(b) MeCP2 S421 phosphorylation does not influence its interaction with DHX9, TDP-43 and LEDGF.

(c) Representative Western blot analysis of MeCP2 immunoprecipitate from WT (+/y), *Mecp2*$^{S421A;S424A/y}$ and *Mecp2*$^{S421E/y}$ mouse.

(d) Quantification of IP/input ratio from four independent experiments as (c).

2.3 Discussion

Using a unique *Mecp2-Flag* knockin mouse line, we performed co-immunoprecipitation and mass spectrometry to systematically screen for MeCP2-interacting proteins and successfully identified a number of novel candidate partners. Although many MeCP2-interacting proteins had been discovered before we set out to perform the systematic screening, the identification of multiple novel interacting proteins in this study suggested that the full map of MeCP2 protein-protein interaction is far from being complete. Future efforts are needed to expand the list of proteins that MeCP2 interact *in vivo*.

While this study was going on, another group performed a similar assay to systematically identified potential MeCP2-interacting protein. They took advantage of a *Mecp2-EGFP* knock-in mouse line and performed co-immunoprecitation using an efficient anti-GFP antibody(Lyst et al., 2013). Mass spectrometry analysis of proteins co-purified with MeCP2-EGFP identified several components of the NcoR/SMRT co-repressor complex, including NCoR1, SMRT, TBL1, TBLR1, and HDAC3. Although NCoR1 and HDAC3 have previously been identified as MeCP2-associated proteins, this study was the first to show that MeCP2 R306C mutation abolishes the interaction with NcoR/SMRT complex, which might underlie the RTT-like phenotypes in *Mecp2*$^{R306C/y}$ mice. Note that the protein list from our study and Lyst et al., 2013, do not have any overlap; this difference could be due to the different mouse line used and other experimental conditions. But it is also possible that Lyst et al., 2013, did not provide a full list of proteins identified by mass spectrometry. Nevertheless, Lyst et al., 2013, and our study demonstrated the usefulness of co-immunoprecipitation and mass spectrometry in the identification of novel MeCP2-interacting proteins.

Although MeCP2 has been previously implicated in the regulation of alternative splicing, only two splicing factors were identified as MeCP2-interacting protein(Long et al., 2011; Young et al., 2005). Our co-immunoprecipitation and mass spectrometry screening greatly substantiated the involvement of MeCP2 in alternative splicing by revealing that MeCP2 interacts with multiple splicing factors. But how the MeCP2 and splicing factor complex regulates alternative splicing is still unclear and worth of further examination.

Understanding the regulation of protein-protein interaction is important for interpreting the behavior of the protein complex and developing methods to modulate the interaction. In response to external stimuli, posttranscriptional modification occurs on MeCP2 and modulates its ability to bind to chromatin or other protein partners. Although our results showed that the interaction between MeCP2 and LEDGF, DHX9, or TDP-43 is not modulated by KA treatment or phosphorylation status on S421, it does not preclude that other posttranscriptional events influences the interaction. Perhaps we could use a peptide array to systematically identify posttranscriptional events that affect interaction between MeCP2 and splicing factors in the future(Nady et al., 2008).

2.4 Materials and Methods

2.4.1 Animals

All animal procedures were performed according to protocols approved by the Institutional Animal Care and Use Committee at the University of Wisconsin-Madison. The *Mecp2*-Flag mice have a Flag sequence inserted intermediately before the stop codon of the *Mecp2* locus(Robinson et al., 2010). Mice were housed in a facility with 12-hr light/12-hr dark cycle.

2.4.2 Plasmids

pRK5-HA-MeCP2-WT, Δ1-77, Δ1-162, Δ78-162 and Δ381-492 were a gift from Dr. Zilong Qiu(Cheng et al., 2014b). DNA encoding Δ163-380, MeCP2^{R168X}, MeCP2^{R255X}, MeCP2^{R270X} and MeCP2^{R290X} were PCR amplified and inserted into pRK5-HA by replacing the sequence between SalI site and NotI site of pRK5-HA-MeCP2 using Gibson cloning (NEB). To construct Myc-tagged protein expression plasmid, cDNA of LEDGF/p52, LEDGF/p75, and DHX9 were amplified from a mouse cortex cDNA library using a Myc sequence-containing primer and inserted into pRK5 backbone. LEDGF is also known as Psip1.

2.4.3 Co-immunoprecipitation and Mass spectrometry

Nuclei were extracted from the whole brain of WT and *Mecp2-Flag* mice as previously described(Jiang et al., 2008). Purified nuclei were resuspended in lysis buffer containing 20mM Tris, 150mM NaCl, 1.5mM $MgCl_2$, 1mM EDTA, 10% Glycerol, 0.2% NP-40 and 1X proteinase inhibitors cocktail (Roche) and sonicated using a Misonix 3000. After centrifuging at 20,000g for 20min at 4°C, supernatant was incubated with 50ul of Anti-Flag M2 Magnetic Beads (Sigma) overnight at 4°C. In the following day, beads were washed with lysis buffer for 6 times. Bound protein was eluted by competition with 100 mg/ml of Flag Peptide (Sigma F3290). Eluted proteins from 5 IPs per genotype were pooled together and precipitated by adding 8 volume of pre-chilled acetone. Pellet was resuspended in 100mM Ammonium Bicarbonate solution. After DTT and IOAA treatment, protein was digested into peptides using Trypsin Gold (Promega) and Proteinase Max (Promega) overnight at 37°C. Peptides were separated by a nano HPLC and analyzed by a Thermo LTQ mass spectrometer. MS/MS spectra data was analyzed using

Bioworks software (Thermo). Only proteins identified in Flag IP eluate from *Mecp2-Flag* mice but not WT mice were considered to be potential MeCP2-interacting proteins.

2.4.4 Co-immunoprecipitation and Western blot

Co-IP was performed as described above except using Dynabeads (Life Technologies). For co-IP with Benzonase treatment, lysate was treated with 250 Unit of Benzonase per mouse brain for 1hr at 4°C before incubating with beads. Proteins were eluted by adding 1X LDS sample buffer (Life Technologies) and heated at 95°C for 10min.

Proteins were resolved in a 10% SDS-PAGE gel and transferred into a nitrocellulose membrane. Membrane was blocked with 5% non-fat milk in PBS for 1 hour followed by incubating with primary antibody overnight at 4°C. Membrane was washed 3 times with PBST and incubated with DyLight Fluor Secondary Antibodies (Pierce) for one hour at room temperature. Membrane was imaged on a LI-COR Odyssey Imager. Western blot quantification was done using ImageJ. Primary antibodies used in this study were: anti-DHX9 (Abcam ab26271, 1:2000), anti-FLAG (Sigma M2, 1:1000), anti-FUS (Bethyl A300-293A, 1:10000), anti-HA (Covance MMS-101P, 1:5000), anti-hnRNP F+H (Abcam ab10689, 1:3000), anti-LEDGF (Bethyl A300-847A, 1:1500), anti-MeCP2 (Abcam ab50005, 1:2000), anti-Myc (Cell signaling 71D10, 1:1000), and anti-TDP-43 (ProteinTech 10782-2-AP, 1:1000).

2.4.5 Transfection and Co-immunoprecipitation

HA-MeCP2 construct was co-transfected with Myc-LEDGF or Myc-DHX9 (1:1 ratio) into HEK293 cells using GenJet transfection reagent (Signagen). 24 hours after transfection, cells were washed with PBS twice and directly lysed with Pierce IP Lysis Buffer (Thermo Scientific)

for 10min on ice. Lysate was centrifuged at 16,000g for 10min at 4°C and pellet was discarded. Six hours before lysate preparation, 30ul Dynabeads protein G was incubated with 3ug of anti-HA (Covance) or anti-Myc (Millipore) at 4°C to form the antibody-proteinG-bead complex. After washing off excess antibody, beads were incubated with lysate overnight at 4°C. Beads were washed with lysis buffer 6 times and then eluted by adding 1X LDS sample buffer (Life Technologies) and heated at 95°C for 10min.

Chapter 3: Loss of MeCP2 affects alternative splicing

3.1 Introduction

MeCP2 binds to methylated cytosine across the whole genome and acts as an interpreter of the information encoded by DNA methylation. Because of the association between DNA methylation and transcription regulation, early studies focused on how MeCP2 translates the methylation information into transcriptional outcomes. Although DNA methylation in gene promoters has been well characterized as a transcriptional silencer, the function of DNA methylation in the gene body is still poorly defined. Bioinformatic studies revealed that exons tend to have higher levels of DNA methylation than flanking introns do, suggesting intragenic DNA methylation might play an important role in pre-mRNA splicing by marking exons(Anastasiadou et al., 2011; Chodavarapu et al., 2010; Choi, 2010; Feng et al., 2010). In support of such an association, a recent study demonstrated that DNA methylation affects alternative splicing through inhibiting CTCF binding and modulating the elongation rate of DNA polymerase II(Shukla et al., 2011).

The identification of interaction between MeCP2 and a RNA-binding protein, YB1, has implicated a role of MeCP2 in the regulation of alternative splicing(Young et al., 2005). Genome wide analysis of MeCP2 binding and splicing data also suggested MeCP2 might promote the inclusion of highly methylated exons(Maunakea et al., 2013). However, because of the limitation of technology at the time the study was performed or the choice of non-relevant cell lines, these two studies failed to provide insights into how aberrant splicing events caused by loss of MeCP2 contribute to RTT phenotypes. Moreover, although inhibition of HDAC results in similar splicing deficit as MeCP2 knockdown in cancer cells, it remains elusive whether such mechanism are responsible for splicing changes in the MeCP2 deficient brain.

Herein, we sought to understand how MeCP2 regulates alternative splicing in the brain and what splicing events are misregulated in *Mecp2* null cortex. RNA-Seq analysis revealed that hundreds of splicing events were misregulated in the cortex of *Mecp2* knockout (KO) mice. ChIP-seq analysis revealed MeCP2 occupancy at exon/intron junctions, which provides additional support of the role for MeCP2 in modulating alternative splicing. More importantly, a specific splicing change in the *Mecp2* KO cortex-a shift in the balance between the flip and flop exon in the AMPA receptor (AMPAR) gene-was causally linked to synaptic phenotypes of faster desensitization kinetics of AMPAR-gated current and altered synaptic transmission. Together, our findings substantiate the role of MeCP2 in regulating alternative splicing of RNA by revealing direct physical interaction between MeCP2 and multiple splicing factors, association of MeCP2 at exon/intron junction, and providing the first functional link between a specific splicing alteration and synaptic phenotypes in RTT mice.

3.2 Results

3.2.1 RNA-Seq reveals alteration of alternative splicing upon loss of MeCP2

The newly identified interactions between MeCP2 and multiple splicing factors prompted us to determine whether there are widespread RNA splicing changes upon loss of MeCP2. We conducted high-throughput sequencing of RNA (RNA-Seq) from the cortex of wild type and *Mecp2* knockout (KO) mice. As a measure of the quality of the RNA-Seq data, we first examined whether our data reflect transcriptional changes consistent with previous findings. We examined transcriptional changes in our RNA-Seq data by applying a negative binomial model in edgeR(Robinson et al., 2010). Recently, a meta-analysis of transcriptional changes across multiple brain regions in *Mecp2* KO or overexpression (OE) mouse identified 466 MeCP2-

repressed genes based on high degree of consistency ($log_2FC > 0$ in KO or $log_2FC < 0$ in OE in at least 7 out of 8 datasets; FC, fold change)(Gabel et al., 2015). Of these genes, 315 genes (~68%) were also found to be up-regulated (log2FC[KO/WT] > 0) in our analysis result, suggesting significant overlap between transcriptional changes identified in our study and previous studies. In addition, we selected seven previously known misregulated genes in *Mecp2* KO(Chen et al., 2015; Gabel et al., 2015) as well as six novel differentially expressed gene identified by our study for further validation. qRT-PCR results show that all of them show similar changes as observed in our RNA-Seq data (Pearson's r = 0.95) (**Fig 8**). Taken together, these data indicate that our RNA-Seq data are robust in identifying transcriptional changes.

Next, we applied the Mixture of Isoforms (MISO)(Katz et al., 2010) algorithm to the RNA-Seq data and identified 263 alternative splicing (AS) events that were significantly changed in the cortex of *Mecp2* KO mice using a stringent filter. Loss of MeCP2 affects various types of AS events, including skipped exon (SE), mutually exclusive exons (MXE), retained intron (RI), alternative 5' ss exon (A5E), and alternative 3' ss exon (A3E) (**Fig 9a**). Subsequent analysis indicated that although more RI or MXE events had slightly reduced percent spliced in (PSI) value, SE, A5E, and A3E events, which in total represented the majority of events, had similar number of events with increased or decreased PSI (**Fig 9b**). These data suggest that the loss of MeCP2 affects alternative splicing in both directions, which is similar to the knockdown or overexpression of a typical splicing factor(Choudhury et al., 2014; Wang et al., 2014a). Additionally, functional enrichment analysis using DAVID showed that genes with splicing changes were enriched with splice variant, alternative splicing, phosphoprotein, cell junction, compositionally biased region (Ser-rich), and plasma membrane part (**Fig 10**). Interestingly, gene expression analysis on the 232 genes associated with splicing changes revealed that a majority of

genes with splicing changes have similar total expression level between WT and *Mecp2* KO (only 15 genes show larger than 1.25-fold change, and only one shows larger than 1.5-fold change) (**Fig 9c**), suggesting that MeCP2-mediated transcriptional regulation and splicing regulation are independent of each other. To validate the splicing changes, we performed qRT-PCR with isoform specific primers to evaluate 20 SE events. We observed consistent changes in 13 genes as identified by MISO (65%), including 6 events with decreased PSI and 7 events with increased PSI in *Mecp2* KO (**Fig 11**). The overall validation rate from our study of using biological replicates of tissue is comparable to the success rate using cell lines in two recent studies (74% and 71%, respectively)(Anczukow et al., 2015; Wang et al., 2014b).

To generalize our observation that loss of MeCP2 leads to global splicing changes, we analyzed RNA-Seq data generated from *Mecp2* KO hypothalamus and visual cortex in two recent studies(Chen et al., 2015; Gabel et al., 2015), respectively. Using a cutoff of $|\Delta PSI| \geq 5\%$ and Bayes factor≥1, 482 and 719 SE events were identified by MISO to be changed in *Mecp2* KO hypothalamus and visual cortex, respectively. 150 of the 482 SE events identified in the *Mecp2* KO hypothalamus and 171 of the 719 SE events identified in the *Mecp2* KO visual cortex were also found in our study. Only 22 events were identified in all three studies using the same filter criteria. We focused our meta-analysis on SE events because this is the best-annotated category of alternative splicing events in the mouse genome. In summary, the large number of alternative splicing changes in independent RNA-seq data sets and the significant overlap between data sets generated from different brain regions of different lines of *Mecp2* KO mice at different ages are consistent with the notion that loss of MeCP2 results in global splicing alterations.

To further study whether MeCP2 may be directly involved in modulating splicing, we examined MeCP2 occupancy across the genome. ChIP-Seq analysis was performed using the anti-Flag antibody on chromatin prepared from the cortex of the *Mecp2-Flag* knockin mice. 20,652 high confidence MeCP2 ChIP-seq peaks were identified (see Methods for detailed description on ChIP-seq analysis and quality control statistics.). Based on statistical ranking and robustness of primer design, five of the identified peaks were selected for independent validation. ChIP-qPCR on a separate cohort of *Mecp2*-Flag mice detected significant occupancy of MeCP2 at the genomic locations corresponding to these five peaks relative to *Gapdh* promoter (**Fig 12**). Gene ontology analysis found that genes with MeCP2 ChIP-seq peak(s) were enriched with GO terms of alternative splicing (**Fig 9d**). Moreover, alignment of MeCP2 ChIP-seq reads with the 5' and 3' ends of exons revealed a significant enrichment of MeCP2 ChIP-seq peaks around the exon/intron boundary and over exons (**Fig 9e**). Taken together, the physical interaction between MeCP2 and splicing factors, the widespread changes in RNA splicing, and the enriched MeCP2 occupancy around exon/intron boundary are consistent with each other and strongly suggest that MeCP2 could play an important role in regulating alternative splicing.

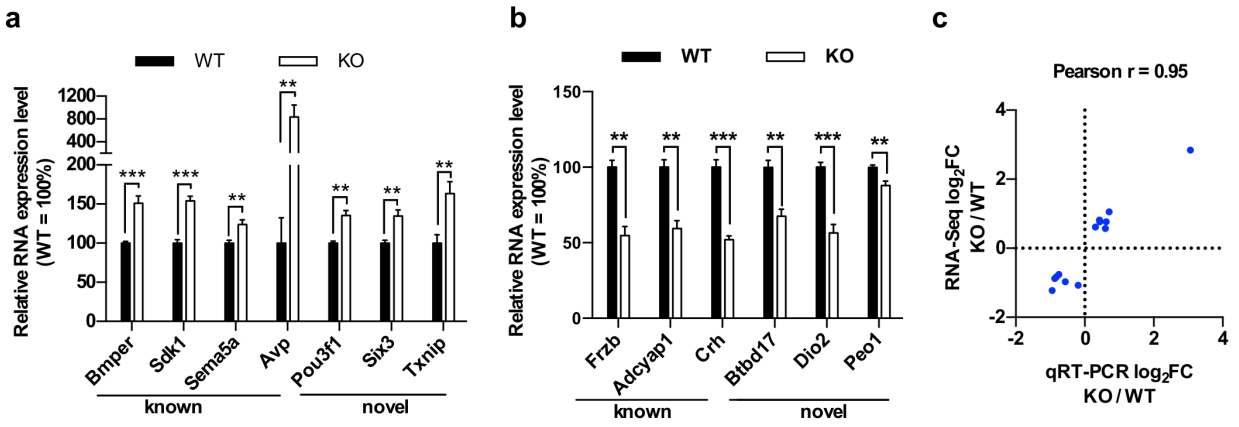

Fig 8. Differential gene expression analysis of RNA-Seq data.

(a-b) Quantification of MeCP2-repressed genes (a) and MeCP2-activated genes (b) in WT and *Mecp2* KO cortex by RT-qPCR. Three to four previously known targets and three novel targets identified only in our RNA-Seq data in each group were selected for validation. Mean ± S.E.M, n = 5-6 per genotype. (** $P < 0.01$, *** $P < 0.001$, Benjamini-Hochberg adjusted P value)

(c) Good correlation between qRT-PCR result and RNA-Seq analysis result of the 13 genes analyzed in b-c. r, correlation coefficient.

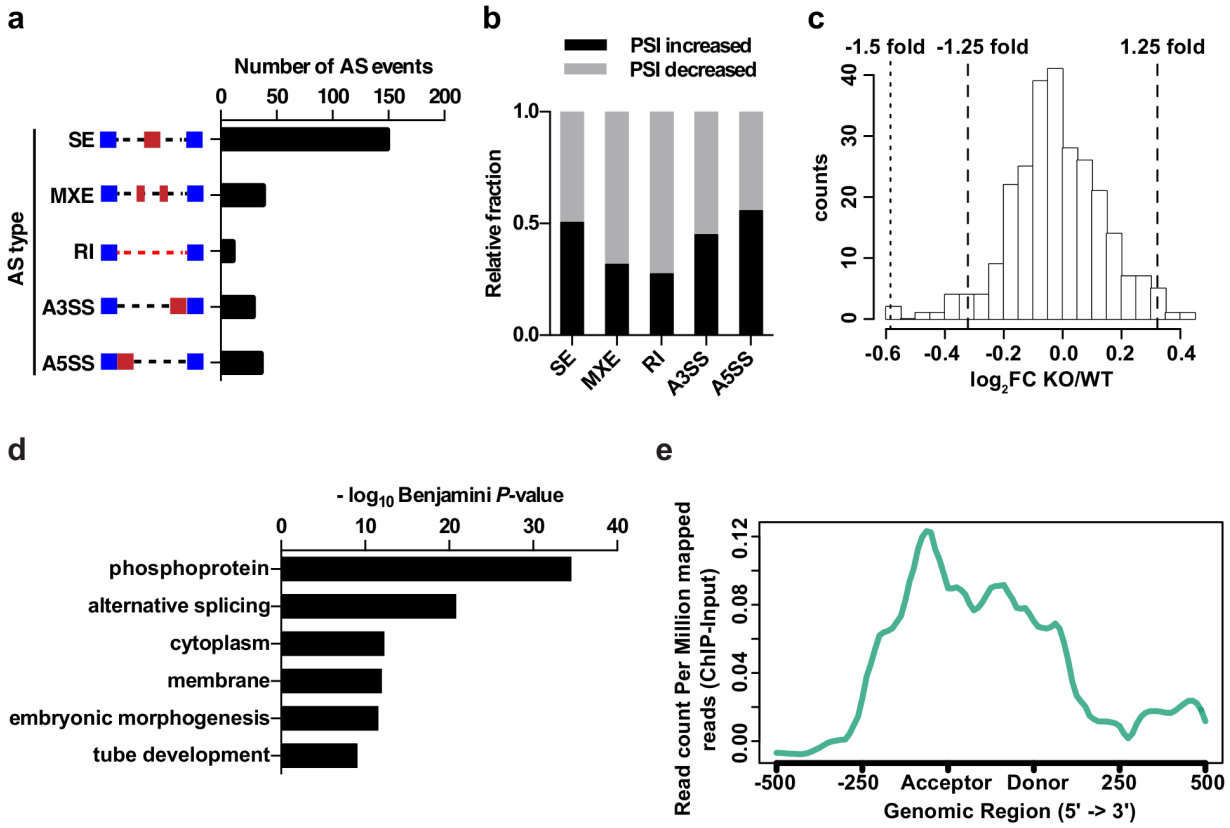

Fig 9. Global splicing changes in *Mecp2* KO mouse cortex and enrichment of MeCP2 around the exon/intron boundary.

(a) Number of misregulated alternative splicing (AS) events by category in *Mecp2* KO cortex.

(b) Relative fraction of each AS events type positively or negatively affected by loss of MeCP2.

(c) Histogram of total gene expression changes in *Mecp2* KO cortex for those 232 genes associated with splicing changes in *Mecp2* KO cortex. FC: fold change.

(d) Functional enrichment analysis of genes with MeCP2 peak(s) identified in ChIP-Seq data from WT mouse cortex. Top six terms are shown and $-\log_{10}$ Benjamini *P*-value is plotted for each GO term.

(e) Read counts per millions of mapped reads (ChIP minus input) across regions spanning from 500bp upstream and 500bp downstream of all exons.

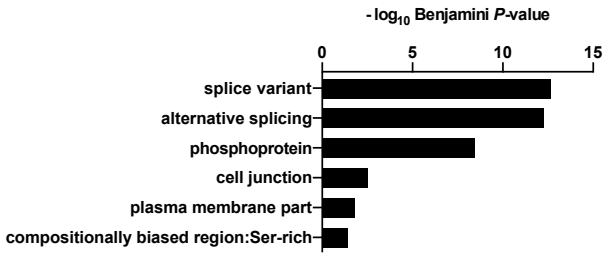

Fig 10. Functional enrichment analysis of genes with splicing changes.

Significant terms (Benjamini *P*-value < 0.05) were shown with one redundant term omitted.

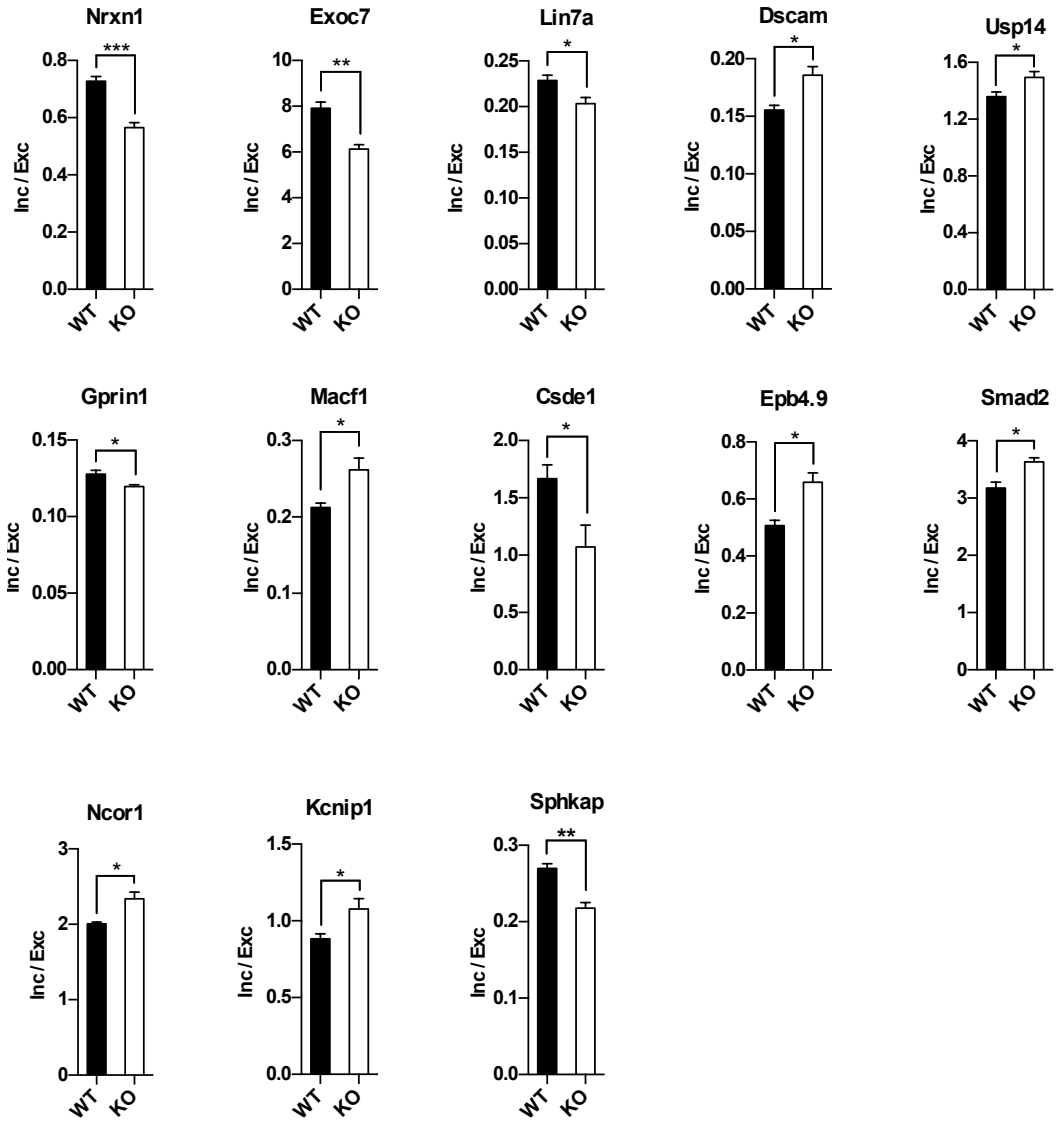

Fig 11. Validation of splicing changes by qRT-PCR.

For each splicing event, specific primers for inclusion isoform and exclusion isoform were designed. Inc / Exc ratio was calculated using $2^{-\Delta Ct}$ method. Mean ± S.E.M is plotted; n = 5-6 per genotype. * $P < 0.05$, ** $P < 0.01$, *** $P < 0.001$; two-tailed *t*-test with Benjamini-Hochberg correction.

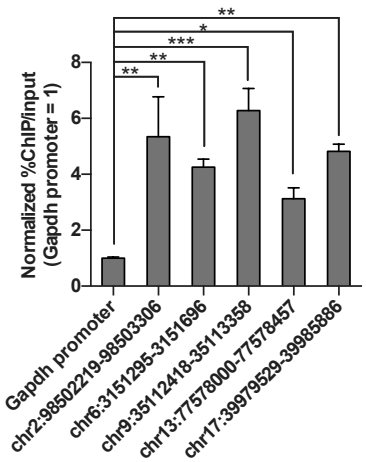

Fig 12. Validation of MeCP2 peaks identified by ChIP-Seq.

ChIP-qPCR was performed using primers specific to each peak. Mean ± S.E.M; n = 4; * $P <$ 0.05, ** $P < 0.01$, *** $P < 0.001$; one-way ANOVA followed with Holm-Sidak's multiple comparisons test.

3.2.2 Altered splicing of the AMPAR genes in the cortex of *Mecp2* KO mice

Gria2 is a major component of the AMPA receptor (AMPAR), which mediates the vast majority of fast synaptic transmission in the CNS. Two electrophysiologically distinct isoforms for Gria2 are generated by a mutually exclusive splicing event of the *Gria2* pre-mRNA. Depending of the usage of either the flip or the flop exon, *Gria2* pre-mRNA can be spliced into either the flip or the flop isoform. Our RNA-Seq data revealed that ~ 51% of all *Gria2* transcripts contained the flip exon in wild type mice. In contrast, only ~ 28% *Gria2* transcripts included the flip exon in the *Mecp2* KO mice (**Fig 13a**). qRT-PCR analysis in a separate cohort of animals confirmed a shift of flip/flop ratio toward a flop dominant state in *Mecp2* KO mice, but the total expression level of the *Gria2* gene remained unchanged (**Fig 13b-c**). The reduction of flip/flop ratio in *Mecp2* KO mice are not likely due to delayed development of the brain because the flip isoform is more abundant during early brain development and the flop isoform gradually increases to a comparable level of the flip isoform toward adulthood(Monyer et al., 1991).

Because alternative splicing of flip/flop exons is a common feature in all AMPAR genes, we asked whether similar changes also occurred in the *Gria1*, *Gria3*, and *Gria4* genes. Quantification result showed that flip/flop ratio of *Gria1*, *Gria3*, and *Gria4* genes was significantly reduced in the cortex of *Mecp2* KO mice (**Fig 13d**), implicating a biased usage of flop exon in the mature transcripts of all AMPAR genes. Importantly, the total mRNA level of *Gria1* was unchanged, and only subtle trend of decreasing *Gria3* and *Gria4* mRNA level was observed in *Mecp2* KO mice (**Fig 13e**).

Interestingly, analysis of RNA-Seq data from visual cortex and hypothalamus of *Mecp2* KO mice also showed that percentage of flip isoform is significantly decreased (**Fig 14**). Note that these two studies used the Bird allele ($Mecp2^{tm1.1Bird}$) and our data was generated from the

Jaenisch allele (*Mecp2*$^{tm1.1jae}$). The consistent flip/flop splicing changes across different brain regions from different knockout mouse lines suggested that reduction of flip/flop ratio is a common defect due solely to loss of MeCP2. More importantly, we also found that the percentage of flip isoform in the hypothalamus of *Mecp2* OE mice was significantly increased, which is opposite to the changes in *Mecp2* KO (**Fig 14**). Together, these results strongly suggest that MeCP2 directly modulates the regulation of *Gria2* flip/flop splicing.

Finally, we tested whether splicing alteration of AMPAR genes also occurs in the cortex of heterozygous female *Mecp2*$^{-/+}$ mice. Although not as drastic as that observed in *Mecp2* KO male mice, *Mecp2*$^{-/+}$ mice also displayed a significant reduction of flip/flop ratio in *Gria1*, *Gria2*, *Gria3*, and *Gria4* (**Fig 13f**). Similar to *Mecp2* KO male mice, *Mecp2*$^{-/+}$ mice had unchanged total mRNA level in all four AMPAR genes (**Fig 13g**). These data suggest similar change in flip/flop usage may exist in female RTT patients.

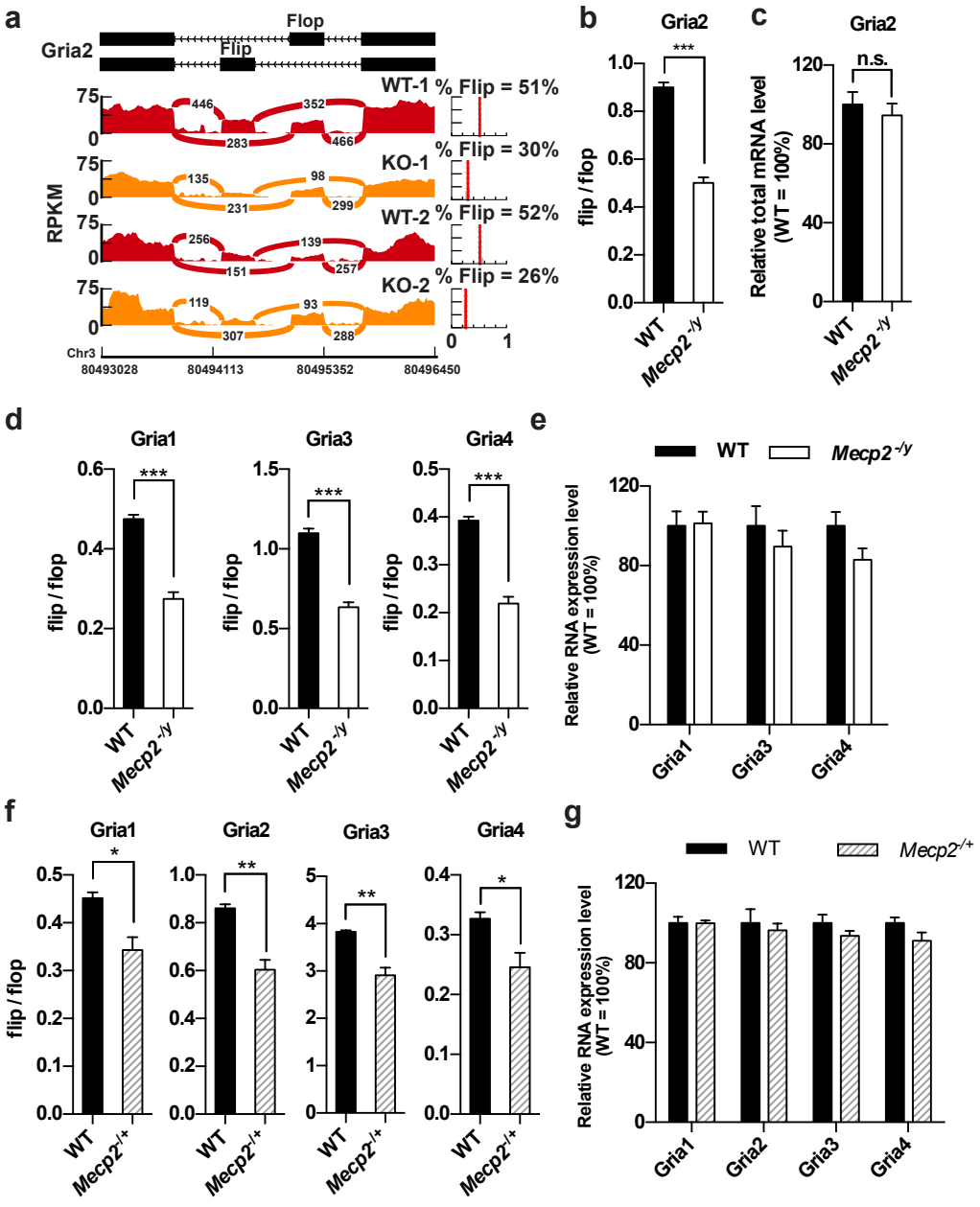

Fig 13. Loss of MeCP2 affects flip/flop splicing of AMPAR genes

(a) Reads distribution surrounding the flip and flop exons of *Gria2* locus from RNA-Seq data of two pairs of WT and *Mecp2* KO mouse cortex. Percentage of flip isoform (% flip) for each sample is estimated by Mixture of Isoform pipeline (MISO) and plotted on the right.

(b) Quantification of flip/flop ratio of *Gria2* gene in the cortex of WT and *Mecp2* KO mice. Mean ± S.E.M is plotted. n = 8 per genotype. *** $P < 0.001$; two-tailed *t*-test.

(c) Quantification of *Gria2* total mRNA level in the cortex of WT and *Mecp2* KO mice. Mean ± S.E.M is plotted. n = 8 per genotype.

(d) Quantification of the flip/flop ratio of *Gria1*, *Gria3* and *Gria4* in the cortex of WT and *Mecp2* KO mice. Mean ± S.E.M is plotted. n = 8 per genotype. *** $P < 0.001$; two-tailed *t*-test.

(e) Quantification of *Gria1, Gria3 and Gria4* total mRNA level in the cortex of WT and *Mecp2* KO mice. Mean ± S.E.M is plotted. n = 8 per genotype.

(f) Quantification of the flip/flop ratio of *Gria1*, *Gria2, Gria3* and *Gria4* in the cortex of WT and *Mecp2*$^{-/+}$ female mice. Mean ± S.E.M is plotted. n = 4 per genotype. * $P < 0.05$, ** $P < 0.01$; two-tailed *t*-test.

(g) Quantification of *Gria1, Gria3 and Gria4* total mRNA level in the cortex of WT and *Mecp2*$^{-/+}$ female mice. Mean ± S.E.M is plotted. n = 4 per genotype.

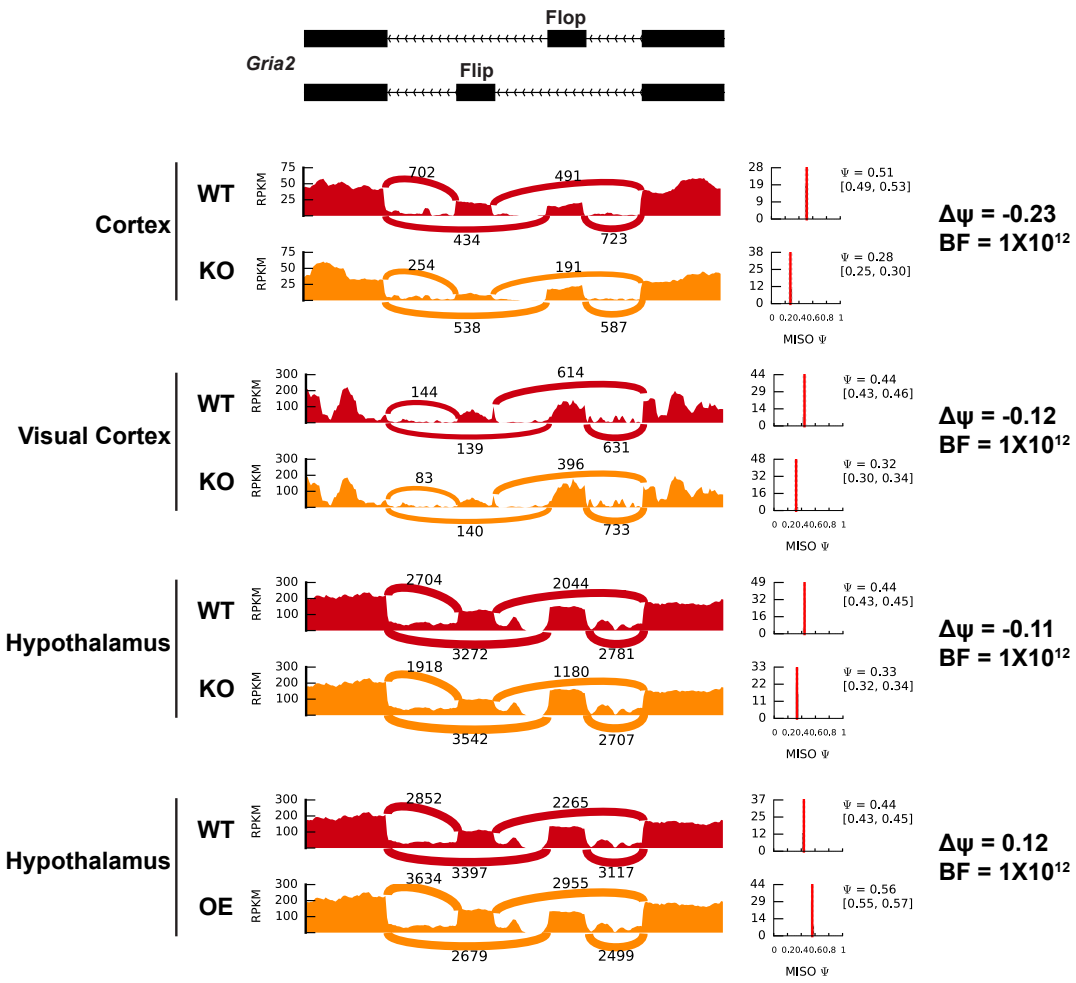

Fig 14. Gria2 flip/flop splicing is altered in multiple brain regions of *Mecp2* KO mouse and the hypothalamus of *Mecp2* overexpression (OE) mouse.

RNA-Seq read density around flip and flop exon in indicated brain region of WT and KO (or OE) mouse. Percentage of flip isoform (ϕ) is shown to the right of density plot. Δϕ (KO or OE - WT) was calculated and the Bayes factor (BF) is shown below. Difference in Δϕ among different studies might reflect difference of brain region, the knockout allele (cortex data was generated from the Jaenisch allele and the others Bird allele), age of mice when tissue was collected (cortex: 6 weeks of age; hypothalamus: 7 weeks of age; visual cortex: 8-9 weeks of age) and other experimental conditions.

3.2.3 AMPA receptor flip/flop splicing is not regulated by activity dependent MeCP2 phosphorylation

AMPA receptor flip/flop splicing is subjected to regulation by neuronal activity. Prior studies showed that percentage of flip splice variant of *Gria1* and *Gria2* decreases upon chronic activity deprivation using Na^+-channel blocker tetrodotoxin (TTX)(Penn et al., 2012). Because MeCP2 directly regulates AMPA receptor flip/flop splicing, we ask whether flip/flop splicing is regulated by activity-dependent MeCP2 phosphorylation. To that end, we performed qRT-PCR to quantify flip/flop ratio in WT, $Mecp2^{S80A/y}$, $Mecp2^{S80D/y}$, $Mecp2^{S421A;S424A/y}$, and $Mecp2^{S421D/y}$ mouse cortex. Serine (S) to alanine (A) substitution abolishes the capability of phosphorylation and represents as phosphor-dead mutant; Serine (S) to Aspartic acid (D) substitution mimics phosphorylation and represents as constitutively phosphorylated mutant. The qRT-PCR results showed that flip/flop ratio of all AMPA receptor genes is similar between WT and $Mecp2^{S80A/y}$, $Mecp2^{S80D/y}$, $Mecp2^{S421A;S424A/y}$, $Mecp2^{S421D/y}$ (**Fig 15a, c, e and g**). In addition, the expression level of the total AMPA receptor genes is also similar between WT and these four different phosphor mutant mice (**Fig 15b, d, f and h**). These data suggest that AMPA receptor flip/flop splicing is not regulated by activity-dependent MeCP2 phosphorylation.

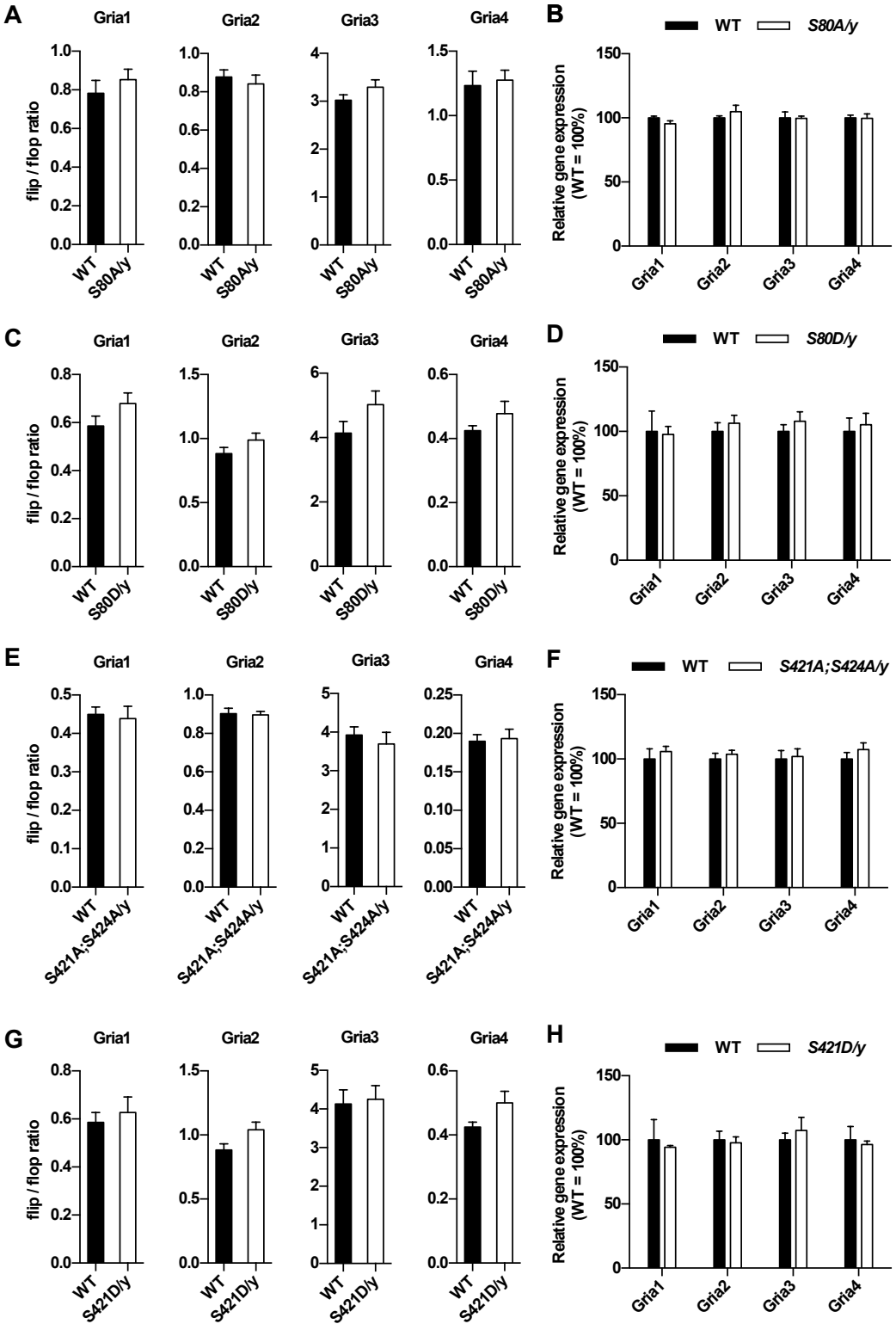
A
Gria1
Gria2
Gria3
Gria4
flip / flop ratio
WT
S80A/y
B
WT
S80A/y
Relative gene expression (WT = 100%)
Gria1
Gria2
Gria3
Gria4
C
S80D/y
D
S80D/y
E
S421A;S424A/y
F
S421A;S424A/y
G
S421D/y
H
S421D/y

Fig 15. Flip/flop ratio of all AMPA receptor genes is similar between WT and *Mecp2*$^{S80A/y}$, *Mecp2*$^{S80D/y}$, *Mecp2*$^{S421A;S424A/y}$, *Mecp2*$^{S421D/y}$.

(A) Quantification of flip/flop ratio of Gria1, Gria2, Gria3 and Gria4 gene in the cortex of WT and Mecp2S80A/y mice. Mean ± S.E.M is plotted. n = 3 per genotype.

(B) Quantification of total gene expression of Gria1, Gria2, Gria3 and Gria4 gene in the cortex of WT and Mecp2S80A/y mice. Mean ± S.E.M is plotted. n = 3 per genotype.

(C) Quantification of flip/flop ratio of Gria1, Gria2, Gria3 and Gria4 gene in the cortex of WT and Mecp2S80D/y mice. Mean ± S.E.M is plotted. n = 3 per genotype.

(D) Quantification of total gene expression of Gria1, Gria2, Gria3 and Gria4 gene in the cortex of WT and Mecp2S80D/y mice. Mean ± S.E.M is plotted. n = 3 per genotype.

(E) Quantification of flip/flop ratio of Gria1, Gria2, Gria3 and Gria4 gene in the cortex of WT and Mecp2S421A;S424A/y mice. Mean ± S.E.M is plotted. n = 4 per genotype.

(F) Quantification of total gene expression of Gria1, Gria2, Gria3 and Gria4 gene in the cortex of WT and Mecp2S421A;S424A/y mice. Mean ± S.E.M is plotted. n = 4 per genotype.

(C) Quantification of flip/flop ratio of Gria1, Gria2, Gria3 and Gria4 gene in the cortex of WT and Mecp2S421D/y mice. Mean ± S.E.M is plotted. n = 3 per genotype.

(D) Quantification of total gene expression of Gria1, Gria2, Gria3 and Gria4 gene in the cortex of WT and Mecp2S421D/y mice. Mean ± S.E.M is plotted. n = 3 per genotype.

3.2.4 LEDGF is involved in the regulation of *Gria2* flip/flop splicing

To determine how loss of MeCP2 affects the splicing of flip/flop exon, we focused on the *Gria2* gene to explore the potential involvement of several recent models of splicing regulation. Modulation of PolII elongation rate has been proposed as one model of how epigenetic mechanisms influence splicing. Slow PolII elongation rate allows longer time for spliceosome to assemble and hence increase the chance of the alternative exon being included in the mature transcript(Luco et al., 2011). A recent study suggested that MeCP2 is enriched in particular alternative exons and facilitates exon inclusion by pausing PolII in cultured cells(Maunakea et al., 2013). We set out to test whether MeCP2 regulates *Gria2* flip/flop splicing through similar mechanism in the brain. Chromatin immunoprecipitation (ChIP) followed by qRT-PCR showed a significant enrichment of MeCP2 on the flip and flop exons of *Gria2* gene (**Fig 16a**). But no significant difference in PolII occupancy on the flip and flop exons between the wild type and *Mecp2* KO mice was found by PolII ChIP (**Fig 16b**), suggesting the involvement of a PolII-independent mechanism underlying the flip/flop splicing change in *Mecp2* KO brain. Another interesting epigenetic model for alternative splicing regulation is that histone modification can be bound by adaptor proteins which in turn recruit specific splicing factor to alternative exons(Luco et al., 2011). It has been previously shown that trimethylated histone H3 lysine 36 (H3K36me3) is enriched on exons and can be bound by LEDGF, which recruits splicing factors such as SRSF1 to regulate splicing(Pradeepa et al., 2012). Although significant LEDGF occupancy was detected on the flip and flop exons (**Fig 16c**), no significant difference in the occupancy of H3K36me3 on the flop and flip exons was detected between the wild type and *Mecp2* KO brain (**Fig 16d**).

To determine whether LEDGF is functionally involved in the regulation of Gria2 flip/flop splicing, we tested the effect of LEDGF knockdown on flip/flop ratio in a neuroblastoma cell line, Neuro-2A, using a *Gria2* minigene. The *Gria2* minigene spans the genomic region from exon 13 to exon 15 of *Gria2* (**Fig 18**, either the flip or flop exon can be included as exon 14). As a control, we co-transfected *Mecp2* shRNA, Gria2 minigene along with a MeCP2 overexpression plasmid into Neuro-2a cells and found that flip/flop ratio is significantly reduced upon *Mecp2* knockdown (**Fig 16e-f**), indicating that this artificial assay is capable of discovering factors that potentially affect flip/flop splicing. Next, we transfected a *Ledgf* shRNA in the cells and tested its effect on flip/flop splicing. Similar to *Mecp2* knockdown, *Ledgf* knockdown also leads to a reduction of flip/flop ratio (**Fig 16g-h**), suggesting that LEDGF is functionally involved in the regulation of Gria2 flip/flop splicing.

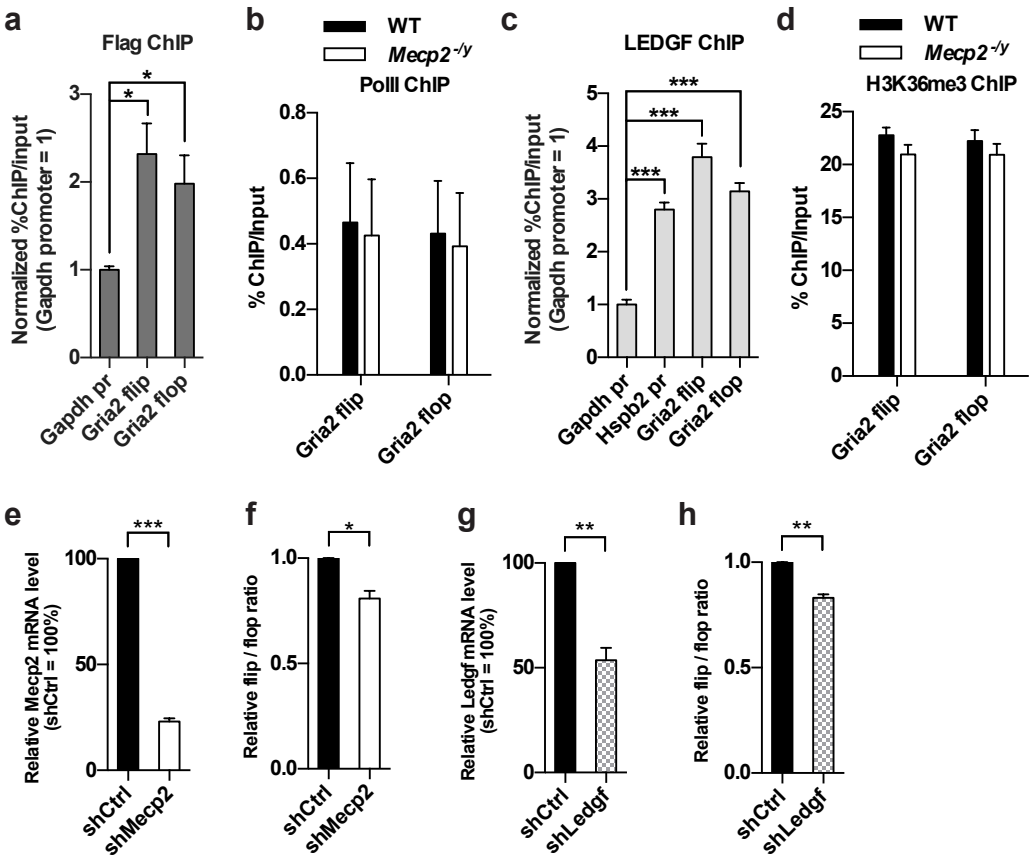

Fig 16. LEDGF is involved in regulation of Gria2 flip/flop splicing.

(a) ChIP-qPCR analysis of MeCP2 occupancy on *Gapdh* promoter, *Gria2* flip and flop exon in *Mecp2-Flag* mouse cortex. pr: promoter. Mean ± S.E.M is plotted. n = 4 per genotype. * $P < 0.05$; one-way ANOVA followed with Holm-Sidak's multiple comparisons test.

(b) ChIP-qPCR analysis of PolII occupancy on *Gria2* flip and flop exon in WT and *Mecp2* KO cortex. Mean ± S.E.M is plotted. n = 4 per genotype.

(c) ChIP-qPCR analysis of LEDGF occupancy on *Gria2* flip and flop exon in WT mouse cortex. Mean ± S.E.M; n = 5; *** $P < 0.001$; one-way ANOVA followed with Holm-Sidak's multiple comparisons test.

(d) ChIP-qPCR analysis of H3K36me3 occupancy on *Gria2* flip and flop exons in WT and *Mecp2* KO cortex. n = 4 per genotype.

(e-f) Quantification of *Mecp2* (e) and flip/flop ratio (f) in Neuro-2A cells co-transfected with *Mecp2* shRNA plasmid, MeCP2 expression plasmid and Gria2 minigene plasmid. Mean ± S.E.M of three independent experiments, * $P < 0.05$, *** $P < 0.001$; two-tailed *t*-test.

(g-h) Quantification of *Ledgf* (g) and flip/flop ratio (h) in Neuro-2A cells co-transfected with *Ledgf* shRNA plasmid and Gria2 minigene plasmid. Mean ± S.E.M of four independent experiments, ** $P < 0.01$; two-tailed *t*-test.

3.2.5 Functional link between altered flip/flop splicing and synaptic phenotypes in the *Mecp2* KO mice

Flip/flop exon encodes a 38 amino acids sequence in the ligand binding domain of AMPARs that controls desensitization rate: flop-containing receptors desensitize with faster kinetics than flip-containing receptors (Mosbacher et al., 1994; Sommer et al., 1990). To determine the functional consequence of altered flip/flop splicing in the cortex of *Mecp2* KO mice, we performed outside-out patch clamp recording of glutamate-evoked current on layer 2/3 pyramidal neurons in acute brain slices. We found that the decay time constant τ was significantly reduced in *Mecp2* KO mice (**Fig 17a-b**). In addition to evoked response, regular whole cell patch clamp recording of spontaneous synaptic events also detected a faster decay in miniature excitatory postsynaptic current (mEPSC) in layer 2/3 pyramidal neurons from the *Mecp2* KO mice. Finally, bath application of cyclothiazide (CTZ), a positive allosteric modulator of AMPARs that inhibits desensitization of AMPARs(Partin et al., 1996), slowed down the decay kinetics in *Mecp2* KO slice to a comparable level of wild type cells (**Fig 17c-d**). Together, these results uncover a previously unappreciated defect of faster desensitization kinetics of AMPAR-gated current in the *Mecp2* KO mice, which correlates with altered flip/flop splicing and can be modulated by pharmacological reagents.

To causally link the change in flip/flop splicing and the altered AMPAR desensitization kinetics, we used engineered splicing factors (ESF)(Wang et al., 2009; Wang et al., 2013) to specifically manipulate flip/flop splicing in the brain of *Mecp2* KO mice. ESF is composed of a sequence-specific RNA-binding domain derived from human Pumilio1 (PUF domain) and a functional domain that suppresses (Gly domain) or enhances (SR domain) inclusion of a specific exon. We evaluated the effect of four ESFs (ESF-flop-Gly [flop suppressor], ESF-flop-SR [flop

enhancer], ESF-flip-Gly [flip suppressor] and ESF-flip-SR [flip enhancer]) on flip/flop splicing using a *Gria2* minigene (**Fig 18a**). We found that ESF-flop-Gly significantly increased the flip/flop ratio (**Fig 17e**), an effect opposite to the change we observed in the cortex of *Mecp2* KO mice. Moreover, ESF-flop-Gly didn't change the level of total *Gria2* gene expression (**Fig 17f**).

To further test the effect of ESF-flop-Gly on flip/flop splicing of the endogenous *Gria2* transcript in neurons, we infected primary cortical neurons with adeno-associated virus (AAV) encoding either mCherry alone or ESF-flop-Gly and mCherry. As expected, AAV-ESF-flop-Gly-mCherry significantly altered the flip/flop splicing balance to favor the use of the flip exon (**Fig 18b-c**), suggesting that ESF-flop-Gly could be used *in vivo* to reverse the flip/flop splicing defect in *Mecp2* KO mice. To that end, we injected lentivirus expressing ESF-flop-Gly into the cortex of *Mecp2* KO mice, and measured the decay time constant τ of glutamate-evoked AMPAR-gated current in the outside-out patch clamp mode in acute brain slices 2 weeks post injection. Compared to neurons infected with control virus (KO+Ctrl), ESF-flop-Gly expressing neurons (KO+ESF) had a significant larger decay time constant τ, which was indistinguishable from that of WT cells (**Fig 17g**). These results strongly suggest that altered flip/flop splicing is required for a specific synaptic phenotype in the *Mecp2* KO mice.

To further examine the effect of altered flip/flop splicing on synaptic transmission, we applied repetitive stimulation on the neurons in an interval of 100 ms and recorded the AMPAR-gated current. Upon repetitive stimulation, a fraction of AMPA receptors desensitizes and the short interval between stimulation does not allow full recovery. As a result, fewer AMPA receptors can respond to the subsequent stimulation, and therefore current diminished. Comparing to WT neurons, KO neurons displayed even more drastic decrease in current amplitude over the course of five stimulations (**Fig 17h-i**). This difference could be partially due to a higher percentage of

flop isoform that are more easily desensitized in the KO neurons. Consistent with this hypothesis, overexpressing ESF-flop-Gly in KO neurons partially rescued this phenotype (**Fig 17h-i**). These data suggest the altered flip/flop splicing ratio has important impact on synaptic transmission in the *Mecp2* KO cortex, which can be reversed by ESF designed to specifically target flip/flop exons.

To determine the functional outcome of *Ledgf* knockdown-induced change in *Gria2* flip/flop splicing, we injected lentivirus encoding shLedgf and control shRNA into the cortex of wild type mice. We found that *Ledgf* knockdown resulted in a significantly reduced decay time constant τ of glutamate-evoked AMPAR-gated current (**Fig 17j**), an effect similar to that caused by the loss of MeCP2 (**Fig 17a-b**). In addition, *Ledgf* knockdown led to significantly weaker response upon repetitive stimulations (**Fig 17k-l**), another phenotype caused by the loss of MeCP2 (**Fig 17h-i**). These data correlate well with the *Gria2* minigene assay in figure 5 and further support that both LEDGF and MeCP2 are required for the normal splicing of *Gria2* flip/flop exons.

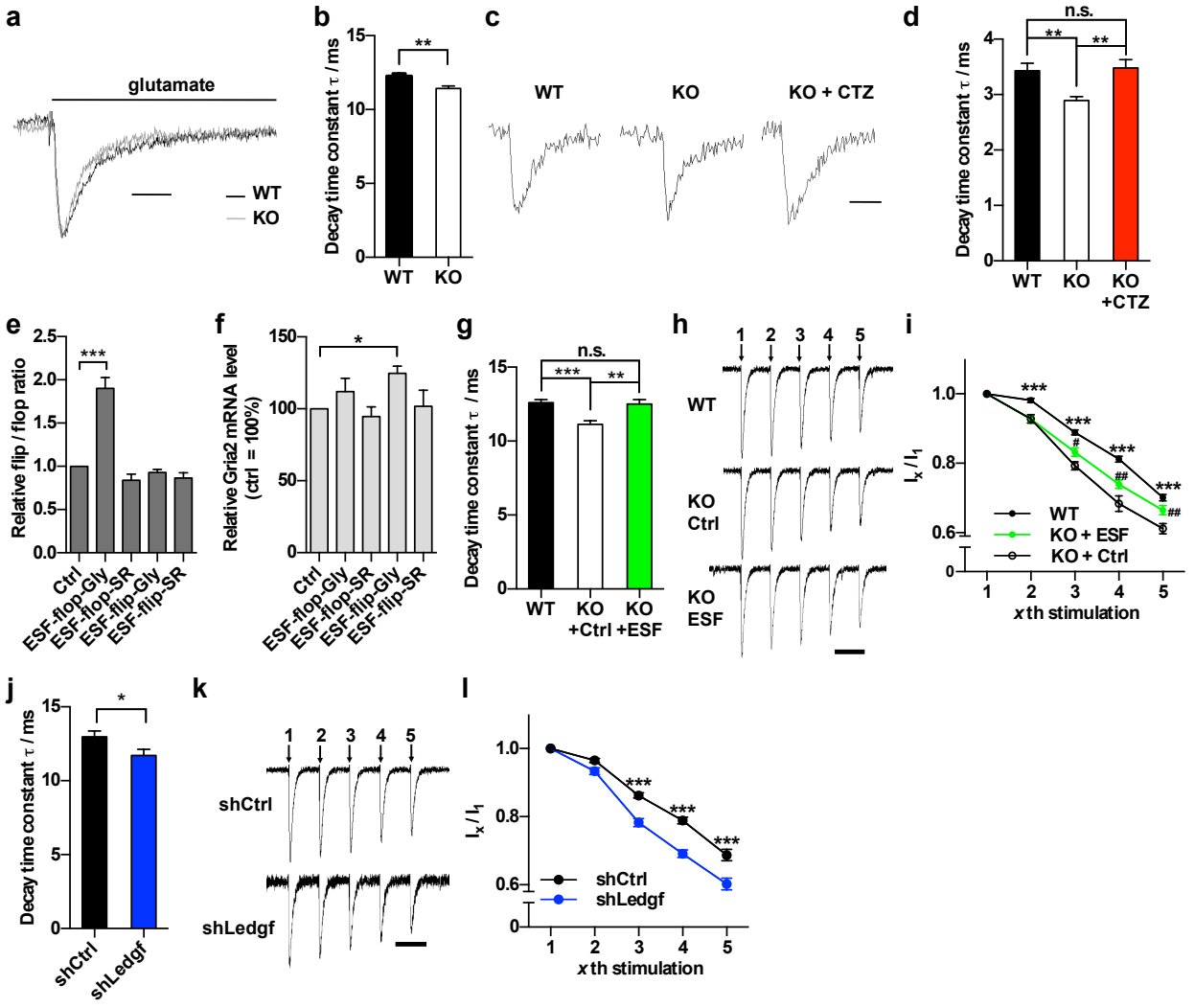

Fig 17. Altered AMPA receptor decay kinetics and synaptic transmission in *Mecp2* KO cortical neurons can be reversed by ESF.

(a) Representative sample trace of glutamate-evoked current in WT and *Mecp2* KO cortical neurons. Scale bar = 15ms.

(b) Quantification of decay time constant τ of glutamate-evoked current in WT and *Mecp2* KO cortical neurons. Mean ± S.E.M is plotted. n = 37 for WT, n = 33 for KO. ** $P < 0.01$; two tailed *t*-test.

(c) Representative mEPSC sample trace in WT and *Mecp2* KO cortical neurons with or without CTZ treatment. Scale bar = 10ms.

(d) Quantification of decay time constant τ of mEPSC. Mean ± S.E.M is plotted. n = 42 for WT, n = 46 for KO, n = 38 for KO + CTZ. ** $P < 0.01$; one-way ANOVA with Tukey's multiple comparisons test.

(e-f) qRT-PCR analysis the flip/flop ratio (e) and total *Gria2* minigene (f) expression in HEK 293 cells co-transfected with indicated ESF and the *Gria2* minigene. Mean ± S.E.M is plotted. n = 4 for each group. * $P < 0.05$, *** $P < 0.001$; two tailed *t*-test.

(g) Quantification of decay time constant τ of glutamate-evoked current in WT, *Mecp2* KO (KO+Ctrl) and *Mecp2* KO cortical neurons infected with ESF-flop-Gly lentivirus (KO+ESF). Recording was done on acute slice from mouse infected with lentivirus two weeks after stereotaxic injection. Mean ± S.E.M is plotted. n = 50 for WT, n = 26 for KO+Ctrl, n = 27 for KO+ESF. ** $P < 0.01$, *** $P < 0.001$; one-way ANOVA with Tukey's multiple comparisons test.

(h) Representative sample trace of AMPAR-mediated current in response to repetitive stimulations in WT and *Mecp2* KO neurons infected with control or ESF-flop-Gly lentivirus (KO+Ctrl or KO+ESF). Scale bar, 100ms.

(i) Relative current amplitude of the xth stimulation to first stimulation in WT and *Mecp2* KO neurons infected with either control or ESF-flop-Gly lentivirus (KO+Ctrl or KO+ESF). Mean ± S.E.M is plotted. n = 36 for WT, n = 18 for KO+Ctrl, n = 18 for KO+ESF. Asterisk denotes *P*-value for comparison between WT and KO+Ctrl, *** $P < 0.001$. Pound sign denotes *P*-value for comparison between KO+ESF and KO+Ctrl, # $P < 0.05$, ## $P < 0.01$; repeated measures two-way ANOVA with Tukey's multiple comparisons test.

(j) Quantification of decay time constant τ of glutamate-evoked current in neurons infected with shCtrl or shLedgf lentivirus. Mean ± S.E.M is plotted. n = 13 for shCtrl, n = 12 for shLedgf, * $P < 0.05$; two-tailed *t*-test.

(k) Representative sample trace of AMPAR-mediated current in response to repetitive stimulations in neurons infected with shCtrl or shLedgf lentivirus. Scale bar, 100ms.

(l) Relative current amplitude of xth stimulation to first stimulation in neurons infected with shCtrl or shLedgf. Mean ± S.E.M is plotted. n = 12 for each group, *** $P < 0.001$; repeated measures two-way ANOVA with Tukey's multiple comparisons test.

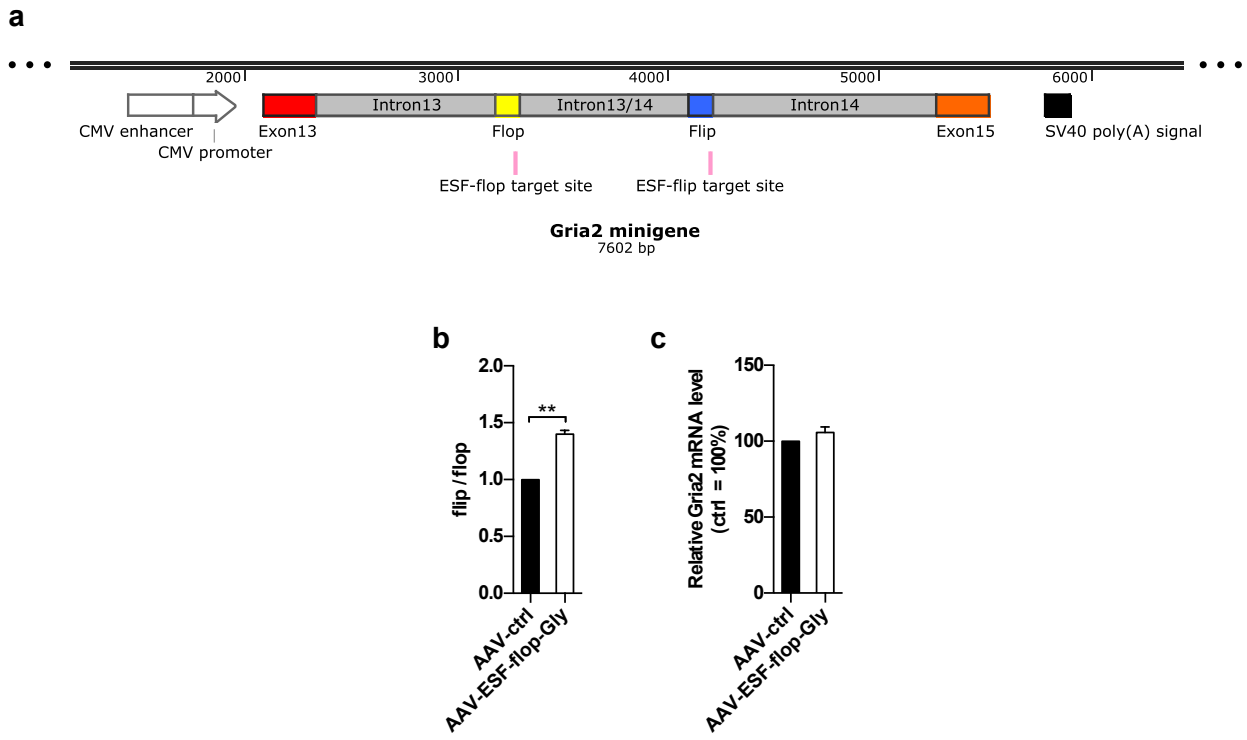

Fig 18. Engineering splice factor (ESF) can modulate *Gria2* flip/flop splicing.

(a) Schematic diagram of the *Gria2* minigene. The ESF binding site on flip or flop exon is shown.

(b-c) Quantification of *Gria2* flip/flop ratio (b) and total *Gria2* mRNA level (c) in primary culture neurons infected with AAV-Ctrl or AAV-ESF-flop-Gly. Mean ± S.E.M of three independent experiments, ** $P < 0.01$; two-tailed *t*-test.

3.2.6 Pharmaceutical correction of AMPA receptor desensitization defect might delay disease progression in *Mecp2* KO mouse

Loss of MeCP2 in the mouse brain leads to favored usage of flop exon over the flip exon, which accelerates desensitization of the AMPA receptor and alters synaptic transmission. To functionally test whether the flip/flop defect is responsible for RTT disease progression, we treated *Mecp2* KO mice with Aniracetam, which could decelerate desensitization of the AMPA receptor. We started the treatment at about 4 weeks of age, when the KO mice are slightly underweight than wild type mice and do not show any RTT-related phenotypes (**Fig 19a-b**). The Aniracetam-treated wild type mice gained weight in a similar manner as vehicle-treated ones during the study, suggesting the dose of drug is well tolerated in mice (**Fig 19a**). In contrast, *Mecp2* KO mice start to lose weight at 7 weeks of age. Although Aniracetam could not delay the weight loss in KO mice, the average weight of Aniracetam-treated KO mice is slightly higher than mice in the vehicle group (**Fig 19a**). Besides body weight, we also monitor the disease progression based on the combined phenotypic scores of six parameters as previously described(Guy et al., 2007) (higher scores indicate more severe syndromes). We observed that KO mice treated with Aniracetam showed slightly less severe phenotypes than vehicle-treated mice (**Fig 19b**). Lastly, Aniracetam seemed to slightly prolong lifespan of the *Mecp2* KO mice compared to vehicle (**Fig 19c**). Taken together, this small pilot experiment of using Aniracetam to treat RTT mice showed some beneficial effects on disease progression of RTT mice and suggest it is worth of further investigation in the future.

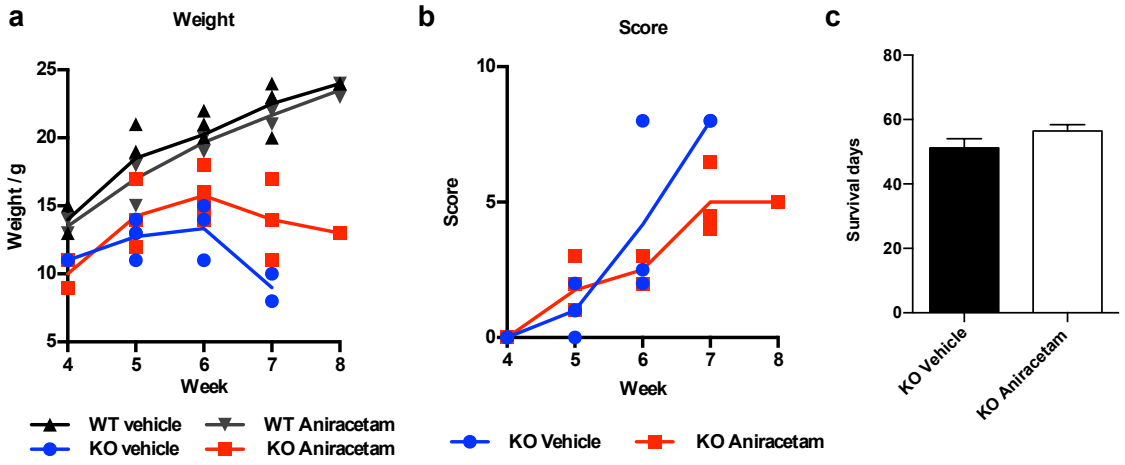

Fig 19. Aniracetam treatment might delay disease progression in RTT mouse.

(a) Weight change over the course of mouse receiving either vehicle or Aniracetam treatment. n=4 per group.

(b) Sum of phenotypic scores on mobility, gait, hindlimb clasping, tremor, breathing, and general condition over the course of mouse receiving either vehicle or Aniracetam treatment. n=4 per group.

(c) Average survival days of *Mecp2* KO mice treated with vehicle or Aniracetam. n=4 per group.

3.3 Discussion

MeCP2 has been previously implicated in regulating alternative splicing of RNA in two studies. In 2005, Young et al. reported RNA-dependent interaction between MeCP2 and YB1 in a neuroblastoma cell line forced to overexpress MeCP2 and some changes in alternative splicing in the *Mecp2*$^{308/y}$ brain(Young et al., 2005). In 2013, Maunakea et al. reported intragenic DNA methylation-dependent MeCP2 binding to alternatively spliced exons in cancer cell lines(Maunakea et al., 2013). Our work substantially extends these previous studies in several ways, and to our knowledge, this is the first report of the functional consequence for MeCP2-mediated splicing.

First, the physical interaction between MeCP2 and its interacting partners identified in our study are independent of any nucleic acid, suggesting that MeCP2 does not need to bind to RNA in order to regulate splicing. Additionally, these physical interactions have more physiological relevance, because they were identified in the mouse brain where MeCP2 is expressed from its endogenous locus. Furthermore, we identified multiple splicing factors as novel MeCP2-interacting partners in the brain. Since these factors are not part of the core splicing machinery but rather affect splicing as accessory splicing factors(Matera and Wang, 2014), the biochemical mechanism underlying their involvement in splicing regulation is not well known. Their interaction with MeCP2, a known chromatin protein, provides novel clues for studying how these factors regulate splicing. In addition, because we used a different RTT mouse model (*Mecp2* KO mice in our study vs. *Mecp2*$^{308/y}$ mice in Young et al) and a more sensitive method to profile alternative splicing (RNA-seq vs. microarray), the altered splicing events identified in our study were different from those previously identified by Young et al. Nonetheless, combining results from three independent unbiased approaches (Co-IP mass spectrometry, RNA-seq and

ChIP-seq), our study provides strong evidences for a significant involvement of MeCP2 in regulating RNA splicing.

Second, we discovered significant MeCP2 occupancy around exon/intron boundary and exons in the mouse brain, and characterized gene exon specific interaction between MeCP2 and two splicing regulators, providing a potential mechanism for MeCP2-dependent splicing regulation. Recent evidence suggests intragenic DNA methylation recruits MeCP2 and regulates pre-mRNA splicing through altering DNA polymerase II elongation rate(Maunakea et al., 2013). Our data, however, suggests that it is not responsible for the altered flip/flop splicing in the cortex of *Mecp2* KO mice. Instead, our results are suggesting a new model that co-occupancy of MeCP2 and LEDGF on the chromatin is required for the normal flip/flop splicing in the *Gria2* gene.

Finally, and most importantly, we established a functional link between specific splicing changes caused by the loss of MeCP2 function to synaptic changes in RTT mice. The fact that a ESF specifically rescues the flip/flop splicing defect can reverse the corresponding synaptic changes in RTT brain strongly suggest that the specific change in synaptic property (AMPAR kinetics) is caused by altered flip/flop splicing. Given the central role of AMPARs in synaptic transmission, it is likely the altered AMPAR kinetics will lead to altered synaptic functions other than the repetitive stimulation paradigm employed in our study. Future study is needed to mechanistically link the altered AMPAR kinetics with specific neuronal defects in RTT symptoms, and to evaluate the effect of reversing flip/flop splicing on RTT disease progression. In addition to the flip/flop choice in AMPARs, alterative splicing of several other genes (e.g. *Nrxn1*, *Dscam*, *lin7a*) that play important roles in synaptic functions were changed in the RTT mouse cortex, indicating that additional synaptic changes may be caused by splicing deficits.

Thus, altered RNA splicing appears to be a novel molecular mechanism underlying synaptic dysfunction in RTT.

Splicing misregulation has been increasingly recognized as a significant contributor to a number of neurological diseases, such as SMA(Pellizzoni et al., 1998), FTDP-17(D'Souza et al., 1999), ALS(Lagier-Tourenne et al., 2012) and myotonic dystrophy(Du et al., 2010). The mechanistic study of how the genes mutated in neurological diseases can directly affect alternative splicing, as well as the functional consequences of splicing alteration in such diseases, will have important implications in human health. Our study adds to the growing list of studies on the novel links between specific events of altered splicing and neurological diseases.

3.4 Methods and Materials

3.4.1 RNA-Seq Analysis

Total RNA was extracted from cortices of 6-weeks-old WT and *Mecp2* KO mice using Qiagen RNeasy Mini Plus kit. Genomic DNA was removed by a gDNA Eliminator column. 150ng total RNA was used to prepare sequencing library according to manufacturer's instructions (Nugen Encore Complete). Each Library was subject to one lane of 100bp single end sequencing using Illumina Hi-Seq 2000. Reads were mapped to the mouse genome (mm9) using Tophat (2.0.8). Reads count for each gene was calculated using htseq-count function in the HTSeq package. Differential gene expression analysis was done using edgeR in R. Splicing analysis was performed using the Mixture of Isoforms pipeline (MISO 0.4.7). Considering the high similarity of the two replicates for each genotype (Correlation = 0.98 for each), reads from two replicates were combined for each genotype and processed with MISO. A stringent filter (total reads for the event ≥ 1000, reads supporting inclusion or exclusion isoform ≥ 50, total reads supporting inclusion and exclusion isoform ≥ 100, $|\Delta PSI| \geq 0.20$ and Bayes-factor ≥ 20) was used to generate a list of differential splicing events. Read density plot was generated using sashimi plot built in MISO.

RNA-Seq data from Chen et al. 2015 PNAS and Gabel et al 2015 Nature were processed as above for splicing analysis. A less stringent filter (total reads for the event ≥ 20, $|\Delta PSI| \geq 0.05$ and Bayes-factor ≥ 1) was applied to allow for generating more events for further overlap analysis.

3.4.2 Gene Ontology Analysis

Gene Ontology (GO) analysis was done using DAVID(Huang da et al., 2009). Briefly, official gene symbols were submitted to DAVID. We used our own RNA-seq data and applied a cutoff of RPKM ≥ 0.5 to generate a list of genes expressed in the mouse cortex (13846 genes). This set of genes expressed in the mouse cortex was used as background for all GO analysis in this manuscript. Terms with Benjamini adjusted *P*-value <= 0.05 was considered as significant.

3.4.3 RNA extraction and qRT-PCR

Total RNA was extracted from cortices of 6-8-week-old wild type (WT) and *Mecp2* KO male mice or 15-18-month-old WT and *Mecp2* KO female mice using Qiagen RNeasy Mini Plus kit with on-column DNase treatment. RNA extraction from HEK293 or N2A cells was performed using TRIzol (Life Technology). RNA was reverse transcribed into cDNA using qScript cDNA SuperMix (Quanta Biosciences). qPCR was performed on an ABI Step-One plus machine using SYBR Green qPCR Master Mix (Biotool). *Gapdh* was used as endogenous control and $2^{-\Delta Ct}$ method was used to calculate fold change. See **Table S8** for primer sequence.

3.4.4 Chromatin Immunoprecipitation

Chromatin immunoprecipitation (ChIP) was performed as previously reported(Li et al., 2011). Briefly, cortex tissue was dissected from 6-8-week-old mice, minced and crosslinked in 1% formaldehyde (wt/vol) and sonicated using a Misonix 3000. Antibody was first bound to Dynabeads and then incubated with sheared chromatin overnight at 4°C. After 4 washes with RIPA buffer and 1 wash with TE buffer, bound chromatin was eluted and reverse crosslinked at 65°C overnight. Eluted DNA was treated with RNase A (Thermo Scientific) and proteinase K

(Promega), purified by phenol-chloroform extraction and dissolved in water. Antibodies used were: anti-Flag (Sigma M2), anti-LEDGF (Bethyl A300-847A), anti-H3K36me3 (Abcam ab9050), and anti-PolII (Abcam ab5408). Primer sequence for ChIP-qPCR is provided in **Table S8**.

3.4.5 ChIP-seq data analysis

ChIP-Seq data were generated from two biological replicates (referred to as WT1 and WT2). Raw data was aligned to the mouse genome version mm9 with Bowtie (0.12.7). After excluding non-mapping reads, we had 72, 221, 924 reads for WT1 ChIP and 31, 333, 769 for its input and 84, 871, 157 reads for WT2 ChIP and 22, 412, 408 for its input. We firstly evaluated the quality of these data with respect to ENCODE's ChIP-seq quality control metrics(Landt et al., 2012). The Normalized Strand Cross Correlation (NSC) for WT1 ChIP and WT2 ChIP is 1.3 and 1.4, respectively. Another quality control measure is PCR Bottleneck Coefficient (PBC), which gives an estimate of the complexity of the ChIP-seq library(Ballester et al., 2014). PBC<0.5 indicates PCR bottlenecks are present in sequenced libraries. The PBC ranged within [0.63 0.83] across WT1 ChIP sample and [0.85, 0.94] for the WT1 input sample. Similarly, the PBC ranged within [0.63 0.83] across WT2 ChIP sample and was 0.93 for the WT2 input sample. These numbers suggest our libraries were of good quality.

We carried out peak calling using MOSAiCS package in R(Kuan et al., 2011) using default parameters except for fdrRelaxed = 0.1 for WT1 and WT2 and fdrRelaxed = 0.2 for pooled replicates. Bin and fragment sizes were set to 200 bps for all the runs. We followed a conservative strategy and obtained peaks for individual replicates at false discovery rate of 0.1 and for pooled sample run at 0.2. Then, we identified the peaks in the intersection of the three

peak lists and filtered them with mosaics parameters: logMinP >= $-\log_{10}(0.05)$ & peakSize >= 150 & aveLog2Ratio >= $\log_2(1.5)$. This resulted in a total of 20, 652 peaks with median size of 1731 bps. We performed location analysis using mm9 Refseq genes and the nomenclature in Blahnik et al(Blahnik et al., 2010).

3.4.6 Gria2 minigene splicing assay

ESF construct was co-transfected into 293 cells with *Gria2* minigene (8:2 ratio) using GenJet transfection reagent (Signagen). To test the effect of *Mecp2* knockdown on *Gria2* splicing, shMecp2, *Mecp2* overexpression construct and Gria2 minigene (4.5:4.5:1 ratio) was co-transfected into N2A cells with using GenJet. To test the effect of *Ledgf* knockdown on *Gria2* splicing, shLedgf construct and *Gria2* minigene (9:1 ratio) was co-transfected into N2A cells using GenJet. Cells were lysed in TRIzol 48 hours after transfection for qRT-PCR analysis.

3.4.7 Electrophysiology

Male mice at 4-6 weeks postnatal were used. Coronal brain slices (400 μm) were prepared in ice-cold modified artificial cerebrospinal fluid (aCSF) (in mM: 124 NaCl, 2.5 KCl, 1 $CaCl_2$, 2 $MgSO_4$, 1.25 NaH_2PO_4, 26 $NaHCO_3$, and 15 glucose) bubbled with 95%O_2/5%CO_2. Then the slices were incubated in normal aCSF (in mM: 124 NaCl, 2.5 KCl, 2.5 $CaCl_2$, 1.2 $MgSO_4$, 1.25 NaH_2PO_4, 25 $NaHCO_3$, and 15 glucose) at room temperature for at least 1 hour and then transferred to a submerged recording chamber perfused with 95%O_2/5%CO_2 saturated aCSF for electrophysiological recordings. Whole-cell recording of mEPSCs and outside-out patch recording of glutamate-evoked currents was performed from the Layer 2/3 pyramidal neurons at room temperature. TTX (1 μM), D-APV (20 μM), bicuculline (50 μM) were added into the

perfused aCSF to block voltage gated Na^+ channels, NMDA receptors and GABA receptors respectively. The patch pipette (3–4 MΩ) solution contained (in mM): 140 Cs-Gluconate, 7.5 CsCl, 10 HEPES, 0.5 EGTA-Cs, 4 Mg-ATP, and 0.3 Li-GTP, pH 7.4. Raw data were amplified with a Multiclamp 700B amplifier and acquired with pClamp10.2 software (Molecular Devices). Neuronal currents were recorded under voltage clamp at the holding potential of -70 mV. An ALA fast perfusion system was used to perform application of glutamate (10 mM). In some experiments, CTZ (50 μM) was added. The detection of mEPSCs and exponential fitting were performed using Clampfit 10.2. The decay of glutamate evoked currents was fitted with double-exponential functions, and the fast- and slow- time constant were obtained. Signals were filtered at 2 Hz and sampled at 10 kHz by Digidata 1440A (Molecular Devices). mEPSCs were analyzed using the Template Search tool of the Clampfit10.2. To create the template, several well-shaped mEPSCs traces were picked and averaged to the template window. The mEPSCs events were accepted manually. Amplitude and the weighted time constant of decay phase of both mEPSCs and glutamate evoked currents were acquired.

To investigate whether enhanced depression of AMPAR responses to burst-type stimulations is expressed at synapses, we recorded excitatory postsynaptic potentials evoked through a bipolar stimulating electrode (FHC Inc.) placed in the white matter (eEPSCs, five pulses at 10 Hz). AMPAR-mediated eEPSCs were recorded in the presence of D-APV (20 μM) and bicuculline(50 μM) at a holding potential of -70 mV. The data was analyzed with Clampfit 10.

3.4.8 Lentivirus preparation and stereotaxic injection.

Lentivirus preparation was performed as described(Ananiev et al., 2011) except that we use minimum amount of media (leftover in the tubes) to resuspend the virus. Stereotaxic injection was done as previously described(Gao et al., 2015).

3.4.9 AAV infection.

Custom AAV was generated by Vigene. DIV7 primary cortical neurons were infected with AAV at a MOI of 10^5. AAV was removed 48 hours after infection and cells were collected 7 days after infection for qRT-PCR analysis.

3.4.10 Statistics.

No statistical procedure was used to predetermine sample size. Student's *t*-test was used to compare means between two groups. Multiple *t*-test comparisons were corrected using Benjamini-Hochberg procedure. One-way ANOVA followed by Tukey's multiple comparison tests was used to test difference in experiments with multiple groups. Two-way ANOVA with repeated measure followed by Bonferroni's multiple comparisons test was used for analysis in the repetitive stimulation experiments. Statistical calculation was performed using Microsoft Excel and Graphpad Prism.

Chapter 4: Conclusions and future directions

4.1 MeCP2-interacting proteins

4.1.1 Cell-type specific protein-protein interaction

Our coIP-Mass spectrometry experiments identified a number of novel MeCP2-interacting proteins. But we do not know whether the interaction between MeCP2 and these novel partners occurs in all cell types of the brain or only a specific group of cells because the information of cell-type specific protein-protein interaction is lost using whole brain homogenate as the starting material for co-immunoprecipitation. Cell-type specific protein-protein interaction is important for us to understand the contribution of a certain cell types and their role in the disease pathogenesis. For example, we know that astrocytes play an important role in the RTT pathogenesis(Ballas et al., 2009), but we know little about whether MeCP2 regulates gene expression in astrocytes through interacting the same set of transcriptional regulators as it does in neurons.

For simplicity, we will use astrocytes as an example to illustrate some potential approaches to answer this question. First, we can take a candidate approach: we can compare the interaction between MeCP2 and a list of known partners by co-immunoprecipitation and Western blot in astrocytes with that in whole brain. To specifically purify astrocytes from the mouse brain, we could take advantage of the resource from The Gene Expression Nervous System Atlas (GENSAT) Project, which has generated multiple transgenic mouse lines that carry a BAC reporter to label astrocytes in the brain. Alternatively, astrocytes differentiated from human pluripotent stem cells are another source that could be used to examine cell type specific protein-protein interactions(Krencik et al., 2011). The effectiveness of the candidate approach to reveal differential protein-protein interactions among different cell types relies on the list of MeCP2-

interacting protein being as complete as possible. Second, unique MeCP2-interacting proteins in astrocytes can be studied systematically by labeling proteins with isotope-coded affinity tag (ICAT) followed with quantitative mass spectrometry analysis(Berggard et al., 2007). By comparing the MeCP2 protein-protein interaction profile between whole brain and astrocytes, we could identify specific MeCP2 protein-protein interaction in astrocytes.

4.1.2 Functional importance of MeCP2-interacting proteins

4.1.2.1 MBD-fusion proteins

Studying protein-protein interactions advances our understanding of the functionality of MeCP2 and helps predict novel functions of this seemingly multifunctional protein. The strategy of inferring new functions of MeCP2 based on the evidence of interaction with proteins had successfully predicted the regulatory role of MeCP2 in alternative splicing, and will achieve more success in the future. The functional significance of the interaction itself, however, is rarely studied. Traditionally, similar questions were addressed by mutating a specific residue of the protein to disrupt the protein-protein interaction. For example, the tyrosine residue 306 (R306) of MeCP2 is frequently mutated in RTT patients and tyrosine to cysteine mutation abolishes interaction with NcoR/SMRT complex(Lyst et al., 2013). Although the R306C renders MeCP2 incapable to repress gene transcription in a reporter assay, it remains unclear whether such effect is mediated by loss of binding to NcoR/SMRT complex or other co-repressors or more likely, the collective loss of interaction with multiple co-repressors. It is hard to experimentally test whether R306C specifically disrupts the interaction of MeCP2 and NcoR/SMRT complex. Although we do not know the identities of other proteins with whom the interaction of MeCP2 is disrupted by R306C, it is highly likely R306C affects interaction with more than one protein complex.

Therefore, it is not ideal to test the functional significance of a protein-protein interaction by mutating the proteins.

MeCP2 binds to methylated DNA genome wide and regulates gene expression. The current model of the action of MeCP2 is that MBD is responsible for binding to DNA and TRD recruits protein partners to repress or activate transcription. Based on this model, TRD serves as an adaptor to recruit other proteins, and would be dispensable if MBD is fused to the interacting protein. Therefore, MBD-fusion protein mimics the MeCP2-protein complex. Using this strategy, we can test the functional significance of any MeCP2-protein interaction by expressing a MBD-fusion protein in MeCP2 deficient cells or animals. If a MBD-fusion protein can rescue one or several aspects of phenotypes due to MeCP2 deficiency, such as misregulation of gene expression, deficit of dendritic development, and shortened lifespan in mice, it would suggest that the MeCP2-protein interaction mediates at least part of the process.

One potential problem is that MBD-fusion protein would bind to chromatin and execute the same function regardless of context. However, MeCP2 interacts various kinds of protein on the chromatin and execute different functions depending on the chromatin context. For example, MeCP2 can serve as transcriptional repressor or activator when binding to different gene loci by interacting with repressors such as HDACs or activators such as CREB(Chahrour et al., 2008). Therefore, to enable the MBD-fusion protein strategy to work, we might need to first identify a few specific sites that the MeCP2-protein complex is at play in normal condition, and then specifically direct the MBD-fusion protein to those sites in MeCP2 deficient cells. CRISPR-Cas9 is versatile genome-editing tool that could be potentially engineered to target the MBD-fusion protein to desired sites. Although this idea of MBD-fusion protein is still in its infancy and needs a lot of further improvement, it is a feasible idea to start testing the functional significance of

MeCP2-protein interactions. It also has the potential to be extended to the study of the functional importance of any protein-protein interaction.

4.1.2.2 *In vivo* imaging of MeCP2-containing complex

Our coIP-MS and the following independent Western blot validation definitively demonstrated the interaction of MeCP2 with multiple splicing factors. We also obtained experimental evidence showing that MeCP2 and LEDGF co-occupy on the Gria2 flip or flop exon. But we have little information regarding when and where the protein-protein interaction occurs. To answer such question, we can label individual protein with respective high affinity mono-specific antibody and infer co-localiztion from signal overlap using fluorescence microscopy. Alternatively, we can tag proteins with different fluorescent proteins and rely on a technology called fluorescence resonance energy transfer (FRET) to visualize the protein-protein interaction in real time. Traditionally, this is achieved by overexpressing florescent protein-tagged proteins in a cell line and perform FRET assay using fluorescent microscopy. Such method suffers from the problem of overexpressing protein at much higher level than its physiological level. With the advent of versatile genome editing tools such as CRISPR-Cas9, one can easily tag any protein in its endogenous locus. In fact, the MeCP2::GFP mouse line has been created and used for immunopricipitation assay(Lyst et al., 2013). As a proof-of-principle experiment, a LEDGF::mCherry mouse line can be created and breed with the MeCP2::GFP line. The resulting MeCP2::GFP; LEDGF::mCherry mice line enables the *in vivo* visualization of MeCP2-LEDGF interaction(Albertazzi et al., 2009). With this tool, we can study the cell-type specific interaction between MeCP2 and LEDGF, the precise subcellular localization of MeCP2-LEDGF complex and the temporal occurrence of the complex using high-resolution microscopy. One more

potential application of this tool is to examine the genome wide distribution of the MeCP2-LEDGF complex using efficient and specific fluorescent protein antibodies. Coupled with data of the global splicing change upon loss of MeCP2 or LEDGF, data of the genome wide distribution of MeCP2-LEDGF enables the examination of potential patterns of the direct effect of MeCP2-LEDGF complex on splicing.

4.2 MeCP2 and alternative splicing

4.2.1 Brain region specific splicing changes

Similar to differential gene expression analysis, comparative analysis of splicing changes across three brain regions-cortex, hypothalamus and visual cortex-showed that only a proportion of splicing events were consistently changed between two different brain regions. An even smaller proportion of splicing events were changed in three brain regions. Two possibilities could account for this phenomenon. One possibility is that only overlapping splicing events of all three studies are MeCP2 direct target events and the other changed splicing events are the result of secondary effect. Integrated analysis of genome wide MeCP2 binding and splicing changes data would help define direct splicing targets for MeCP2. The other possibility is that some of the non-overlapping events were region-specific splicing changes upon loss of MeCP2. It is highly possible that splicing events in different brain regions react differently upon loss of MeCP2. The differential pattern of splicing changes could explain the distinct contributions of different brain regions to disease pathogenesis. In the future, experiments should be performed to identify brain region specific splicing changes because it will not only shed light on disease mechanism but also provide potential direction for therapeutic development.

4.2.2 Profiling splicing changes in specific cell types

Previous experiments using conditional knock out mouse have showed a differential contribution of different cell types in the brain to the RTT phenotypes(Guy et al., 2011). To understand how loss of MeCP2 causes malfunction of specific cell types, it is critical to profile both transcriptional changes and splicing changes because loss of MeCP2 has been repeatedly shown to regulate both gene transcription and pre-mRNA splicing. As mentioned in 4.1.1, astrocytes are an important cell type that affects the disease progression of Rett syndrome. MeCP2 deficient astrocytes have adverse non-cell autonomous effects on wild type and mutant neurons, but the underlying mechanism is not clear(Williams et al., 2014). We propose to profile the splicing changes in *Mecp2* null astrocytes as the first step to understand how loss of MeCP2 leads to malfunction of astrocytes. We will primarily focus on the alternative splicing of secreted factors because secreted factors might mediate the non-cell autonomous effects of the *Mecp2* null astrocytes.

4.2.3 Dynamics of flip/flop splicing changes

The flip/flop alternative splicing is developmentally regulated. The flip isoform is expressed at a high level in newborn mice and maintains a similar level throughout development, whereas the flop isoform gradually increase to a comparable level as the flip isoform in adulthood(Sommer et al., 1990). Therefore, the flip/flop ratio is gradually decreasing over the course of development. Our data reflects such a transition of the flip/flop ratio (ratio is higher is 4-5 weeks old WT mice compared with 6-weeks old WT mice). Loss of MeCP2 accelerates the transition and results in significant lower flip/flop ratio in *Mecp2* KO at both 4-5 and 6 weeks of age. Interestingly, the flip/flop ratio is not changed at postnatal day 0 (P0) probably because MeCP2 is expressed at a

low level at P0. As MeCP2 rises during the early postnatal development, any effect mediated by loss of MeCP2 would become more drastic. Therefore, we expect that the differential flip/flop ratio would begin to show during this period. We propose to examine the flip/flop ratio at P7, P14 and P21 in WT and *Mecp2* KO mice so that we can define the exact starting time point when significant flip/flop change occurs. Such information would help us determine the timing to start correcting the flip/flop splicing defect in the *Mecp2* KO mice without causing any undesired changes.

4.2.4 Contribution of splicing changes to RTT phenotypes

Our experimental data shows that reversing flip/flop change specifically by ESF-flop-Gly can rescue the deficits of AMPA receptor desensitization and synaptic transmission. Moreover, administration of an AMPA receptor modulator, Aniracetam, might alleviate RTT features and slightly prolong lifespan of the *Mecp2* KO mice, indicating that flip/flop splicing change contributes to the RTT pathogenesis. We only observed modest effect of Aniracetam in improving the syndromes probably because flip/flop splicing change is just one of hundreds of splicing abnormalities in the *Mecp2* KO mice. To evaluate the potential contribution of other splicing defects to RTT phenotypes, we should correct them and test whether the phenotypes can be rescued. We propose to start with splicing changes that could affect synaptic functions, such as splicing alteration in *Nrxn1*, *Usp14*, *let-7a*, *Dscam,* and *Gprin1*, because splicing dysfunction is a hallmark of RTT syndrome.

CRISPR-Cas9 is a versatile genome-editing tool that could potentially be used to edit RNA and modulate the activity of RNA-processing enzymes(Nelles et al., 2016; O'Connell et al., 2014). By attaching a splicing modulation domain to the Cas9 protein, we could program the

CRISPR-Cas9 to bind to any specific sequence of pre-mRNA and modulate the alternative splicing of any desired exon. The programmable nature of CRISPR-Cas9 also enables splicing regulation in multiple pre-mRNA transcripts simultaneously. With this tool, we can potentially correct the splicing defect in multiple synaptic genes simultaneously in the *Mecp2* KO mice so that we could evaluate the contribution of aberrant splicing of this group of genes to the disease pathogenesis.

4.2.5 Mechanism underlying MeCP2-mediated splicing regulation on *Gria2* flip/flop exons

Splicing analysis of RNA-Seq data from *Mecp2* KO and *MECP2*^{tg} mice suggested MeCP2 directly regulates the alternative splicing of *Gria2* flip/flop exon. Moreover, knockdown of MeCP2 also resulted in misregulation of *Gria2* flip/flop splicing, further supporting the direct regulatory role of MeCP2 in the flip/flop splicing. To understand the underlying mechanism, we explored whether MeCP2 regulates flip/flop splicing through affecting the elongation rate of PolII complex or enrichment of H3K36me3, two well-established models in how epigenetic information can modulate splicing. Our experimental data, however, rejected these hypotheses. In addition, although occupancy of H3K9me3 is significantly reduced on flip and flop exon in MeCP2 deficient cortex, these changes are not unique to flip or flop exon and might be just a global effect due to reduced expression of a H3K9 trimethylation enzyme, Suv39h2. H3K36me3 and H3K9me3 are not the only histone modifications involved in splicing regulation. In the future, experiments should be performed to systematically profile the histone modification change on *Gria2* locus between wild type and *Mecp2* KO cortex.

LEDGF knockdown mimics the effect of loss of MeCP2 in the regulation of flip/flop splicing, suggesting LEDGF is involved in the process. To further understand the significance of LEDGF

in the regulation of splicing, we could conditionally delete *Ledgf* in the brain and profile splicing changes to see whether loss of LEDGF results in similar splicing changes as loss of MeCP2. To examine the role of LEDGF in RTT syndrome pathogenesis, we could test whether the deletion of *Ledgf* accelerates the disease progression of *Mecp2* KO mice and overexpression of LEDGF rescues some aspects of RTT phenotypes.

4.2.6 Correction of aberrant flip/flop splicing in *Mecp2* KO mice

Administration of an AMPA receptor modulator, Aniracetam, only slightly improves RTT syndromes in *Mecp2* KO mice. A number of factors could account for the modest effect of Aniracetam. One factor is the timing of starting the treatment. We began injecting Aniracetam to mice at around 4-weeks of age when *Mecp2* KO mice are still at the presyndromatic phase. Our qRT-PCR result showed that flip/flop splicing is significantly changed in *Mecp2* KO mice at 4-5 weeks of age. To maximize the efficacy of Aniracetam, we need to determine the earliest time point when aberrant flip/flop splicing occurs, and start treating mice with Aniracetam on or before that time point. Another factor is the way of the treatment. We administered Aniracetam to mice daily by intraperitoneal injection. Such treatment scheme, although well tolerated in wild type animals, might cause adverse yet unnoticeable effects.

ESF-Gly-flop can specifically reverse the aberrant flip/flop splicing in the *Mecp2* KO mice. AAV delivery of ESF-Gly-flop can serve as an alternative method to test whether correction of aberrant flip/flop splicing is beneficial to *Mecp2* KO mice. To that end, we injected AAV encoding ESF-Gly-flop into the ventricles of wild type and *Mecp2* KO mice at about one week of age. Unfortunately, both wild type and *Mecp2* KO mice died or chewed by their mother within 2 weeks after injection, but the same procedure on litters of different genetic background did not

result in early death of pups. We generated the male *Mecp2* KO mice by crossing a heterozygous female with wild type male mice. We have always noticed that the heterozygous mothers have problems in taking care of pups and are unable to retrieve dispersed pups. In the future, we could avoid using $Mecp2^{+/-}$ mice as breeder but instead breed $Mecp2^{2loxP/2loxP}$ female with Nestin-Cre male mice to generate conditional knockout mice. Besides the problem of unexpected early death, injecting AAV into ventricles of mice within one week after birth only results in infection of about 50% of all cells in the brain. To increase infection efficiency, we could adjust the dose of virus or perform systematic tail vein injection instead of brain-directed ventricle injection in the future.

Alternatively, we can generate a transgenic mouse by inserting the inducible ESF-Gly-flop expression cassette in the *AAVS* locus. By crossing with the $Mecp2^{+/-}$ female mice, we could place the inducible ESF-Gly-flop expression cassette in the *Mecp2* KO mice and start expressing ESF-Gly-flop at any desired time point. With this tool, we can easily manipulate the flip/flop splicing and test its effects on RTT pathogenesis.

References

Adams, V.H., McBryant, S.J., Wade, P.A., Woodcock, C.L., and Hansen, J.C. (2007). Intrinsic disorder and autonomous domain function in the multifunctional nuclear protein, MeCP2. The Journal of biological chemistry *282*, 15057-15064.
Agarwal, N., Hardt, T., Brero, A., Nowak, D., Rothbauer, U., Becker, A., Leonhardt, H., and Cardoso, M.C. (2007). MeCP2 interacts with HP1 and modulates its heterochromatin association during myogenic differentiation. Nucleic Acids Res *35*, 5402-5408.
Albertazzi, L., Arosio, D., Marchetti, L., Ricci, F., and Beltram, F. (2009). Quantitative FRET analysis with the EGFP-mCherry fluorescent protein pair. Photochem Photobiol *85*, 287-297.
Amir, R.E., Van den Veyver, I.B., Wan, M., Tran, C.Q., Francke, U., and Zoghbi, H.Y. (1999). Rett syndrome is caused by mutations in X-linked MECP2, encoding methyl-CpG-binding protein 2. Nat Genet *23*, 185-188.
Amir, R.E., and Zoghbi, H.Y. (2000). Rett syndrome: methyl-CpG-binding protein 2 mutations and phenotype-genotype correlations. Am J Med Genet *97*, 147-152.
Ananiev, G., Williams, E.C., Li, H., and Chang, Q. (2011). Isogenic pairs of wild type and mutant induced pluripotent stem cell (iPSC) lines from Rett syndrome patients as in vitro disease model. PloS one *6*, e25255.
Anastasiadou, C., Malousi, A., Maglaveras, N., and Kouidou, S. (2011). Human epigenome data reveal increased CpG methylation in alternatively spliced sites and putative exonic splicing enhancers. DNA Cell Biol *30*, 267-275.
Anczukow, O., Akerman, M., Clery, A., Wu, J., Shen, C., Shirole, N.H., Raimer, A., Sun, S., Jensen, M.A., Hua, Y.*, et al.* (2015). SRSF1-Regulated Alternative Splicing in Breast Cancer. Mol Cell *60*, 105-117.
Armstrong, D., Dunn, J.K., Antalffy, B., and Trivedi, R. (1995). Selective dendritic alterations in the cortex of Rett syndrome. J Neuropathol Exp Neurol *54*, 195-201.
Armstrong, D.D., Dunn, K., and Antalffy, B. (1998). Decreased dendritic branching in frontal, motor and limbic cortex in Rett syndrome compared with trisomy 21. J Neuropathol Exp Neurol *57*, 1013-1017.
Auboeuf, D., Honig, A., Berget, S.M., and O'Malley, B.W. (2002). Coordinate regulation of transcription and splicing by steroid receptor coregulators. Science *298*, 416-419.
Baker, S.A., Chen, L., Wilkins, A.D., Yu, P., Lichtarge, O., and Zoghbi, H.Y. (2013). An AT-hook domain in MeCP2 determines the clinical course of Rett syndrome and related disorders. Cell *152*, 984-996.
Ballas, N., Lioy, D.T., Grunseich, C., and Mandel, G. (2009). Non-cell autonomous influence of MeCP2-deficient glia on neuronal dendritic morphology. Nat Neurosci *12*, 311-317.
Ballester, B., Medina-Rivera, A., Schmidt, D., Gonzalez-Porta, M., Carlucci, M., Chen, X., Chessman, K., Faure, A.J., Funnell, A.P., Goncalves, A.*, et al.* (2014). Multi-species, multi-transcription factor binding highlights conserved control of tissue-specific biological pathways. Elife *3*, e02626.
Balmer, D., Goldstine, J., Rao, Y.M., and LaSalle, J.M. (2003). Elevated methyl-CpG-binding protein 2 expression is acquired during postnatal human brain development and is correlated with alternative polyadenylation. J Mol Med (Berl) *81*, 61-68.
Bauman, M.L., Kemper, T.L., and Arin, D.M. (1995). Pervasive neuroanatomic abnormalities of the brain in three cases of Rett's syndrome. Neurology *45*, 1581-1586.

Becker, A., Zhang, P., Allmann, L., Meilinger, D., Bertulat, B., Eck, D., Hofstaetter, M., Bartolomei, G., Hottiger, M.O., Schreiber, V.*, et al.* (2016). Poly(ADP-ribosyl)ation of Methyl CpG Binding Domain Protein 2 Regulates Chromatin Structure. The Journal of biological chemistry *291*, 4873-4881.
Belichenko, P.V., Oldfors, A., Hagberg, B., and Dahlstrom, A. (1994). Rett syndrome: 3-D confocal microscopy of cortical pyramidal dendrites and afferents. Neuroreport *5*, 1509-1513.
Berggard, T., Linse, S., and James, P. (2007). Methods for the detection and analysis of protein-protein interactions. Proteomics *7*, 2833-2842.
Beyer, A.L., and Osheim, Y.N. (1988). Splice site selection, rate of splicing, and alternative splicing on nascent transcripts. Genes Dev *2*, 754-765.
Blahnik, K.R., Dou, L., O'Geen, H., McPhillips, T., Xu, X., Cao, A.R., Iyengar, S., Nicolet, C.M., Ludascher, B., Korf, I.*, et al.* (2010). Sole-Search: an integrated analysis program for peak detection and functional annotation using ChIP-seq data. Nucleic Acids Res *38*, e13.
Bracaglia, G., Conca, B., Bergo, A., Rusconi, L., Zhou, Z., Greenberg, M.E., Landsberger, N., Soddu, S., and Kilstrup-Nielsen, C. (2009). Methyl-CpG-binding protein 2 is phosphorylated by homeodomain-interacting protein kinase 2 and contributes to apoptosis. EMBO Rep *10*, 1327-1333.
Calfa, G., Percy, A.K., and Pozzo-Miller, L. (2011). Experimental models of Rett syndrome based on Mecp2 dysfunction. Exp Biol Med (Maywood) *236*, 3-19.
Cartegni, L., and Krainer, A.R. (2002). Disruption of an SF2/ASF-dependent exonic splicing enhancer in SMN2 causes spinal muscular atrophy in the absence of SMN1. Nat Genet *30*, 377-384.
Chahrour, M., Jung, S.Y., Shaw, C., Zhou, X., Wong, S.T.C., Qin, J., and Zoghbi, H.Y. (2008). MeCP2, a key contributor to neurological disease, activates and represses transcription. Science *320*, 1224-1229.
Chahrour, M., and Zoghbi, H.Y. (2007). The story of Rett syndrome: from clinic to neurobiology. Neuron *56*, 422-437.
Chandler, S.P., Guschin, D., Landsberger, N., and Wolffe, A.P. (1999). The methyl-CpG binding transcriptional repressor MeCP2 stably associates with nucleosomal DNA. Biochemistry *38*, 7008-7018.
Chang, Q., Khare, G., Dani, V., Nelson, S., and Jaenisch, R. (2006). The disease progression of Mecp2 mutant mice is affected by the level of BDNF expression. Neuron *49*, 341-348.
Chao, H.T., Chen, H., Samaco, R.C., Xue, M., Chahrour, M., Yoo, J., Neul, J.L., Gong, S., Lu, H.C., Heintz, N.*, et al.* (2010). Dysfunction in GABA signalling mediates autism-like stereotypies and Rett syndrome phenotypes. Nature *468*, 263-269.
Chasin, L.A. (2007). Searching for splicing motifs. Adv Exp Med Biol *623*, 85-106.
Chen, L., Chen, K., Lavery, L.A., Baker, S.A., Shaw, C.A., Li, W., and Zoghbi, H.Y. (2015). MeCP2 binds to non-CG methylated DNA as neurons mature, influencing transcription and the timing of onset for Rett syndrome. Proc Natl Acad Sci U S A *112*, 5509-5514.
Chen, M., and Manley, J.L. (2009). Mechanisms of alternative splicing regulation: insights from molecular and genomics approaches. Nat Rev Mol Cell Biol *10*, 741-754.
Chen, R.Z., Akbarian, S., Tudor, M., and Jaenisch, R. (2001). Deficiency of methyl-CpG binding protein-2 in CNS neurons results in a Rett-like phenotype in mice. Nat Genet *27*, 327-331.
Chen, W.G., Chang, Q., Lin, Y., Meissner, A., West, A.E., Griffith, E.C., Jaenisch, R., and Greenberg, M.E. (2003). Derepression of BDNF transcription involves calcium-dependent phosphorylation of MeCP2. Science *302*, 885-889.

Cheng, J., Huang, M., Zhu, Y., Xin, Y.J., Zhao, Y.K., Huang, J., Yu, J.X., Zhou, W.H., and Qiu, Z. (2014a). SUMOylation of MeCP2 is essential for transcriptional repression and hippocampal synapse development. J Neurochem *128*, 798-806.
Cheng, T.L., Wang, Z., Liao, Q., Zhu, Y., Zhou, W.H., Xu, W., and Qiu, Z. (2014b). MeCP2 suppresses nuclear microRNA processing and dendritic growth by regulating the DGCR8/Drosha complex. Dev Cell *28*, 547-560.
Cheung, A.Y., Horvath, L.M., Grafodatskaya, D., Pasceri, P., Weksberg, R., Hotta, A., Carrel, L., and Ellis, J. (2011). Isolation of MECP2-null Rett Syndrome patient hiPS cells and isogenic controls through X-chromosome inactivation. Hum Mol Genet *20*, 2103-2115.
Cheval, H., Guy, J., Merusi, C., De Sousa, D., Selfridge, J., and Bird, A. (2012). Postnatal inactivation reveals enhanced requirement for MeCP2 at distinct age windows. Hum Mol Genet *21*, 3806-3814.
Chodavarapu, R.K., Feng, S., Bernatavichute, Y.V., Chen, P.Y., Stroud, H., Yu, Y., Hetzel, J.A., Kuo, F., Kim, J., Cokus, S.J.*, et al.* (2010). Relationship between nucleosome positioning and DNA methylation. Nature *466*, 388-392.
Choi, J.K. (2010). Contrasting chromatin organization of CpG islands and exons in the human genome. Genome Biol *11*, R70.
Choudhury, R., Roy, S.G., Tsai, Y.S., Tripathy, A., Graves, L.M., and Wang, Z. (2014). The splicing activator DAZAP1 integrates splicing control into MEK/Erk-regulated cell proliferation and migration. Nature communications *5*, 3078.
Cirignotta, F., Lugaresi, E., and Montagna, P. (1986). Breathing impairment in Rett syndrome. Am J Med Genet Suppl *1*, 167-173.
Cohen, S., Gabel, H.W., Hemberg, M., Hutchinson, A.N., Sadacca, L.A., Ebert, D.H., Harmin, D.A., Greenberg, R.S., Verdine, V.K., Zhou, Z.*, et al.* (2011). Genome-wide activity-dependent MeCP2 phosphorylation regulates nervous system development and function. Neuron *72*, 72-85.
Collins, A.L., Levenson, J.M., Vilaythong, A.P., Richman, R., Armstrong, D.L., Noebels, J.L., David Sweatt, J., and Zoghbi, H.Y. (2004). Mild overexpression of MeCP2 causes a progressive neurological disorder in mice. Hum Mol Genet *13*, 2679-2689.
Coy, J.F., Sedlacek, Z., Bachner, D., Delius, H., and Poustka, A. (1999). A complex pattern of evolutionary conservation and alternative polyadenylation within the long 3"-untranslated region of the methyl-CpG-binding protein 2 gene (MeCP2) suggests a regulatory role in gene expression. Hum Mol Genet *8*, 1253-1262.
D'Souza, I., Poorkaj, P., Hong, M., Nochlin, D., Lee, V.M., Bird, T.D., and Schellenberg, G.D. (1999). Missense and silent tau gene mutations cause frontotemporal dementia with parkinsonism-chromosome 17 type, by affecting multiple alternative RNA splicing regulatory elements. Proceedings of the National Academy of Sciences of the United States of America *96*, 5598-5603.
Daoud, H., Valdmanis, P.N., Kabashi, E., Dion, P., Dupre, N., Camu, W., Meininger, V., and Rouleau, G.A. (2009). Contribution of TARDBP mutations to sporadic amyotrophic lateral sclerosis. J Med Genet *46*, 112-114.
de la Mata, M., Alonso, C.R., Kadener, S., Fededa, J.P., Blaustein, M., Pelisch, F., Cramer, P., Bentley, D., and Kornblihtt, A.R. (2003). A slow RNA polymerase II affects alternative splicing in vivo. Mol Cell *12*, 525-532.
de la Mata, M., Lafaille, C., and Kornblihtt, A.R. (2010). First come, first served revisited: factors affecting the same alternative splicing event have different effects on the relative rates of intron removal. RNA *16*, 904-912.

del Gaudio, D., Fang, P., Scaglia, F., Ward, P.A., Craigen, W.J., Glaze, D.G., Neul, J.L., Patel, A., Lee, J.A., Irons, M.*, et al.* (2006). Increased MECP2 gene copy number as the result of genomic duplication in neurodevelopmentally delayed males. Genet Med *8*, 784-792.
Du, H., Cline, M.S., Osborne, R.J., Tuttle, D.L., Clark, T.A., Donohue, J.P., Hall, M.P., Shiue, L., Swanson, M.S., Thornton, C.A.*, et al.* (2010). Aberrant alternative splicing and extracellular matrix gene expression in mouse models of myotonic dystrophy. Nat Struct Mol Biol *17*, 187-193.
Ebert, D.H., Gabel, H.W., Robinson, N.D., Kastan, N.R., Hu, L.S., Cohen, S., Navarro, A.J., Lyst, M.J., Ekiert, R., Bird, A.P.*, et al.* (2013). Activity-dependent phosphorylation of MeCP2 threonine 308 regulates interaction with NCoR. Nature *499*, 341-345.
Feng, S., Cokus, S.J., Zhang, X., Chen, P.Y., Bostick, M., Goll, M.G., Hetzel, J., Jain, J., Strauss, S.H., Halpern, M.E.*, et al.* (2010). Conservation and divergence of methylation patterning in plants and animals. Proc Natl Acad Sci U S A *107*, 8689-8694.
Forlani, G., Giarda, E., Ala, U., Di Cunto, F., Salani, M., Tupler, R., Kilstrup-Nielsen, C., and Landsberger, N. (2010). The MeCP2/YY1 interaction regulates ANT1 expression at 4q35: novel hints for Rett syndrome pathogenesis. Hum Mol Genet *19*, 3114-3123.
Fuks, F., Hurd, P.J., Wolf, D., Nan, X., Bird, A.P., and Kouzarides, T. (2003). The methyl-CpG-binding protein MeCP2 links DNA methylation to histone methylation. The Journal of biological chemistry *278*, 4035-4040.
Fyffe, S.L., Neul, J.L., Samaco, R.C., Chao, H.T., Ben-Shachar, S., Moretti, P., McGill, B.E., Goulding, E.H., Sullivan, E., Tecott, L.H.*, et al.* (2008). Deletion of Mecp2 in Sim1-expressing neurons reveals a critical role for MeCP2 in feeding behavior, aggression, and the response to stress. Neuron *59*, 947-958.
Gabel, H.W., Kinde, B., Stroud, H., Gilbert, C.S., Harmin, D.A., Kastan, N.R., Hemberg, M., Ebert, D.H., and Greenberg, M.E. (2015). Disruption of DNA-methylation-dependent long gene repression in Rett syndrome. Nature *522*, 89-93.
Gao, Y., Su, J., Guo, W., Polich, E.D., Magyar, D.P., Xing, Y., Li, H., Smrt, R.D., Chang, Q., and Zhao, X. (2015). Inhibition of miR-15a Promotes BDNF Expression and Rescues Dendritic Maturation Deficits in MeCP2-Deficient Neurons. Stem Cells *33*, 1618-1629.
Gemelli, T., Berton, O., Nelson, E.D., Perrotti, L.I., Jaenisch, R., and Monteggia, L.M. (2006). Postnatal loss of methyl-CpG binding protein 2 in the forebrain is sufficient to mediate behavioral aspects of Rett syndrome in mice. Biol Psychiatry *59*, 468-476.
Georgel, P.T., Horowitz-Scherer, R.A., Adkins, N., Woodcock, C.L., Wade, P.A., and Hansen, J.C. (2003). Chromatin compaction by human MeCP2. Assembly of novel secondary chromatin structures in the absence of DNA methylation. The Journal of biological chemistry *278*, 32181-32188.
Giacometti, E., Luikenhuis, S., Beard, C., and Jaenisch, R. (2007). Partial rescue of MeCP2 deficiency by postnatal activation of MeCP2. Proc Natl Acad Sci U S A *104*, 1931-1936.
Goffin, D., Allen, M., Zhang, L., Amorim, M., Wang, I.T., Reyes, A.R., Mercado-Berton, A., Ong, C., Cohen, S., Hu, L.*, et al.* (2012). Rett syndrome mutation MeCP2 T158A disrupts DNA binding, protein stability and ERP responses. Nat Neurosci *15*, 274-283.
Gonzales, M.L., Adams, S., Dunaway, K.W., and LaSalle, J.M. (2012). Phosphorylation of distinct sites in MeCP2 modifies cofactor associations and the dynamics of transcriptional regulation. Mol Cell Biol *32*, 2894-2903.

Goren, A., Ram, O., Amit, M., Keren, H., Lev-Maor, G., Vig, I., Pupko, T., and Ast, G. (2006). Comparative analysis identifies exonic splicing regulatory sequences--The complex definition of enhancers and silencers. Mol Cell *22*, 769-781.
Guo, J.U., Su, Y., Shin, J.H., Shin, J., Li, H., Xie, B., Zhong, C., Hu, S., Le, T., Fan, G.*, et al.* (2014). Distribution, recognition and regulation of non-CpG methylation in the adult mammalian brain. Nat Neurosci *17*, 215-222.
Guy, J., Cheval, H., Selfridge, J., and Bird, A. (2011). The role of MeCP2 in the brain. Annu Rev Cell Dev Biol *27*, 631-652.
Guy, J., Gan, J., Selfridge, J., Cobb, S., and Bird, A. (2007). Reversal of neurological defects in a mouse model of Rett syndrome. Science *315*, 1143-1147.
Guy, J., Hendrich, B., Holmes, M., Martin, J.E., and Bird, A. (2001). A mouse Mecp2-null mutation causes neurological symptoms that mimic Rett syndrome. Nat Genet *27*, 322-326.
Hagberg, B. (1985). Rett's syndrome: prevalence and impact on progressive severe mental retardation in girls. Acta Paediatr Scand *74*, 405-408.
Hagberg, B. (2002). Clinical manifestations and stages of Rett syndrome. Ment Retard Dev Disabil Res Rev *8*, 61-65.
Hagberg, B., Aicardi, J., Dias, K., and Ramos, O. (1983). A progressive syndrome of autism, dementia, ataxia, and loss of purposeful hand use in girls: Rett's syndrome: report of 35 cases. Ann Neurol *14*, 471-479.
Hagberg, B.A., and Skjeldal, O.H. (1994). Rett variants: a suggested model for inclusion criteria. Pediatr Neurol *11*, 5-11.
Han, K., Gennarino, V.A., Lee, Y., Pang, K., Hashimoto-Torii, K., Choufani, S., Raju, C.S., Oldham, M.C., Weksberg, R., Rakic, P.*, et al.* (2013). Human-specific regulation of MeCP2 levels in fetal brains by microRNA miR-483-5p. Genes Dev *27*, 485-490.
Han, S.P., Tang, Y.H., and Smith, R. (2010). Functional diversity of the hnRNPs: past, present and perspectives. Biochem J *430*, 379-392.
Harikrishnan, K.N., Chow, M.Z., Baker, E.K., Pal, S., Bassal, S., Brasacchio, D., Wang, L., Craig, J.M., Jones, P.L., Sif, S.*, et al.* (2005). Brahma links the SWI/SNF chromatin-remodeling complex with MeCP2-dependent transcriptional silencing. Nat Genet *37*, 254-264.
Hu, K., Nan, X., Bird, A., and Wang, W. (2006). Testing for association between MeCP2 and the brahma-associated SWI/SNF chromatin-remodeling complex. Nat Genet *38*, 962-964; author reply 964-967.
Huang da, W., Sherman, B.T., and Lempicki, R.A. (2009). Systematic and integrative analysis of large gene lists using DAVID bioinformatics resources. Nature protocols *4*, 44-57.
Itoh, M., Tahimic, C.G., Ide, S., Otsuki, A., Sasaoka, T., Noguchi, S., Oshimura, M., Goto, Y., and Kurimasa, A. (2012). Methyl CpG-binding protein isoform MeCP2_e2 is dispensable for Rett syndrome phenotypes but essential for embryo viability and placenta development. The Journal of biological chemistry *287*, 13859-13867.
Jellinger, K., Armstrong, D., Zoghbi, H.Y., and Percy, A.K. (1988). Neuropathology of Rett syndrome. Acta Neuropathol *76*, 142-158.
Jellinger, K., and Seitelberger, F. (1986). Neuropathology of Rett syndrome. Am J Med Genet Suppl *1*, 259-288.
Jiang, Y., Matevossian, A., Huang, H.S., Straubhaar, J., and Akbarian, S. (2008). Isolation of neuronal chromatin from brain tissue. BMC Neurosci *9*, 42.

Johnson, R.A., Lam, M., Punzo, A.M., Li, H., Lin, B.R., Ye, K., Mitchell, G.S., and Chang, Q. (2012). 7,8-dihydroxyflavone exhibits therapeutic efficacy in a mouse model of Rett syndrome. J Appl Physiol (1985) *112*, 704-710.
Jones, P.L., Veenstra, G.J., Wade, P.A., Vermaak, D., Kass, S.U., Landsberger, N., Strouboulis, J., and Wolffe, A.P. (1998). Methylated DNA and MeCP2 recruit histone deacetylase to repress transcription. Nat Genet *19*, 187-191.
Kabashi, E., Valdmanis, P.N., Dion, P., Spiegelman, D., McConkey, B.J., Vande Velde, C., Bouchard, J.P., Lacomblez, L., Pochigaeva, K., Salachas, F.*, et al.* (2008). TARDBP mutations in individuals with sporadic and familial amyotrophic lateral sclerosis. Nat Genet *40*, 572-574.
Kadener, S., Cramer, P., Nogues, G., Cazalla, D., de la Mata, M., Fededa, J.P., Werbajh, S.E., Srebrow, A., and Kornblihtt, A.R. (2001). Antagonistic effects of T-Ag and VP16 reveal a role for RNA pol II elongation on alternative splicing. EMBO J *20*, 5759-5768.
Kashima, T., Rao, N., and Manley, J.L. (2007). An intronic element contributes to splicing repression in spinal muscular atrophy. Proc Natl Acad Sci U S A *104*, 3426-3431.
Katz, Y., Wang, E.T., Airoldi, E.M., and Burge, C.B. (2010). Analysis and design of RNA sequencing experiments for identifying isoform regulation. Nature methods *7*, 1009-1015.
Kernohan, K.D., Jiang, Y., Tremblay, D.C., Bonvissuto, A.C., Eubanks, J.H., Mann, M.R., and Berube, N.G. (2010). ATRX partners with cohesin and MeCP2 and contributes to developmental silencing of imprinted genes in the brain. Dev Cell *18*, 191-202.
Kerr, A.M., Armstrong, D.D., Prescott, R.J., Doyle, D., and Kearney, D.L. (1997). Rett syndrome: analysis of deaths in the British survey. Eur Child Adolesc Psychiatry *6 Suppl 1*, 71-74.
Kimura, H., and Shiota, K. (2003). Methyl-CpG-binding protein, MeCP2, is a target molecule for maintenance DNA methyltransferase, Dnmt1. The Journal of biological chemistry *278*, 4806-4812.
Kishi, N., and Macklis, J.D. (2004). MECP2 is progressively expressed in post-migratory neurons and is involved in neuronal maturation rather than cell fate decisions. Mol Cell Neurosci *27*, 306-321.
Kokura, K., Kaul, S.C., Wadhwa, R., Nomura, T., Khan, M.M., Shinagawa, T., Yasukawa, T., Colmenares, C., and Ishii, S. (2001). The Ski protein family is required for MeCP2-mediated transcriptional repression. The Journal of biological chemistry *276*, 34115-34121.
Krencik, R., Weick, J.P., Liu, Y., Zhang, Z.J., and Zhang, S.C. (2011). Specification of transplantable astroglial subtypes from human pluripotent stem cells. Nat Biotechnol *29*, 528-534.
Kriaucionis, S., and Bird, A. (2004). The major form of MeCP2 has a novel N-terminus generated by alternative splicing. Nucleic Acids Res *32*, 1818-1823.
Kuan, P.F., Chung, D., Pan, G., Thomson, J.A., Stewart, R., and Keles, S. (2011). A Statistical Framework for the Analysis of ChIP-Seq Data. J Am Stat Assoc *106*, 891-903.
Lagier-Tourenne, C., Polymenidou, M., Hutt, K.R., Vu, A.Q., Baughn, M., Huelga, S.C., Clutario, K.M., Ling, S.C., Liang, T.Y., Mazur, C.*, et al.* (2012). Divergent roles of ALS-linked proteins FUS/TLS and TDP-43 intersect in processing long pre-mRNAs. Nature neuroscience *15*, 1488-1497.
Landt, S.G., Marinov, G.K., Kundaje, A., Kheradpour, P., Pauli, F., Batzoglou, S., Bernstein, B.E., Bickel, P., Brown, J.B., Cayting, P.*, et al.* (2012). ChIP-seq guidelines and practices of the ENCODE and modENCODE consortia. Genome Res *22*, 1813-1831.

Lawson-Yuen, A., Liu, D., Han, L., Jiang, Z.I., Tsai, G.E., Basu, A.C., Picker, J., Feng, J., and Coyle, J.T. (2007). Ube3a mRNA and protein expression are not decreased in Mecp2R168X mutant mice. Brain Res *1180*, 1-6.
Leoh, L.S., van Heertum, B., De Rijck, J., Filippova, M., Rios-Colon, L., Basu, A., Martinez, S.R., Tungteakkhun, S.S., Filippov, V., Christ, F.*, et al.* (2012). The stress oncoprotein LEDGF/p75 interacts with the methyl CpG binding protein MeCP2 and influences its transcriptional activity. Mol Cancer Res *10*, 378-391.
Lewis, J.D., Meehan, R.R., Henzel, W.J., Maurer-Fogy, I., Jeppesen, P., Klein, F., and Bird, A. (1992). Purification, sequence, and cellular localization of a novel chromosomal protein that binds to methylated DNA. Cell *69*, 905-914.
Li, H., Zhong, X., Chau, K.F., Santistevan, N.J., Guo, W., Kong, G., Li, X., Kadakia, M., Masliah, J., Chi, J.*, et al.* (2014). Cell cycle-linked MeCP2 phosphorylation modulates adult neurogenesis involving the Notch signalling pathway. Nat Commun *5*, 5601.
Li, H., Zhong, X., Chau, K.F., Williams, E.C., and Chang, Q. (2011). Loss of activity-induced phosphorylation of MeCP2 enhances synaptogenesis, LTP and spatial memory. Nat Neurosci *14*, 1001-1008.
Li, Y., Wang, H., Muffat, J., Cheng, A.W., Orlando, D.A., Loven, J., Kwok, S.M., Feldman, D.A., Bateup, H.S., Gao, Q.*, et al.* (2013). Global transcriptional and translational repression in human-embryonic-stem-cell-derived Rett syndrome neurons. Cell Stem Cell *13*, 446-458.
Lioy, D.T., Garg, S.K., Monaghan, C.E., Raber, J., Foust, K.D., Kaspar, B.K., Hirrlinger, P.G., Kirchhoff, F., Bissonnette, J.M., Ballas, N.*, et al.* (2011). A role for glia in the progression of Rett's syndrome. Nature *475*, 497-500.
Long, J.C., and Caceres, J.F. (2009). The SR protein family of splicing factors: master regulators of gene expression. Biochem J *417*, 15-27.
Long, S.W., Ooi, J.Y., Yau, P.M., and Jones, P.L. (2011). A brain-derived MeCP2 complex supports a role for MeCP2 in RNA processing. Biosci Rep *31*, 333-343.
Lorson, C.L., Hahnen, E., Androphy, E.J., and Wirth, B. (1999). A single nucleotide in the SMN gene regulates splicing and is responsible for spinal muscular atrophy. Proc Natl Acad Sci U S A *96*, 6307-6311.
Luco, R.F., Allo, M., Schor, I.E., Kornblihtt, A.R., and Misteli, T. (2011). Epigenetics in alternative pre-mRNA splicing. Cell *144*, 16-26.
Lugaresi, E., Cirignotta, F., and Montagna, P. (1985). Abnormal breathing in the Rett syndrome. Brain Dev *7*, 329-333.
Luikenhuis, S., Giacometti, E., Beard, C.F., and Jaenisch, R. (2004). Expression of MeCP2 in postmitotic neurons rescues Rett syndrome in mice. Proc Natl Acad Sci U S A *101*, 6033-6038.
Lunyak, V.V., Burgess, R., Prefontaine, G.G., Nelson, C., Sze, S.H., Chenoweth, J., Schwartz, P., Pevzner, P.A., Glass, C., Mandel, G.*, et al.* (2002). Corepressor-dependent silencing of chromosomal regions encoding neuronal genes. Science *298*, 1747-1752.
Lyst, M.J., Ekiert, R., Ebert, D.H., Merusi, C., Nowak, J., Selfridge, J., Guy, J., Kastan, N.R., Robinson, N.D., de Lima Alves, F.*, et al.* (2013). Rett syndrome mutations abolish the interaction of MeCP2 with the NCoR/SMRT co-repressor. Nat Neurosci *16*, 898-902.
Maezawa, I., and Jin, L.W. (2010). Rett syndrome microglia damage dendrites and synapses by the elevated release of glutamate. J Neurosci *30*, 5346-5356.
Maezawa, I., Swanberg, S., Harvey, D., LaSalle, J.M., and Jin, L.W. (2009). Rett syndrome astrocytes are abnormal and spread MeCP2 deficiency through gap junctions. J Neurosci *29*, 5051-5061.

Marchetto, M.C., Carromeu, C., Acab, A., Yu, D., Yeo, G.W., Mu, Y., Chen, G., Gage, F.H., and Muotri, A.R. (2010). A model for neural development and treatment of Rett syndrome using human induced pluripotent stem cells. Cell *143*, 527-539.
Martinowich, K., Hattori, D., Wu, H., Fouse, S., He, F., Hu, Y., Fan, G., and Sun, Y.E. (2003). DNA methylation-related chromatin remodeling in activity-dependent BDNF gene regulation. Science *302*, 890-893.
Matera, A.G., and Wang, Z. (2014). A day in the life of the spliceosome. Nat Rev Mol Cell Biol *15*, 108-121.
Maunakea, A.K., Chepelev, I., Cui, K., and Zhao, K. (2013). Intragenic DNA methylation modulates alternative splicing by recruiting MeCP2 to promote exon recognition. Cell research *23*, 1256-1269.
Maxwell, S.S., Pelka, G.J., Tam, P.P., and El-Osta, A. (2013). Chromatin context and ncRNA highlight targets of MeCP2 in brain. RNA Biol *10*, 1741-1757.
McGraw, C.M., Samaco, R.C., and Zoghbi, H.Y. (2011). Adult neural function requires MeCP2. Science *333*, 186.
Meehan, R.R., Lewis, J.D., and Bird, A.P. (1992). Characterization of MeCP2, a vertebrate DNA binding protein with affinity for methylated DNA. Nucleic Acids Res *20*, 5085-5092.
Mellen, M., Ayata, P., Dewell, S., Kriaucionis, S., and Heintz, N. (2012). MeCP2 binds to 5hmC enriched within active genes and accessible chromatin in the nervous system. Cell *151*, 1417-1430.
Mnatzakanian, G.N., Lohi, H., Munteanu, I., Alfred, S.E., Yamada, T., MacLeod, P.J., Jones, J.R., Scherer, S.W., Schanen, N.C., Friez, M.J.*, et al.* (2004). A previously unidentified MECP2 open reading frame defines a new protein isoform relevant to Rett syndrome. Nat Genet *36*, 339-341.
Monyer, H., Seeburg, P.H., and Wisden, W. (1991). Glutamate-operated channels: developmentally early and mature forms arise by alternative splicing. Neuron *6*, 799-810.
Mosbacher, J., Schoepfer, R., Monyer, H., Burnashev, N., Seeburg, P.H., and Ruppersberg, J.P. (1994). A molecular determinant for submillisecond desensitization in glutamate receptors. Science *266*, 1059-1062.
Muotri, A.R., Marchetto, M.C., Coufal, N.G., Oefner, R., Yeo, G., Nakashima, K., and Gage, F.H. (2010). L1 retrotransposition in neurons is modulated by MeCP2. Nature *468*, 443-446.
Nady, N., Min, J., Kareta, M.S., Chedin, F., and Arrowsmith, C.H. (2008). A SPOT on the chromatin landscape? Histone peptide arrays as a tool for epigenetic research. Trends Biochem Sci *33*, 305-313.
Nan, X., Campoy, F.J., and Bird, A. (1997). MeCP2 is a transcriptional repressor with abundant binding sites in genomic chromatin. Cell *88*, 471-481.
Nan, X., Hou, J., Maclean, A., Nasir, J., Lafuente, M.J., Shu, X., Kriaucionis, S., and Bird, A. (2007). Interaction between chromatin proteins MECP2 and ATRX is disrupted by mutations that cause inherited mental retardation. Proc Natl Acad Sci U S A *104*, 2709-2714.
Nan, X., Meehan, R.R., and Bird, A. (1993). Dissection of the methyl-CpG binding domain from the chromosomal protein MeCP2. Nucleic Acids Res *21*, 4886-4892.
Nan, X., Ng, H.H., Johnson, C.A., Laherty, C.D., Turner, B.M., Eisenman, R.N., and Bird, A. (1998). Transcriptional repression by the methyl-CpG-binding protein MeCP2 involves a histone deacetylase complex. Nature *393*, 386-389.
Nan, X., Tate, P., Li, E., and Bird, A. (1996). DNA methylation specifies chromosomal localization of MeCP2. Mol Cell Biol *16*, 414-421.

Nelles, D.A., Fang, M.Y., O'Connell, M.R., Xu, J.L., Markmiller, S.J., Doudna, J.A., and Yeo, G.W. (2016). Programmable RNA Tracking in Live Cells with CRISPR/Cas9. Cell.
Neul, J.L., Fang, P., Barrish, J., Lane, J., Caeg, E.B., Smith, E.O., Zoghbi, H., Percy, A., and Glaze, D.G. (2008). Specific mutations in methyl-CpG-binding protein 2 confer different severity in Rett syndrome. Neurology *70*, 1313-1321.
Nikitina, T., Shi, X., Ghosh, R.P., Horowitz-Scherer, R.A., Hansen, J.C., and Woodcock, C.L. (2007). Multiple modes of interaction between the methylated DNA binding protein MeCP2 and chromatin. Mol Cell Biol *27*, 864-877.
Nuber, U.A., Kriaucionis, S., Roloff, T.C., Guy, J., Selfridge, J., Steinhoff, C., Schulz, R., Lipkowitz, B., Ropers, H.H., Holmes, M.C*., et al.* (2005). Up-regulation of glucocorticoid-regulated genes in a mouse model of Rett syndrome. Hum Mol Genet *14*, 2247-2256.
O'Connell, M.R., Oakes, B.L., Sternberg, S.H., East-Seletsky, A., Kaplan, M., and Doudna, J.A. (2014). Programmable RNA recognition and cleavage by CRISPR/Cas9. Nature *516*, 263-266.
Pagani, F., Raponi, M., and Baralle, F.E. (2005). Synonymous mutations in CFTR exon 12 affect splicing and are not neutral in evolution. Proc Natl Acad Sci U S A *102*, 6368-6372.
Pan, Q., Shai, O., Lee, L.J., Frey, B.J., and Blencowe, B.J. (2008). Deep surveying of alternative splicing complexity in the human transcriptome by high-throughput sequencing. Nat Genet *40*, 1413-1415.
Partin, K.M., Fleck, M.W., and Mayer, M.L. (1996). AMPA receptor flip/flop mutants affecting deactivation, desensitization, and modulation by cyclothiazide, aniracetam, and thiocyanate. The Journal of neuroscience : the official journal of the Society for Neuroscience *16*, 6634-6647.
Pellizzoni, L., Kataoka, N., Charroux, B., and Dreyfuss, G. (1998). A novel function for SMN, the spinal muscular atrophy disease gene product, in pre-mRNA splicing. Cell *95*, 615-624.
Penn, A.C., Balik, A., Wozny, C., Cais, O., and Greger, I.H. (2012). Activity-mediated AMPA receptor remodeling, driven by alternative splicing in the ligand-binding domain. Neuron *76*, 503-510.
Phillips, M., and Pozzo-Miller, L. (2015). Dendritic spine dysgenesis in autism related disorders. Neurosci Lett *601*, 30-40.
Phizicky, E.M., and Fields, S. (1995). Protein-protein interactions: methods for detection and analysis. Microbiol Rev *59*, 94-123.
Polymenidou, M., Lagier-Tourenne, C., Hutt, K.R., Huelga, S.C., Moran, J., Liang, T.Y., Ling, S.C., Sun, E., Wancewicz, E., Mazur, C*., et al.* (2011). Long pre-mRNA depletion and RNA missplicing contribute to neuronal vulnerability from loss of TDP-43. Nat Neurosci *14*, 459-468.
Pradeepa, M.M., Sutherland, H.G., Ule, J., Grimes, G.R., and Bickmore, W.A. (2012). Psip1/Ledgf p52 binds methylated histone H3K36 and splicing factors and contributes to the regulation of alternative splicing. PLoS Genet *8*, e1002717.
Quaderi, N.A., Meehan, R.R., Tate, P.H., Cross, S.H., Bird, A.P., Chatterjee, A., Herman, G.E., and Brown, S.D. (1994). Genetic and physical mapping of a gene encoding a methyl CpG binding protein, Mecp2, to the mouse X chromosome. Genomics *22*, 648-651.
Rajaei, S., Erlandson, A., Kyllerman, M., Albage, M., Lundstrom, I., Karrstedt, E.L., and Hagberg, B. (2011). Early infantile onset "congenital" Rett syndrome variants: Swedish experience through four decades and mutation analysis. J Child Neurol *26*, 65-71.
Ramocki, M.B., Peters, S.U., Tavyev, Y.J., Zhang, F., Carvalho, C.M., Schaaf, C.P., Richman, R., Fang, P., Glaze, D.G., Lupski, J.R*., et al.* (2009). Autism and other neuropsychiatric symptoms are prevalent in individuals with MeCP2 duplication syndrome. Ann Neurol *66*, 771-782.

Reichwald, K., Thiesen, J., Wiehe, T., Weitzel, J., Poustka, W.A., Rosenthal, A., Platzer, M., Stratling, W.H., and Kioschis, P. (2000). Comparative sequence analysis of the MECP2-locus in human and mouse reveals new transcribed regions. Mamm Genome *11*, 182-190.
Reiss, A.L., Faruque, F., Naidu, S., Abrams, M., Beaty, T., Bryan, R.N., and Moser, H. (1993). Neuroanatomy of Rett syndrome: a volumetric imaging study. Ann Neurol *34*, 227-234.
Rett, A. (1966). [On a unusual brain atrophy syndrome in hyperammonemia in childhood]. Wien Med Wochenschr *116*, 723-726.
Robinson, M.D., McCarthy, D.J., and Smyth, G.K. (2010). edgeR: a Bioconductor package for differential expression analysis of digital gene expression data. Bioinformatics *26*, 139-140.
Samaco, R.C., Mandel-Brehm, C., Chao, H.T., Ward, C.S., Fyffe-Maricich, S.L., Ren, J., Hyland, K., Thaller, C., Maricich, S.M., Humphreys, P.*, et al.* (2009). Loss of MeCP2 in aminergic neurons causes cell-autonomous defects in neurotransmitter synthesis and specific behavioral abnormalities. Proc Natl Acad Sci U S A *106*, 21966-21971.
Samaco, R.C., Mandel-Brehm, C., McGraw, C.M., Shaw, C.A., McGill, B.E., and Zoghbi, H.Y. (2012). Crh and Oprm1 mediate anxiety-related behavior and social approach in a mouse model of MECP2 duplication syndrome. Nat Genet *44*, 206-211.
Schmid, D.A., Yang, T., Ogier, M., Adams, I., Mirakhur, Y., Wang, Q., Massa, S.M., Longo, F.M., and Katz, D.M. (2012). A TrkB small molecule partial agonist rescues TrkB phosphorylation deficits and improves respiratory function in a mouse model of Rett syndrome. J Neurosci *32*, 1803-1810.
Shahbazian, M., Young, J., Yuva-Paylor, L., Spencer, C., Antalffy, B., Noebels, J., Armstrong, D., Paylor, R., and Zoghbi, H. (2002). Mice with truncated MeCP2 recapitulate many Rett syndrome features and display hyperacetylation of histone H3. Neuron *35*, 243-254.
Shukla, S., Kavak, E., Gregory, M., Imashimizu, M., Shutinoski, B., Kashlev, M., Oberdoerffer, P., Sandberg, R., and Oberdoerffer, S. (2011). CTCF-promoted RNA polymerase II pausing links DNA methylation to splicing. Nature *479*, 74-79.
Skene, P.J., Illingworth, R.S., Webb, S., Kerr, A.R., James, K.D., Turner, D.J., Andrews, R., and Bird, A.P. (2010). Neuronal MeCP2 is expressed at near histone-octamer levels and globally alters the chromatin state. Mol Cell *37*, 457-468.
Sommer, B., Keinanen, K., Verdoorn, T.A., Wisden, W., Burnashev, N., Herb, A., Kohler, M., Takagi, T., Sakmann, B., and Seeburg, P.H. (1990). Flip and flop: a cell-specific functional switch in glutamate-operated channels of the CNS. Science *249*, 1580-1585.
Song, C.X., Szulwach, K.E., Fu, Y., Dai, Q., Yi, C., Li, X., Li, Y., Chen, C.H., Zhang, W., Jian, X.*, et al.* (2011). Selective chemical labeling reveals the genome-wide distribution of 5-hydroxymethylcytosine. Nat Biotechnol *29*, 68-72.
Sugino, K., Hempel, C.M., Okaty, B.W., Arnson, H.A., Kato, S., Dani, V.S., and Nelson, S.B. (2014). Cell-type-specific repression by methyl-CpG-binding protein 2 is biased toward long genes. J Neurosci *34*, 12877-12883.
Tai, D.J., Liu, Y.C., Hsu, W.L., Ma, Y.L., Cheng, S.J., Liu, S.Y., and Lee, E.H. (2016). MeCP2 SUMOylation rescues Mecp2-mutant-induced behavioural deficits in a mouse model of Rett syndrome. Nat Commun *7*, 10552.
Tao, J., Hu, K., Chang, Q., Wu, H., Sherman, N.E., Martinowich, K., Klose, R.J., Schanen, C., Jaenisch, R., Wang, W.*, et al.* (2009). Phosphorylation of MeCP2 at Serine 80 regulates its chromatin association and neurological function. Proc Natl Acad Sci U S A *106*, 4882-4887.
Tennyson, C.N., Klamut, H.J., and Worton, R.G. (1995). The human dystrophin gene requires 16 hours to be transcribed and is cotranscriptionally spliced. Nat Genet *9*, 184-190.

Trappe, R., Laccone, F., Cobilanschi, J., Meins, M., Huppke, P., Hanefeld, F., and Engel, W. (2001). MECP2 mutations in sporadic cases of Rett syndrome are almost exclusively of paternal origin. Am J Hum Genet *68*, 1093-1101.
Tudor, M., Akbarian, S., Chen, R.Z., and Jaenisch, R. (2002). Transcriptional profiling of a mouse model for Rett syndrome reveals subtle transcriptional changes in the brain. Proc Natl Acad Sci U S A *99*, 15536-15541.
Ule, J. (2008). Ribonucleoprotein complexes in neurologic diseases. Curr Opin Neurobiol *18*, 516-523.
Urdinguio, R.G., Fernandez, A.F., Lopez-Nieva, P., Rossi, S., Huertas, D., Kulis, M., Liu, C.G., Croce, C.M., Calin, G.A., and Esteller, M. (2010). Disrupted microRNA expression caused by Mecp2 loss in a mouse model of Rett syndrome. Epigenetics *5*, 656-663.
von Mering, C., Krause, R., Snel, B., Cornell, M., Oliver, S.G., Fields, S., and Bork, P. (2002). Comparative assessment of large-scale data sets of protein-protein interactions. Nature *417*, 399-403.
Wang, E.T., Sandberg, R., Luo, S., Khrebtukova, I., Zhang, L., Mayr, C., Kingsmore, S.F., Schroth, G.P., and Burge, C.B. (2008). Alternative isoform regulation in human tissue transcriptomes. Nature *456*, 470-476.
Wang, Y., Chen, D., Qian, H., Tsai, Y.S., Shao, S., Liu, Q., Dominguez, D., and Wang, Z. (2014a). The splicing factor RBM4 controls apoptosis, proliferation, and migration to suppress tumor progression. Cancer Cell *26*, 374-389.
Wang, Y., Cheong, C.G., Hall, T.M., and Wang, Z. (2009). Engineering splicing factors with designed specificities. Nature methods *6*, 825-830.
Wang, Y., Ma, M., Xiao, X., and Wang, Z. (2012). Intronic splicing enhancers, cognate splicing factors and context-dependent regulation rules. Nat Struct Mol Biol *19*, 1044-1052.
Wang, Y., Wang, Z., and Tanaka Hall, T.M. (2013). Engineered proteins with Pumilio/fem-3 mRNA binding factor scaffold to manipulate RNA metabolism. Febs J *280*, 3755-3767.
Wang, Z., Murigneux, V., and Le Hir, H. (2014b). Transcriptome-wide modulation of splicing by the exon junction complex. Genome Biol *15*, 551.
Wang, Z., Rolish, M.E., Yeo, G., Tung, V., Mawson, M., and Burge, C.B. (2004). Systematic identification and analysis of exonic splicing silencers. Cell *119*, 831-845.
Williams, E.C., Zhong, X., Mohamed, A., Li, R., Liu, Y., Dong, Q., Ananiev, G.E., Mok, J.C., Lin, B.R., Lu, J.*, et al.* (2014). Mutant astrocytes differentiated from Rett syndrome patients-specific iPSCs have adverse effects on wild-type neurons. Hum Mol Genet *23*, 2968-2980.
Young, J.I., Hong, E.P., Castle, J.C., Crespo-Barreto, J., Bowman, A.B., Rose, M.F., Kang, D., Richman, R., Johnson, J.M., and Berget, S. (2005). Regulation of RNA splicing by the methylation-dependent transcriptional repressor methyl-CpG binding protein 2. Proceedings of the National Academy of Sciences of the United States of America *102*, 17551-17558.
Zhou, Z., Hong, E.J., Cohen, S., Zhao, W.N., Ho, H.Y., Schmidt, L., Chen, W.G., Lin, Y., Savner, E., Griffith, E.C.*, et al.* (2006). Brain-specific phosphorylation of MeCP2 regulates activity-dependent Bdnf transcription, dendritic growth, and spine maturation. Neuron *52*, 255-269.
Zoghbi, H. (1988). Genetic aspects of Rett syndrome. J Child Neurol *3 Suppl*, S76-78.